Engineered In Vitro Disease Models

Kambez H. Benam,[1] Stephanie Dauth,[1,2]
Bryan Hassell,[1,2] Anna Herland,[1] Abhishek Jain,[1]
Kyung-Jin Jang,[1] Katia Karalis,[1,3,4] Hyun Jung Kim,[1]
Luke MacQueen,[1,2] Roza Mahmoodian,[1,2]
Samira Musah,[1] Yu-suke Torisawa,[1]
Andries D. van der Meer,[1] Remi Villenave,[1]
Moran Yadid,[1,2] Kevin K. Parker,[1,2]
and Donald E. Ingber[1,2,5]

[1]Wyss Institute for Biologically Inspired Engineering at Harvard University, Boston, Massachusetts 02115; email: don.ingber@wyss.harvard.edu

[2]Harvard School of Engineering and Applied Sciences, Cambridge, Massachusetts 02139

[3]Division of Endocrinology, Boston Children's Hospital, Boston, Massachusetts 02115

[4]Center for Clinical, Experimental Surgery and Translational Research, Biomedical Research Foundation Academy of Athens (BRFAA), 11527 Athens, Greece

[5]Vascular Biology Program and Departments of Pathology and Surgery, Boston Children's Hospital and Harvard Medical School, Boston, Massachusetts 02115

Keywords

Abstract

The ultimate goal of most biomedical research is to gain greater insight into mechanisms of human disease or to develop new and improved therapies or diagnostics. Although great advances have been made in terms of developing disease models in animals, such as transgenic mice, many of these models fail to faithfully recapitulate the human condition. In addition, it is difficult to identify critical cellular and molecular contributors to disease or to vary them independently in whole-animal models. This challenge has attracted the interest of engineers, who have begun to collaborate with biologists to leverage recent advances in tissue engineering and microfabrication to develop novel in vitro models of disease. As these models are synthetic systems, specific molecular factors and individual cell types, including parenchymal cells, vascular cells, and immune cells, can be varied independently while simultaneously measuring system-level responses in real time. In this article, we provide some examples of these efforts, including engineered models of diseases of the heart, lung, intestine, liver, kidney, cartilage, skin and vascular, endocrine, musculoskeletal, and nervous systems, as well as models of infectious diseases and cancer. We also describe how engineered in vitro models can be combined with human inducible pluripotent stem cells to enable new insights into a broad variety of disease mechanisms, as well as provide a test bed for screening new therapies.

INTRODUCTION

The ultimate goal of virtually all biomedical research is to understand the molecular basis of human disease in order to develop new and more effective modes of diagnosis, prevention, or therapeutic intervention. Because it is not possible to carry out fundamental research investigations using humans as "guinea pigs," scientists have had to develop alternative models of human disease. Most commonly, animal models, such as transgenic mice with specific gene alterations, are used for this purpose. Although many of these animal models reconstitute disease manifestations and phenotypes that are ostensibly similar to those observed in humans, recent studies in sepsis, for example, show that the underlying molecular mechanisms can actually differ greatly between mice and humans with the same disease phenotype (1). This inability to effectively mimic human disease is becoming evident in increasing numbers of animal models, and it is likely the reason why many drugs fail to show efficacy and safety when advanced from animal studies to human clinical trials. For this reason, many investigators and pharmaceutical companies have placed greater emphasis on studies with cultured human cells, including primary cells, established cell lines, and, more recently, derivatives of induced pluripotent stem cells (iPSCs). Some cells cultured on standard culture dishes might exhibit differentiated cell functions, but they commonly fail to mimic tissue- and organ-level structures and functions that are central to disease etiology. Thus, there is a great need to develop alternative experimental systems containing living human cells that recapitulate tissue- and organ-level pathophysiology in vitro.

In this article, we review recent advances in the development of in vitro disease models made by leveraging recent advances in tissue engineering and microfabrication. Human diseases are hugely complex, and different responses can be observed in the same organ depending on disease location, influences of the physical and chemical microenvironment, immune and inflammatory responses, and whether the condition is acute or chronic; disease manifestations can also differ depending on genetic variation between different patients. For these reasons, it will be difficult to model every facet of human disease in vitro. However, the goal in this emerging field of engineered disease models is not to solve all these problems at once. Rather, investigators take a synthetic approach by starting to build simple tissue and organ models and then constructing progressively more complex in vitro experimental systems that recapitulate more and more features that are critical for disease etiology and progression. Importantly, although this field is still in its infancy, there already have been a few exciting examples of major successes in terms of both mimicking organ-level functions and recapitulating key features of human disease in vitro. Below, we describe multiple examples of engineered in vitro disease models ranging from two-dimensional (2D) networks composed of neuronal cells derived from human iPSCs to three-dimensional (3D) reconstructions of complex heart valve structures lined by living valvular endothelial cells. In addition, we describe recently developed organ-on-a-chip cell culture devices, created with microchip manufacturing methods, that contain hollow microchannels inhabited by human cells; these devices recreate the specialized tissue-tissue interfaces, physicochemical microenvironments, and vascular perfusion characteristics of the lung, liver, gut, kidney, and many other living organs. We also describe how these organs-on-chips are being used to create novel in vitro models of human disease.

STEM CELLS AND IN VITRO DISEASE MODELS

The development of in vitro human disease models hinges on the availability of tissue- and organ-specific cell types that accurately recapitulate disease phenotypes. To date, most tissue engineering strategies rely on established cell lines (often transformed cell lines) or primary cells derived from patients with or without the disease of interest. Although primary cells are more representative of

the functional units of the tissue from which they are derived, they are difficult to obtain, proliferate slowly, have limited life span, and are often poorly characterized. Stem cells, particularly iPSCs (2), provide tremendous opportunities to overcome these limitations. Human iPSCs, which are derived from somatic cells by overexpression of a few transcription factors (3, 4), can be generated from patients with or without a specific disease, and the resulting pluripotent cells can self-renew indefinitely. Under appropriate conditions, these self-renewing human iPSCs can be differentiated into virtually any cell type. Although techniques for direct conversion of some differentiated cell types into other specialized cells (without reverting to the stem cell state) have also been reported (5–7), human iPSCs potentially offer an unlimited supply of cells for tissue engineering, therapeutic discovery, and modeling of diseases that affect almost all human tissues or organs.

A growing number of reports have employed human iPSC-derived cells to model several diseases in vitro and, in some cases, aid drug testing and therapeutic discovery by illuminating disease mechanisms. Although these lines of investigation remain largely underexplored, a few reports have focused on uniting the principles of tissue engineering and stem cell biology to develop in vitro models of human disease, as we describe below. However, it is important to note that almost all specialized cell types derived by differentiation of iPSCs still exhibit immature phenotypes. Such immature cells may be relevant for studying early-onset disease processes, but it is less clear whether their biological responses can be extrapolated to mature and functional cell types that normally compose adult organs. As such, robust methods to not only differentiate iPSCs but also facilitate their maturation and expression of adult-like functionalities are needed. It is also less clear what combinations of soluble, insoluble, and mechanical signals are necessary to coax human iPSCs to commit to specific lineages. Given the importance of soluble, insoluble, and mechanical signals within the extracellular microenvironment for cell fate switching (8, 9) and human pluripotent stem cell self-renewal (10, 11), it is conceivable that robust methods for directed differentiation and maturation of human iPSCs into specialized and functional cell types could be developed by employing combinatorial tissue engineering strategies, including the use of biomimetic scaffolds (12), bioreactors (13), organ-on-a-chip microphysiological systems (14), and 3D biological printing technologies (15). In fact, these types of engineered models are currently being used to facilitate iPSC differentiation, as we describe below, and they may be necessary for realizing the full potential of human iPSCs as tools for in vitro disease modeling and therapeutic discovery. Below we present our review of engineered disease models organized by organ system. We also discuss the relevance of iPSCs for these models.

HEART DISEASE

The heart is a complex organ, with a hierarchical architecture and multiple cell types, that responds to external stimuli and systemic changes by sensing humoral and neurogenic factors while simultaneously being regulated by internal feedback mechanisms (16). Therefore, the mere use of human cells in culture is not enough to construct a reliable heart disease model, a limitation confirmed by studies of cultured cardiomyocytes, which do not recapitulate organ-level structure or functionality (e.g., contractility). Additionally, it is difficult to maintain cardiac cell cultures for extended times, making long-term studies impossible. In contrast, as described below, engineered cardiac tissue constructs can exhibit a genotype and phenotype more similar to those of the native myocardium, reconstitute heart tissue microarchitecture, enable cell-cell and cell–extracellular matrix (ECM) interactions, promote tissue maturation, and enable reliable functional measurements.

Cardiac Stem Cell Models

To appreciate the value of engineered models of heart disease, it is helpful to first understand the power and limitations of recent advances in stem cell biology, which have made it possible to generate unlimited amounts of human cardiomyocytes from healthy individuals and patients with various cardiac diseases for disease studies. This ability has enabled major improvements in understanding the pathogenesis of inherited cardiomyopathies and developing drug-based treatments, by circumventing one of the main limitations of animal disease models—the substantial differences between human and animal genomes. For example, the human congenital long QT (LQT) syndrome, which is characterized by prolonged QT interval, delayed repolarization, and, consequently, lethal polymorphic ventricular tachycardia (PVT), was recently modeled in vitro (17). Human iPSCs were generated from dermal fibroblasts obtained from a 28-year-old patient diagnosed with familial type 2 LQT syndrome due to a missense mutation in exon 9 of the *KCNH2* gene, and they were then differentiated into cardiomyocytes. Intracellular recordings revealed that LQT iPSC-derived cardiomyocytes had a markedly prolonged action potential duration compared with control iPSC-derived cardiomyocytes, both while paced and while spontaneously beating. Voltage clamp studies demonstrated a more than 60% reduction in the I_{Kr} currents of LQT cells, consistent with recordings from heterologous expression systems. Extracellular recording with microelectrode arrays was also used to evaluate the electrophysiological properties at the multicellular level. In agreement with the patch clamp data, LQT cells displayed prolonged field potential duration, but also marked arrhythmogenicity, as manifested by the frequent occurrence of early afterdepolarizations, many of which developed into sustained triggered activity.

This LQT syndrome model was further employed to evaluate drugs that may either aggravate or ameliorate the disease phenotype. On one hand, the I_{Kr} blocker E-4031 significantly increased the action potential duration and increased arrhythmogenesis in LQT cells in both single-cell and multicellular assays. This finding suggested that LQT syndrome patients may be susceptible to PVT in response to I_{Kr}-inhibiting drugs. On the other hand, nifedipine, a calcium channel blocker, decreased LQT cells' action potential duration by 57% and completely abolished all early afterdepolarizations and triggered activities. Additional studies also have employed iPSC-derived cardiomyocytes to model other rhythm disorders, such as type 1 LQT syndrome (18), Brugada syndrome (19), and PVT (20). Human iPSCs can thus be used to characterize the disease phenotype in heart arrhythmias and provide meaningful mechanistic insight at the cellular level in vitro.

Cardiomyopathies, such as hypertrophy and pathological dilatation of the ventricles, have been hard to study in vitro because of the difficulty of obtaining cardiomyocytes from patients with these conditions. However, the availability of iPSC-derived cardiomyocytes recently enabled a study of familial dilated and hypertrophic cardiomyopathies characterized by dilatation of the ventricles and impaired systolic function (21, 22). Human cardiomyocytes were generated from iPSCs prepared from members of three generations of a family with dilated cardiomyopathy due to a point mutation in exon 12 of *TNNT2*, which encodes cardiac troponin T, and from a healthy individual from the same family who did not carry the mutation (21). Sarcomeric α-actinin immunostaining and transmission electron microscopy both demonstrated decreased sarcomeric organization and scattered patterns of condensed Z bodies in iPSC-derived cardiomyocytes from the diseased patients compared with controls. Calcium imaging of single cells revealed decreased Ca^{2+} transient amplitude and time to peak and increased transient duration in the diseased cardiomyocytes compared with the healthy cells. Ca^{2+} measurements with caffeine yielded consistent results, implying that the diseased iPSC-derived cells have relatively less storage of Ca^{2+} in their sarcoplasmic reticulum. Using atomic force microscopy to measure contractile forces in single adherent cells,

the investigators found that diseased cardiomyocytes produced significantly lower forces compared with controls, a finding consistent with clinical data and with genetic mouse models bearing the same mutation and showing impaired systolic function (22). Furthermore, overexpression of the *Serca2a* gene, an intervention that is currently in preclinical testing for treatment of dilated cardiomyopathy (23), partially rescued the disease phenotype. Transfection of *Serca2a* into the diseased iPSC-derived cardiomyocytes returned gene expression to the levels measured in control cardiomyocytes, restored contractile forces to control levels, and elevated Ca^{2+} amplitudes without altering sarcomere organization. This study also revealed several new pathways, not previously linked to this disease, that appeared to contribute to the rescue of function, including cardiogenesis, integrin and cytoskeletal signaling, and ubiquitination.

Hypertrophic cardiomyopathy is an autosomal dominant disease of the cardiac sarcomeres caused by various mutations in genes encoding sarcomeric proteins; these mutations induce pathological thickening of the left ventricular wall and fibrosis, thereby increasing the risk for progressive heart failure, arrhythmia, and sudden cardiac death (22, 24, 25). Although genetic causes of hypertrophic cardiomyopathy have been widely studied, the pathways by which these mutations lead to a hypertrophic phenotype are not well understood. Human iPSC-derived cardiomyocytes were prepared from a family of 10 individuals, half of whom carry an autosomal dominant missense mutation in exon 18 of the β-myosin heavy chain gene (*MYH7*) (26). The cells from diseased patients exhibited several hallmarks of hypertrophic cardiomyopathy, such as increased cell size, multinucleation, atrial natriuretic factor expression, elevation of the β/α myosin ratio, and disorganized sarcomeres. Whole-cell patch clamping also showed arrhythmic waveforms similar to delayed afterdepolarizations in the diseased cells starting at day 30 after induction of differentiation. Moreover, single-cell assays revealed that elevation of cytosolic calcium is a key mechanism underlying the pathogenesis of the disease, and overexpression of the patient-specific myosin mutation in normal human embryonic stem cell (hESC)-derived cardiomyocytes recapitulated the calcium-handling abnormalities of cardiomyocytes prepared from the patients with hypertrophic cardiomyopathy. Most interestingly, Ca^{2+} transient abnormalities were observed in both the diseased cardiomyocytes and mutated hESC-derived cells before noticeable cellular hypertrophy, suggesting abnormal calcium handling as a causal factor for expression of a hypertrophic phenotype. Moreover, treatment with verapamil, an L-type calcium channel blocker, not only ameliorated Ca^{2+} transient abnormalities and arrhythmia but also rescued the hypertrophic phenotype.

2D Engineered Cardiac Tissue Models

Although human induced iPSC-derived cardiomyocytes provide several significant advantages over animal models for study of disease mechanisms, they still exhibit several limitations. First, these cardiomyocytes are usually immature, and they show gene expression profiles characteristic for fetal cardiomyocytes as well as lower β-myosin levels compared with adult cardiac muscle cells (17, 27). Second, the assays described above may not faithfully reflect the human disease phenotype, as they do not recapitulate significant environmental and epigenetic factors. Third, disease models utilizing single cardiomyocytes cannot exhibit disease phenotypes at the tissue level, such as decreased conduction velocity, fibrosis, scarring, myocyte disarray, and tissue-level electromechanical coupling.

Tissue engineering techniques have been used to construct cardiac tissues that mimic the native myocardium's structure and function more closely than do cardiomyocyte cell cultures. In early studies, substrates containing ECM deposited in specific patterns were used to engineer aligned strands or pairs of cardiomyocytes to study conduction abnormalities (28–30). The creation of heart tissues composed of aligned cardiac muscle cells reconstitutes more normal structure-function

relations from the sarcomere to the tissue level (31–34), promotes cell maturation, restores natural directional propagation of action potentials, enhances cell-cell coupling, and, as a result, facilitates stress generation with values comparable to those obtained with ex vivo preparations (isolated fibers) (35–37).

Building 2D tissues with aligned cardiomyocytes has become a popular technique for the in vitro study of electrophysiology and rhythm disorders, due to the spatial heterogeneity of the tissue and to its conduction velocity, which is similar to that of native cardiac tissue. These factors play a dominant role in arrhythmogenesis following decreased cell-cell electrical coupling, myocardial infarction, and tissue fibrosis (30, 38–41). Patterned anisotropic cardiac tissue monolayers can be built by seeding cardiomyocytes on substrates containing geometrical or chemical cues. For example, alignment cues can be engineered into culture surfaces by using microcontact printing of ECM proteins, microabrasion of coverslips, or micromolding of soft substrates (32, 42–44).

In microcontact printing, soft lithography techniques originally developed as an inexpensive way to make computer chips are used to create a flexible stamp with defined surface microtopography that can be used to transfer ECM molecules in a similar microscale pattern onto the surface of a culture substrate. Specifically, a photomask with the desired line patterns (e.g., a set of thin lines) is created using computer-assisted design software and standard photolithography methods, and then the mask is used to shadow a wafer glass covered with a photoresist when exposed to UV light. The depth of the grooves is determined by the thickness of the photoresist layer, and their width is determined by the photomask line patterns when the light-exposed areas of the photoresist are dissolved away. This etched surface is then used as a master form onto which liquid polydimethylsiloxane (PDMS) silicone rubber is cast and allowed to polymerize overnight at 65°C. The product of this process is a PDMS stamp that can be used either to directly stamp (microcontact print) ECM molecules in patterns that match those designed into the master onto a culture substrate, or to micromold soft polymerizable materials, such as alginate or gelatin, creating grooves and ridges in desired patterns that similarly direct anisotropic tissue formation.

Microcontact printing of the ECM protein fibronectin was used in combination with microabrasion of substrates to create linear adhesive substrates that pattern cardiac tissues and dictate cardiac myofiber directions and anisotropy in vitro (32). The cells on the line-patterned substrates appeared elongated, with preferential orientation in the direction of the lines (stamped fibronectin or microabraded grooves). Cell elongation in anisotropic cultures was associated with coalignment of actin fibers along the cell's long axis, parallel arrangement of sarcomeres, and elongation of cell nuclei, as observed in native tissue.

Importantly, upon electrical point stimulation, the electrical wave propagated faster through the engineered cardiac tissue along the direction of the line patterns and significantly slower in the transverse direction. When the direction of the lines sharply varied, a border zone formed where the direction of the fastest propagation of an electrical pulse abruptly changed when crossing. Essentially, the border zone acted as a secondary source following field stimulation, causing far-field activation to initiate along the border zone line and propagate through the rest of the culture.

This method has been extended to create cocultures of patterned monolayers, which have been used to study reentry cardiac rhythm dynamics in an in vitro model of a healed infarct border zone (39). Myocardial infarct border regions have a nonuniform anisotropic structure resulting from fibrosis and gap junction remodeling, both of which result in decreased electrical coupling of cardiomyocytes (40), which causes these zones to be highly susceptible to tachyarrhythmic events (41). To create a 2D in vitro model of arrhythmia generation within a healed infarct border zone, human skeletal myotubes were cocultured with neonatal rat ventricular cardiomyocytes. The skeletal myotubes were chosen to simulate the fibrosis seen in these border zones because they lack gap junctions, exhibit linear morphology similar to that observed in regions of fibrosis,

and orient neighboring cardiomyocytes into bundles, resulting in nonuniform anisotropic architecture. A healed "epicardial" infarct border zone was simulated by plating a mixture of these cells on fibronectin-coated coverslips, whereas a "lateral" infarct border zone was created by micropatterning a sector composed of a similar coculture juxtaposed with a fibronectin-coated region of a PDMS-treated coverslip lined only with ventricular cardiomyocytes. This model succeeded in reproducing the decreased conduction velocity with increased dispersion while maintaining the cell excitability and easy induction of sustained reentrant arrhythmias observed in healed myocardial infarcts (40). In addition, the reentrant arrhythmias induced in this engineered model could be consistently terminated by addition of the L-type calcium channel blocker nifedipine, but not by addition of sodium or potassium channel blockers. These findings provide a possible reason why sodium channel blockers, such as lidocaine, have low efficacy in terminating sustained ventricular tachycardias in patients with old myocardial infarcts.

Following a myocardial infarct, cardiac fibroblasts also undergo a phenotypic change to become α smooth muscle actin (α-SMA)-positive cells (42), which exert strong contractile forces to stabilize scar tissue. They persist in and around the scar tissues formed following myocardial infarction, affecting neighboring cardiomyocytes through biochemical, mechanical, and electrical interactions and by modulating ECM production (43–46). To study this process and model these cell-cell interactions between cardiac myofibroblasts and myocytes, linear islands of ECM created with microcontact printing were employed to build 2D anisotropic cardiac tissues containing both cell types (47). Slowing of both longitudinal and transverse conduction velocities in ventricular cardiomyocytes was demonstrated within 30 min after the myofibroblasts were plated on top of the anisotropic myocyte layer, and cadherin expression levels increased within 1 h. Real-time time-lapse microscopic imaging enabled by this 2D tissue engineering method revealed that the cardiac myofibroblasts were highly motile and constantly interacted with cardiomyocytes, indicating dynamic formation and breakdown of heterocellular connections, mainly via N-cadherins, that supported contractility-mediated deformation of the cardiomyocytes. These mechanical linkages appear to enable transmission of contractile forces from the myofibroblasts to the cardiomyocytes, which deform their membranes, thereby altering the activity of stretch-activated ion channels and impairing electrical wave conduction in the scar tissue area.

The heterogeneous connexin 43 (Cx43) distribution that is observed in the ventricular myocardium of heart failure patients is associated with dispersed conduction and ventricular arrhythmias (48, 49). A chimeric mouse model in which the heart contains a macroscopic mosaic of tissues with or without normal Cx43 expression exhibits irregular macroscopic electric propagation and poor heart contractility (50). Because this observation suggests that abnormal heterogeneous patterns of cell-cell coupling could affect the electromechanical function of the whole heart, tissue engineering was used to create defined cell pairs and cell strands by seeding ventricular cardiomyocytes on coverslips coated with adjacent, microcontact-printed, rectangular ECM islands (30). Ventricular myocytes settle on the ECM islands and extend cell processes across the intervening nonadhesive regions to form well-defined cell-cell adhesions linking cells on neighboring islands. Long (4–5 mm) adhesive islands were also created using photolithography and ECM coating. Ventricular myocytes obtained from Cx43 knockout (KO) or wild-type (WT) mice were cultured on these ECM islands, and dual-voltage patch clamp assays were used to assess intracellular conductance between heterogeneous and homogeneous cell pairs. Calculation of conduction velocity using high-resolution optical mapping revealed that the inclusion of one Cx43 KO cell in a cell pair reduced the conduction velocity by 94% compared with WT-WT cell pairs, and KO-KO pairs showed an even further decrease in conductivity. Analysis of longer cell strands containing various mixtures of KO and WT cells revealed that the macroscopic conduction velocity significantly decreased with increasing Cx43 KO:WT ratios, with the most significant decrease occurring for

strands composed of more than 50% KO cells. KO clusters were consistently excitable, but they were electrically dissociated from neighboring WT clusters.

Although these engineered 2D anisotropic cardiac tissues are useful for studying cardiac arrhythmias, they lack a critical feature necessary for modeling many heart diseases: the ability to generate the mechanical contraction that normally pushes blood throughout the entire body. To study muscle contraction in vitro, the 2D cardiac muscle engineering approach was modified by creating muscle tissues on freestanding, elastic thin films microcontact-printed with ECM that allow three degrees of freedom during contraction and facilitate quantitation of stresses generated by the cells (**Figure 1**) (51). These muscular thin films (MTFs) remain planar during culture and
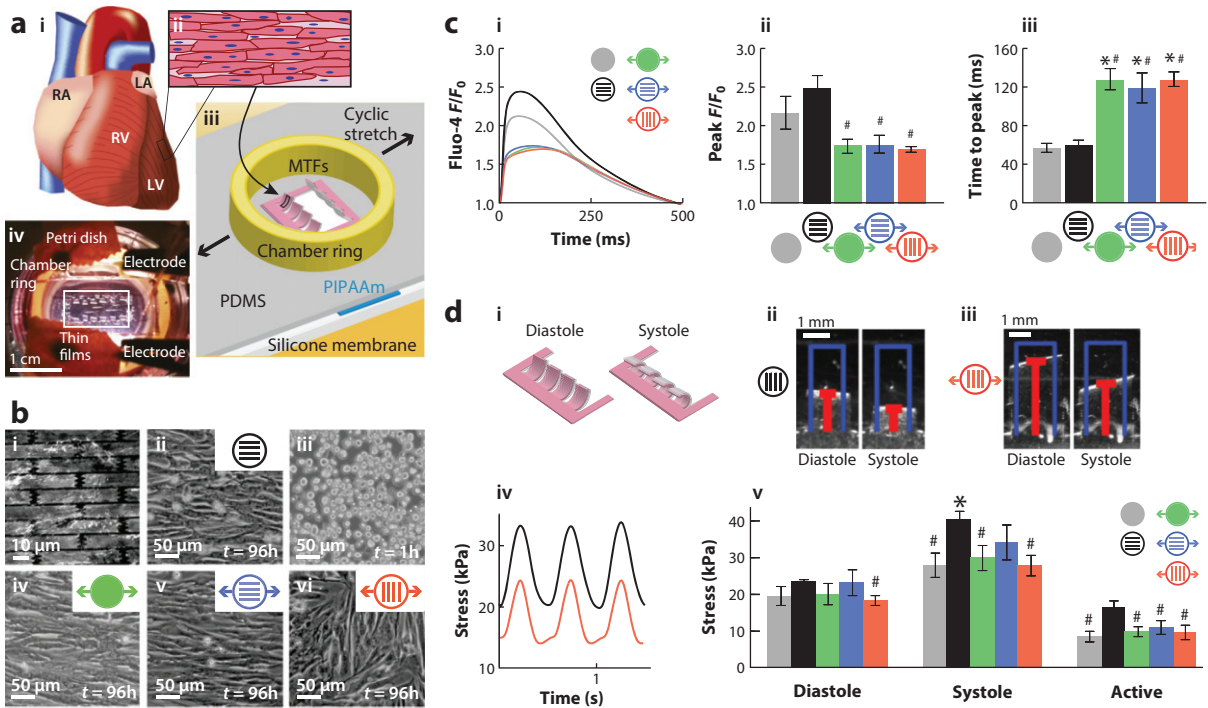

Figure 1

Modeling failing myocardium in vitro. (*a*) Overview of the muscular thin film (MTF) model. (*i*) Schematic of the heart, illustrating the right atrium (RA), left atrium (LA), right ventricle (RV), and left ventricle (LV). (*ii*) Diagram of the arrangement of the ventricular myocardium, which consists of aligned, elongated cardiac myocytes. (*iii*) Schematic of the failing myocardium-on-a-chip system adapted for the MTF assay. (*iv*) Photograph of an experiment in which the MTF is stretched laterally. Other abbreviations: PDMS, polydimethylsiloxane; PIPAAm, poly(*N*-isopropylacrylamide). (*b*) Electron micrographs. (*i*) Elastomeric silicone membrane micropatterned with fibronectin (*white*) in a brick wall pattern. (*ii*) The same membrane seeded with neonatal rat ventricular myocytes. (*iii*, *iv*) Myocytes seeded onto membranes coated with isotropic fibronectin (*iii*) cultured for 1 h and (*iv*) cyclically stretched. (*v*) Myocytes patterned and stretched in the longitudinal direction. (*vi*) Myocytes patterned and stretched in the transverse direction. (*c*) Measuring contractile function. Cyclic stretch reduces contractile function, as shown by a reduction of the average fluorescence intensity *F* of Fluo-4 normalized to F_0 and plotted for (*i*) a cardiac cycle, (*ii*) peak F/F_0, and (*iii*) time to peak for each condition (mean ± SE; $n = 5$; asterisks denote $p < 0.05$ versus static, isotropic tissues; pound signs denote $p < 0.05$ versus static, patterned tissues). (*d*) Measuring stress generation. (*i*) Schematic of stretchable MTFs at diastole and systole. Contraction of MTFs was recorded from above, as shown for representative (*ii*) patterned and (*iii*) transversely stretched films transitioning from diastole to systole. (*iv*) Displacement of these films was used to determine stress generation over time. (*v*) Average diastolic, systolic, and active stress for each condition (mean ± SE; $n = 16$; asterisks denote $p < 0.05$ versus static, isotropic tissues; pound signs denote $p < 0.05$ versus static, patterned tissues). Figure modified with permission from Reference 52.

then can be released partially or completely to enable free cell contraction. Active contraction and shortening of the cardiomyocytes following electrical stimulation causes the PDMS to bend during systole and return to its original position upon relaxation. The polymeric thin films are manufactured by spin coating a thermally sensitive sacrificial layer of poly(N-isopropylacrylamide) (PIPAAm) on glass coverslips and then spin coating a thin film of PDMS on top of the PIPAAm. The thickness of the film can be adjusted by modulating the viscosity of the PDMS and the spin coating parameters; ECM patterns are microcontact-printed on the top surface of the thin PDMS layer after it has cured.

2D laminar organized cardiac tissues form within 5 days after rat ventricular cardiomyocytes are plated on these substrates. The desired shape of the MTFs can be cut by hand or using lasers, and the PIPAAm layer can be dissolved to release the undersurface of the MTFs from the coverslip by cooling the cultures to room temperature. By retaining adhesion of a rectangular MTF to the coverslip at one edge, it is possible to measure deflection of the MTF relative to its remaining fixed edge along the longitudinal axis of the anisotropic tissue by video tracking and to calculate changes in its curvature (31). MTF deflection was shown to depend on the film geometry (aspect ratio and thickness) and on the tissue alignment and contractile forces. Resulting changes in MTF curvature can be converted to the contractile stresses generated by the active muscular tissue by using engineering modeling approaches in which the MTFs are assumed to be two-layered beams and the geometry and mechanical properties of the PDMS film are known.

Importantly, rat cardiac MTFs respond actively to electrical stimulation, and the generated contractile stresses change in response to pharmacological manipulation to a similar degree as measured in the whole-rat ventricular strips that are often used by the pharmaceutical industry to study heart contractility (31, 33). The MTF assay also has been used to mimic maladaptive remodeling of failing myocardium in response to volume overload (**Figure 1**) (52). In this study, the anisotropic cardiac tissues were built on stretchable PDMS membranes rather than on glass coverslips, and the substrates were uniaxially and cyclically stretched for four days at 10% strain and a frequency of 3 Hz. Cyclic stretch decreased the α/β myosin heavy chain mRNA ratio and activated markers of pathological cardiac hypertrophy, including genes encoding T-type calcium channels, myocardin, and cytoskeletal proteins, consistent with results obtained in animal models of hypertrophic remodeling. In addition, the longitudinally stretched tissues exhibited elongated cardiomyocytes with a 10:1 cell aspect ratio, whereas unstretched and normal tissues contained cells with a 7:1 aspect ratio. Calcium measurements demonstrated remodeled Ca^{2+} transients, with longer time to peak and lower amplitudes, similar to the Ca^{2+} transients reported for hypertrophic and failing heart (53, 54). Finally, measuring the deflection of the MTFs enabled calculation of the stresses generated by stretched and control tissue and demonstrated the functional deficiency of these abnormally stretched tissues, which were characterized by lower systolic and twitch stresses compared with controls. Thus, this study demonstrates that tissue engineering approaches can be used to model the abnormal contractile responses of a failing myocardium in vitro.

3D Engineered Cardiac Tissue Models

2D tissue monolayers have provided a relatively simple tool to advance the understanding of cardiac cell function, interactions between neighboring cardiac cells, and electrical properties of cardiac tissues. Yet they lack the complex 3D structures whereby different cell types interact and exert forces on each other. Several groups have been working toward developing 3D constructs of heart cells (55–57). A widely used technique is to mix isolated cardiomyocytes with biodegradable matrices (e.g., collagen, Matrigel, fibrin) that are then polymerized into different geometrical shapes, such as cylinders, rings, or sheets. The cells contained in the ECMs are aligned with the

direction of the principal stresses acting on the structure, forming aligned cardiac tissues. During culture of these constructs, the matrix is gradually remodeled and the cardiac tissue condenses. Similar to 2D cultures, the 3D tissues start to beat spontaneously, gaining synchronicity.

Tissue differentiation and maturation can be promoted in these engineered heart tissues using electrical or cyclic mechanical stimuli. The fiber-like or ring-like formed tissues are usually grown wrapped around bendable posts of known elasticity, which are used for calculating the forces generated by the contraction of the 3D cardiac tissue constructs. Cardiac tissue constructs have been built from neonatal rat ventricular myocytes and from cells extracted from genetically modified mouse models of heart disease. One of the challenges of using mouse-derived cells is the relatively small numbers of cells that can be extracted (58). This problem is being addressed by constantly refining the process of building 3D engineered cardiac tissues and by minimizing the construct's size (59, 60).

An automated, miniaturized, 24-well assay of engineered heart tissues has been used to study a mouse model of homozygous and heterozygous hypertrophic cardiomyopathy (60). Homozygous Mybpc3-targeted knock-in (KI) mice express different splice variants of cardiac myosin-binding protein C (cMyBP-C) and exhibit a 90% reduction of total cMyBP-C protein levels along with early cardiac hypertrophy, left ventricular dilation, and reduced fractional shortening in young adulthood (61). Heterozygous (Het) mice have only slight reduction in cMyBP-C levels, as well as diastolic dysfunction without hypertrophy and no apparent cardiac phenotype until the age of 18 months (61, 62). Het mice thus represent the mild phenotype of cMyBP-C-associated hypertrophic cardiac myopathy. To engineer fiber-like tissues to study these processes in vitro, cardiomyocytes isolated from these mice were suspended in fibrinogen and 10% Matrigel, mixed briefly with thrombin, and pipetted into rectangular agarose casting molds of $12 \times 3 \times 4$ mm in a 24-well plate. Prior to casting, silicone racks with four pairs of elastic silicone posts each were placed onto the 24-well plate (six racks per plate), such that the posts reached into the casting molds from above. Once the fibrin polymerized, rectangular cell-containing gels formed around the tips of the posts. The racks were then transferred into fresh 24-well plates containing culture medium and maintained in cell culture for up to 4 weeks. Spontaneous contractility of the engineered tissue constructs was recorded over time using a video camera and evaluated automatically by designated software (59). The extracted parameters were frequency, force, and contraction and relaxation times. The same parameters could be evaluated under constant beating conditions with electrical stimulation of the tissues.

These studies revealed that cMyBP-C protein and Mybpc3 mRNA levels were 70% lower in KI and 20% lower in Het compared with WT cells when measured after 20 days in culture. The levels of β-MHC and Myh7 mRNAs were 3- to 4-fold higher in Het and KI than in WT. α-Skeletal actin protein and Acta1 mRNA levels were similarly increased, and sarcoplasmic reticulum Ca^{2+}-ATPase and sodium-calcium exchanger mRNA levels did not differ between the groups. The gene and protein expression data suggest the presence of hypertrophy in KI and Het tissues, with no significant changes in calcium-handling functionality. Engineered tissues composed of KI cells showed abnormal spontaneous activity, with a burst beating pattern. Under electrical stimulation at near-physiological conditions, KI tissues exhibited accelerated kinetics and increased sensitivity to external Ca^{2+}. The relative contractile responses to β-adrenergic agonist, isoprenaline, calcium sensitizer, EMD 57033, and verapamil at maximally effective concentrations were significantly smaller than in WT tissues, likely reflecting the high sensitivity of KI engineered cardiac tissues to external calcium levels. This reasoning was supported by showing the lack of positive inotropic effect of EMD 57033 in KI mice in vivo. The Het engineered constructs were apparently normal under spontaneous conditions but showed increased sensitivity to external Ca^{2+} and relatively lower inotropic responses to isoprenaline and EMD, similar to KI.

The results of this study substantiate the hypothesis that reduced inotropic responses can be mainly attributed to the cMyBP-C mutation altering myofilament function. Other studies have recapitulated and extended previous findings obtained in isolated cardiomyocytes (62, 63), engineered cardiac tissues (64), and intact heart preparations (63) from mice, suggesting that tissues engineered from mouse-derived cells are useful to model inherited diseases, particularly the Mybpc3-related hypertrophic cardiomyopathy phenotype in vitro.

Engineered cardiac tissues built using dry Gelfoam collagen sponges as scaffolds, seeding them with neonatal rat ventricular myocytes in Matrigel (65), and culturing them for 8 or 16 days under static conditions also have been used to model the diabetic myocardium (66). These constructs were cultured under four different conditions: normal glucose without insulin (N), normal glucose with insulin (NI), high glucose without insulin (H), and high glucose with insulin (HI). The results demonstrated diabetes-induced gene expression in H engineered cardiac tissues, similar to that observed in animal models, as well as contractile dysfunction and decreased electrical excitability. Insulin increased cell viability, improved excitability, and normalized gene expression profiles in both NI and HI engineered tissues. Antidiabetic drugs showed antiapoptotic effects, with improvement of electrical excitability in H tissues, but did not rescue gene expression profiles. This study demonstrates the feasibility of using engineered tissue constructs as platforms for screening drugs and studying diabetic cardiomyopathies.

Engineered cardiac tissues also have been used to study ischemia-reperfusion conditions in vitro (65–67) and to compare them to previous results obtained with adult myocardium under hypoxic stress. This approach employed ring-shaped scaffolds in which cells were cultured for 5 days to form tissues and then exposed to cyclic mechanical stretch for 1 week to promote maturation. When the engineered tissues were exposed to ischemic conditions with 1% O_2 for 6 h followed by reoxygenation, they exhibited conduction defects, dephosphorylation of Cx43, and downregulation of cell survival proteins, similar to adult ischemic heart (68). Importantly, these effects also were inhibited by pretreating the engineered tissues with protective agents such as cyclosporine and acetylcholine (68–70).

Most recently, a 3D paper-based model for cardiac ischemia was developed that recapitulates the fibrotic process that occurs in ischemic tissue and provides a mechanistic view of ischemic injury (71). In this model, thin porous sheets of paper are impregnated with ECM gels containing cardiac cells and then stacked to create controlled oxygen and nutrient gradients across the 3D tissue construct; the model also facilitates coculturing of multiple cell types and paracrine signaling between different cell populations. Additional advantages of this new approach include simplicity of system assembly, low cost, compatibility with high throughput, and amenability to rapid data analysis.

In this cells-in-gels-in-paper (CiGiP) approach, which was originally developed to study hypoxia in cancer (72–74), 190-mm-thick chromatography paper was patterned with a wax printer to yield 20 separated circular hydrophilic islands (each 3 mm in diameter) in hydrophobic surroundings; this setup yielded 20 experimental replicates in a single experiment. The islands were seeded with neonatal rat ventricular myocytes suspended in Matrigel and cultured for 3 days. Six paper sheets were prepared identically and were stacked in layers after the 3 culture days to form a tissue-like construct. The stack was then placed in an impermeable Derlin holder to block diffusion of nutrients from the bulk medium to the stack, except for the top layer, which was directly exposed to the medium. The nutrients and oxygen diffused into the stack and were metabolized by the cardiomyocytes, resulting in nutrient depletion and ischemic conditions in the bottom layers of the stack. After 1 week, the layers were unstacked and analyzed separately.

This study demonstrated that cardiomyocytes respond to ischemic conditions by undergoing changes in morphology to become round rather than elongated. Cell viability also decreased and was lowest in the bottom layer. Ischemic conditions promoted the release of signaling molecules

from cardiomyocytes as well. Moreover, when layers of fibroblasts were stacked above the cardiomyocyte layers, fibroblasts migrated toward the ischemic cardiac layers. The severity of the ischemia could be increased by increasing the number of fibroblast layers stacked on top of the heart cells. This produced a further decrease in myocyte viability and an increase in fibroblast migration into the ischemic zone due to secretion of cytokines by the cardiomyocytes. Although this method provides a relatively simple way to study complex cocultures in 3D hypoxic environments, it lacks the ability to measure contractile function, which is a major drawback in developing a reliable heart disease model.

All the techniques presented so far for engineering 3D cardiac tissues involve casting of ECM gels containing cardiomyocytes. These ECM scaffolds are animal derived and may introduce uncontrolled variability to the experiments. The scaffolds generated from different batches or vials of these ECM proteins may vary in structure and mechanical properties due to vial-to-vial variability. To address this limitation, a laser writing technique based on two-photon absorption, termed two-photon-initiated polymerization (TPIP), was used to produce scaffolds with accurately defined composition and micro- and nanoscale features (75). In this technique, photoresists can be cured only near the laser focal volume, which enables fabrication of 3D structures with spatial resolution down to 100 nm (76). This technique was used to create a cardiac tissue model containing 3D filamentous matrices consisting of synthetic parallel fibers with tunable spacing and diameter. The fabricated filamentous scaffolding controlled the mechanical microenvironment and dictated the structural alignment of the cardiomyocytes cultured within it. The scaffolds were populated with human cardiomyocytes derived from iPSCs from healthy individuals and patients with type 3 LQT (LQT3) syndrome. The disease-specific 3D human cardiac tissues were evaluated by measuring gene expression, structure, electrophysiology, and contractility by using motion-tracking analysis of bright-field microscopy video recordings. Quantitative reverse transcriptase polymerase chain reaction (RT-qPCR) analysis showed upregulation of cardiac-specific genes, and beating was observed 3 days after seeding. The cells were optimally packed and aligned along the filamentous scaffold when the fibers were spaced 50 mm apart.

Tissues engineered with cells from LQT3 syndrome patients exhibited prolonged QT intervals and abnormalities in contractility compared with those generated with cells from healthy heart tissues, but only when the filament diameter was 5 mm. The model was validated by recapitulating known responses of LQT3 tissues to caffeine, nifedipine, and propranolol. LQT3 tissues also were more susceptible to propranolol-induced cardiotoxicity when grown on filamentous matrices with low fiber stiffness. This study demonstrates the advantages of building reproducible, accurately controlled scaffolds for 3D cardiac tissue engineering, but it also reveals the high sensitivity of these tissues to microscale geometrical cues. The WT and LQT3 tissues differed in contractility only when seeded on specific scaffold configurations, demonstrating the immense importance of scaffold fine-tuning and engineering-system optimization.

Engineered Heart Valve Models

Tissue engineering has been used to model diseases of the heart valve in vitro. Cardiac valves exhibit pronounced structure-function relationships, and valvular heart disease (VHD) can result from abnormal valve leaflet number, thickness, rigidity, composition, and/or organization (77–79). Valve leaflets are thin, multilayer tissues containing valvular interstitial cells (VICs), which are associated with remodeling and repair (80), and valvular endothelial cells (VECs), which coat the leaflet surfaces. VIC dysregulation can lead to valve fibrosis and calcification that progress to sclerosis and stenosis (81, 82). VECs also modulate VIC fate, undergo endothelial-mesenchymal transformation, and likely replenish VIC populations (83).

Traditionally viewed as wear-and-tear phenomena, valve fibrosis and calcification are now recognized to be actively regulated, but they are rarely diagnosed at early stages of disease progression (81, 84). Although congenital defects are increasingly diagnosed (85), early detection and nonsurgical treatment of progressive VHD require clarification of the cellular and molecular mechanisms underlying disease progression and improvements in the use of noninvasive imaging modalities (86, 87). Thus, there is a need for good in vitro VHD models.

Emerging in vitro VHD platforms mimic key aspects of the native valve environment in miniaturized and arrayed formats amenable to high-throughput screening. These include the use of hydrogel-based culture substrates to mimic valve tissue stiffness (88–91), trilaminar leaflet structure (92), and 3D valve morphology (93, 94). Because native cardiac valves operate within mechanically and hemodynamically demanding environments (84), in vitro VHD models increasingly incorporate fluid flow (95, 96) and mechanically active culture capabilities (97–99) that are lacking in traditional cell culture platforms.

To screen the combined effects of soluble cues, ECM composition, and dynamic mechanical deformation on small VIC populations isolated from distinct layers of the aortic valve leaflet, a cell culture chamber array was constructed with integrated mechanical actuation capabilities (99). The platform consisted of 12 segregated groups of 9 circular suspended films, a setup that permitted 12 combinations of matrix proteins, chemical cues, and cell types to be simultaneously probed on a device measuring 7.5 × 5 cm. VICs cultured on the films experienced radial and circumferential strains when the films were distended by the application of pressure via a network of underlying microchannels. VICs isolated from distinct valve layers (fibrosa versus ventricularis) exhibited myofibroblast-specific expression of SMA stress fibers as a function of mechanical loading and ECM protein coatings, either with or without the addition of transforming growth factor β1 (TGF-β1). Increased levels of myofibroblast differentiation were observed in cells from the ventricularis over cells from the fibrosa for all culture conditions, and fibrosa VICs demonstrated increased myofibroblast differentiation on fibronectin compared with collagen substrates. On collagen, fibrosa cells exhibited an increase in myofibroblast differentiation only at high strain levels; however, this increase also was observed at low strains if TGF-β1 was added simultaneously. These experiments provided novel insights into the relationships between soluble (TGF-β1) and nonsoluble (e.g., cell source and ECM composition) factors affecting valvular fibrosis. By allowing investigators to independently vary these factors in a small form-factor platform and to use small quantities of primary VICs, this work reaffirmed the advantages of microfabricated in vitro VHD models.

To examine VEC modulation of VIC activation within a physiologically relevant valve tissue architecture, a bilayer membrane microfluidic device was built that incorporated two microfluidic channels (upper "luminal" and lower "mural" channels) separated by a porous membrane, permitting heterotypic cell interactions between cells cultured in the different microcompartments while allowing passage of macromolecules and extravasation of cells (96). In the bottom channel, VICs were embedded in a 3D photopolymerizable gelatin-based hydrogel (gelatin methacrylate). VEC monolayers were cultured in the top channel, either under static conditions or under steady flow-induced shear stress (20 dyn/cm^2) for 24 h. The presence of endothelial cells significantly suppressed pathological differentiation of VICs into α-SMA-positive myofibroblasts, and this effect was enhanced when the endothelium was exposed to flow-induced shear stress.

These in vitro methods permit direct observations of VEC effects on pathological differentiation of VICs that cannot be done in vivo due to difficulties in arresting fluid flow and removing VECs from native valves. Future iterations of these platforms would benefit from the addition of pulsatile fluid flow conditions and, for some applications, improved mimicry of valve geometry. Future VHD platforms that mimic valve geometry may ultimately bridge the gap between flow duplicators and on-chip platforms, but valve scaling laws must be established to achieve this aim

(100, 101). Importantly, microphysiological platforms are also ideally suited to support toxicology screening and the nascent field of VHD induced by drugs [e.g., ergot derivatives, fenfluramine-phentermine (fen-phen)-based appetite suppressants, 5-hydroxytryptamine].

LUNG

Asthma

Asthma is a complex, multifactorial disease of the airways with genetic and environmental components that involves airway remodeling (e.g., increased hyperplasia of goblet cells, smooth muscle cells, fibroblast cells, and capillary endothelial cells), bronchoconstriction (due to smooth muscle hyperresponsiveness and mucus obstruction), increased inflammation (including edema and induction of cytokines and chemokines), and enhanced immune responses (abundant Th2 cytokines, IgG and IgE secretion, mast cells, eosinophils, T cells) (102). Because of its multifactorial nature and complexity, it has been possible to model only some components of the disease. The most complete models of asthma are animal models, such as mice, rats, cats, dogs, pigs, horses, and primates. Although other animal models of asthma exist, most use mice that do not spontaneously develop the disease (103) and that must be sensitized with ovalbumin and locally challenged with allergens or other stimuli. Most importantly, although promising antiasthmatic drugs have been discovered using mouse models (e.g., IL-5, IL-4, VLA4, and PAF antagonists), ongoing clinical trials have been so far disappointing (104–109). Thus, there is a great need for models of asthma in humans.

To overcome the limitations of animal models, ex vivo and in vitro models of asthma have been developed using tissue explants and cultured human cells, respectively. Whereas many different types of cells (e.g., airway epithelial and smooth muscle cells, fibroblasts, endothelial cells, immune cells) and ECM are involved in asthma pathogenesis, these simplified models generally permit analysis of the contribution of only one of these components at a time (110–115). Given the central role that the airway epithelium plays in the pathogenesis of asthma (102), there have been recent efforts to engineer human airway epithelium (HAE) in vitro. The complexity of these models ranges from a simple monolayer of airway cells to physiologically relevant, 3D airway structures lined by several cell types (116). Most of these models use the Transwell technology, which is composed of a two-compartment culture well separated by a rigid, ECM-coated, semipermeable membrane that supports the growth of cells or excised explants on one or both sides of the membrane (117). Using Transwell inserts, human primary airway epithelial cells have been cultured and differentiated at the air-liquid interface with the addition of retinoic acid to suppress the squamous phenotype (118). Following differentiation, a pseudostratified mucociliary airway epithelium is formed, recapitulating normal in vivo morphology (118). Fully differentiated cultures of HAE cells grown in Transwell inserts have been used to study the role of the airway epithelium in asthma pathogenesis. HAE cultures derived from patients with asthma exhibit higher numbers of mucus-producing cells and fewer ciliated cells than HAE cultures derived from healthy donors (115). Moreover, IL-13-induced goblet cell hyperplasia and mucus hypersecretion, critical hallmarks of allergic asthma, have been reproduced in HAE cultures (119).

Human fetal lung fibroblasts have also been grown in a type I collagen matrix in a Transwell device while HAE cells that differentiate, form beating cilia, and produce mucus were cultured on top of the matrix (120). ECM remodeling can be demonstrated over time in this system, which could be useful to study asthma-associated matrix remodeling (121). In addition, ECM gels have been used to develop a model of matrix stiffness–induced fibroblast differentiation, which could be used to analyze how ECM reorganization affects differentiation of cells in the airway wall, a central hallmark of asthma (122).

Most recently, tissue engineering approaches have been used to develop better models of airway physiology. A model of the human bronchiole was engineered to study cell-cell interactions and remodeling by coculturing in a bioreactor system (cylindrical-shaped bronchioles constructed from human lung primary cells, lung fibroblasts, airway smooth muscle cells, and ECM) (123). Because of the cylindrical geometry of the engineered bronchiole, the tissue applies radial tension, inducing mechanotransduction, and the air pumping through the lumen provides a natural environment for the epithelial cells. This engineered model of the bronchiole can be used to investigate individual components of airway remodeling such as subepithelial fibrosis, smooth muscle hyperplasia and hypertrophy, and epithelial cell metaplasia.

Chronic Obstructive Pulmonary Disease

Chronic obstructive pulmonary disease (COPD) is a progressive and chronic lung disorder characterized by chronic bronchitis, which predominantly affects small airways (conducting airways with diameter <2 mm), and emphysema, which causes gradual destruction of alveolar walls (124). To date, there are no validated in vitro models of COPD (125). The best-established in vitro model of COPD uses cultured HAE cells derived from COPD patients (or healthy donors), which are differentiated at an air-liquid interface in Transwell inserts. These systems are generally used to mechanistically address how and why COPD develops. For example, similar to the situation in asthma, goblet cell hyperplasia and mucus hypersecretion are two of the characteristic features of COPD epithelial lining in vivo (126). Goblet cell hyperplasia can be induced by exposing HAE cells in Transwells to cigarette smoke total particulate matter (127). The effect of cigarette smoke on the conducting airways, which can exacerbate COPD, also can be mimicked by exposing the cultures directly to smoke or cigarette smoke extract (128). In fact, addition of smoke extract attenuates inflammatory responses to endotoxin in HAE cells derived from COPD patients, but not in similar cells from nonsmoking individuals (129). Squamous cell metaplasia, another hallmark of COPD, can be modeled in HAE cells by simply omitting retinoic acid from the culture medium (130). HAE cells have been cocultured with monocytes, which results in synergistic augmentation of CXCL10 and CCL2 secretion following rhinovirus infection (131). Coculture of HAE cells and fibroblasts from COPD patients showed that inducing squamous metaplasia resulted in IL-1β secretion, leading to a fibrotic response in the airway fibroblasts (132). This work led to identification of a pivotal role for TGF-β in squamous metaplasia and fibrosis, two key features of COPD.

Lung Granulomas

Granulomas are aggregates of organized chronic inflammatory reactions predominantly composed of macrophages and/or lymphocytes. Macrophages in granulomas are often described as epithelioid cells and the granulomas as epithelioid granulomas (133). The lungs, along with the skin and lymph nodes, are the most common sites of granuloma formation (133). The etiology of the granuloma has been attributed to persistent infectious irritants (e.g., mycobacteria, fungi) and noninfectious agents that are not cleared or killed by acute inflammatory reactions. Granulomas can be immunogenic or nonimmune, foreign-body granulomas. Various 2D models of immune-mediated granulomas have been developed in which macrophages are exposed to pathogens (134, 135) and pathogen-coated beads (136); however, a 3D in vitro model of foreign-body granulomas has also been created using biopersistent nanomaterials as inducers (137). In this study, granuloma formation was induced in murine macrophages cultured in agarose gels by adding high-aspect-ratio nanomaterials, such as carbon nanotubes. Carbon black particles (Printex 90) and crocidolite

asbestos fibers were used as negative and positive controls, respectively, for granuloma generation. Three different high-molecular-weight carbon nanotubes induced macrophage activation, TNF-α and IL-1β expression, and granuloma formation. One major limitation of the model was that macrophages were used in a static culture, whereas in vivo macrophages and monocytes are dynamically recruited from the circulation or neighboring interstitial tissue, a process that may be important for aggregate formation and subsequent inflammatory responses.

Pneumonia

Pneumonia is an acute inflammation of the lung induced by microbial infection of the alveoli. Recently, a microfluidic human breathing lung-on-a-chip was developed to meet the challenge of mimicking the physiologically relevant tissue-tissue interfaces, physicochemical microenvironments, and vascular perfusion that are necessary to recapitulate organ-level physiology of the lung, as well as inflammation due to lung infection, in vitro (138). Organs-on-chips are cell culture devices created with microchip manufacturing methods that contain hollow, micrometer-sized chambers inhabited by living cells. The lung-on-a-chip contains a lower capillary channel separated from an upper air-filled alveolar channel by an intervening porous ECM-coated membrane that has human lung alveolar epithelial cells cultured on its top surface and pulmonary capillary endothelial cells cultured on its bottom to recreate the alveolar-capillary interface of the living lung (**Figure 2**) (138). These two microchannels are lined along each side by full-height hollow chambers through which cyclic suction is rhythmically applied; this distorts the central porous membrane and results in the application of cyclic mechanical strain (10%; 0.25 Hz) that mimics the forces living cells experience in the alveolus due to breathing motions. By generating an air-liquid interface in the alveolar channel, flowing fluid through the vascular channel, and applying cyclic mechanical distortion, it is possible to greatly enhance the differentiation of the established human alveolar epithelial (NCI-H441) and lung microvascular endothelial cell lines that line the microchannels, as demonstrated by increased surfactant production and enhanced vascular barrier function (measured by both quantitating transepithelial electrical resistance and assessing macromolecular transport). Importantly, this microengineered device also permits one to flow primary human neutrophils through the vascular channel, which do not bind to the quiescent endothelium under baseline conditions. When inflammation is simulated by adding either TNF-α or living bacteria to the upper channel, the endothelium rapidly becomes activated, as indicated by a rapid increase in expression of cell surface ICAM-1 and active recruitment of human neutrophils perfused through the microvascular channel. Interestingly, because this engineered organ-on-a-chip device permits the use of real-time, high-resolution microscopy, the immune cells that bind the endothelium can be observed to undergo diapedesis and migrate through both cell layers to the upper chamber, where they actively engulf the living bacteria on-chip.

Importantly, the use of this human lung-on-a-chip led to new mechanistic insights into how mechanical breathing motions contribute to lung function and disease. For example, when silica nanoparticle simulants of environmental airborne particulates that can induce lung inflammation and injury were introduced into the upper channel, breathing motions were found to be critical for production of reactive oxygen species, cellular uptake of nanoparticles, and transport of nanoparticles across both cell layers and into the vascular channel. Moreover, the dependence of nanoparticle absorption on breathing motions was confirmed using a mouse ex vivo ventilation-perfusion model (138), demonstrating the power of the organ-on-a-chip approach. Thus, this ability to recreate a physiologically relevant mechanical microenvironment simultaneously involving flow and cyclic strain is a key aspect of this engineered model that cannot be easily incorporated in 2D cell culture models.
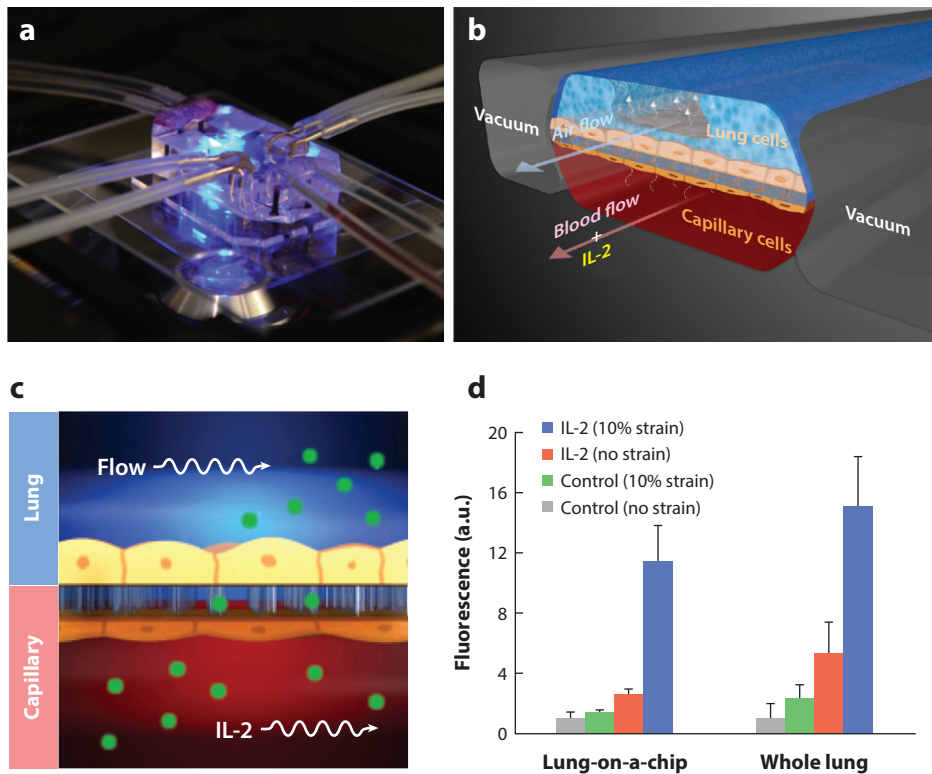
Figure 2

Recapitulating human lung pathophysiology in vitro. (*a*) Human lung-on-a-chip: a photograph of the polydimethylsiloxane lung-on-a-chip microfluidic device placed on a microscope stage. (*b*) On-chip pulmonary edema model: a diagram of the microfluidic lung-on-a-chip design and how it was modified to create an in vitro model of human pulmonary edema. This device recapitulates the alveolar-capillary interface by culturing human alveolar epithelial cells on top of a flexible, porous, extracellular matrix–coated membrane and human capillary cells on the bottom; air is passed through the upper (alveolar epithelium) channel while culture medium is flowed through the lower (vascular) channel. Breathing motions are mimicked by applying cyclic suction to the side channels, which rhythmically deform and relax the flexible polydimethylsiloxane side walls and the porous membrane to which the cell layers are attached. To create an on-chip model of human pulmonary edema, IL-2 was infused into the vascular channel, which resulted in a shift of fluid into the air space, as observed in human patients. (*c*) Measuring vascular leakage: a diagram showing how pulmonary vascular leakage was measured on-chip by quantifying the passage of fluorescent inulin (*green circles*) from the lower to the upper channels in the presence of IL-2. (*d*) Chip results mimic whole lung: a graph showing the increase in fluorescent inulin leakage into the airspace measured on-chip compared with that measured in whole mouse lung in the absence (control) or presence of IL-2, with (10% strain) or without (no strain) mechanical breathing motions. IL-2 induced much greater vascular leakage in the presence of physiological breathing motions both on-chip and in vivo. Figure modified with permission from References 138 and 139.

Pulmonary Edema

The same human lung-on-a-chip microfluidic device was used to create a model of pulmonary edema (**Figure 2**) (139). To do this, the cancer drug IL-2 was perfused through the vascular channel, as it has been reported to produce pulmonary vascular permeability and lung edema as its major dose-limiting side effect. Administration of IL-2 at the same dose used in patients resulted in fluid

permeation into the air channel, blood clot formation in the air space, and associated compromise of oxygen transport, and this occurred over the same time course (2–4 days) observed in humans. In addition, this study revealed that physiological breathing motions also contribute to the development of increased vascular leakage induced by IL-2 (e.g., as measured by increases in gaps within both endothelial and epithelial monolayers and decreased barrier function), and that circulating immune cells are not required for the development of this form of pulmonary edema. Once again, these effects of breathing motions observed on-chip were experimentally confirmed in an animal model (**Figure 2**), thus demonstrating the power of the organ-on-a-chip approach for human disease modeling. Importantly, the potential clinical value of this disease model was reinforced by showing that it could be used to identify a new therapeutic (TRPV4 inhibitor, GSK2193874) that suppresses IL-2-induced pulmonary edema on-chip; this compound also suppressed cardiogenic pulmonary edema in dogs and rabbits, as shown in a sister publication (139).

INTESTINE

Inflammatory Bowel Disease

Crohn's disease and ulcerative colitis are forms of inflammatory bowel disease (IBD) that involve chronic inflammation of the human intestine and result in mucosal injury with villus destruction (140). The etiology of these diseases is thought to involve complex interactions between gut microbes, intestinal mucosa, immune components, and wall peristalsis (141). However, due to the complexity of animal models, it is not possible to study the independent contributions of these different potential contributing factors.

Existing in vitro models of human IBD rely on culturing an intestinal epithelial cell monolayer in a static Transwell culture (142–148) and then adding microbes and immune cells to the apical and basolateral side of the culture well, respectively. Because intestinal cells cultured in Transwell plates often fail to produce mucus (e.g., Caco-2 cells) or undergo differentiation of intestinal villi that become injured in IBD, these models do not effectively recapitulate the pathophysiology of this disease in living intestine. Recently developed 3D organoid cultures (149–151) produce higher levels of intestinal differentiation; however, the cells in organoids also do not experience physiological peristalsis-like motions and cannot be cultured with a living microbiome under these static conditions because bacterial overgrowth will result in death of the epithelium (152). This is a critical limitation, because the resident gut microbiome is a crucial contributor to early IBD progression (153) and because mechanical deformations resulting from peristalsis both influence normal epithelial cell differentiation (154) and restrain microbial overgrowth in vivo (155, 156).

To confront these limitations, the lung-on-a-chip device was modified to create a human gut-on-a-chip lined by human intestinal epithelial (Caco-2) cells (**Figure 3a,b**). This is an established cell line, originally derived from an intestinal tumor, that is poorly differentiated when cultured in standard static cultures. When the same Caco-2 cells are exposed to trickling flow analogous to that experienced in the gut lumen and cyclic mechanical distortion that mimics peristalsis-like motions of the living intestine in the gut-on-a-chip microfluidic device, they spontaneously reorganize into 3D intestinal villi lined by columnar epithelial cells (**Figure 3c**) (152, 157). These villi closely mimic the architecture of the small intestine and exhibit multiple differentiated features, including reestablishment of basal proliferative cell crypts, differentiation of all four cell types of the small intestine (absorptive, mucus-secretory, enteroendocrine, and Paneth), production of high levels of mucus, and creation of a much higher resistance epithelial barrier. Thus, this system is well designed to study the etiology and mechanisms underlying intestinal diseases, such as IBD; however, these phenomena remain largely unexplored.
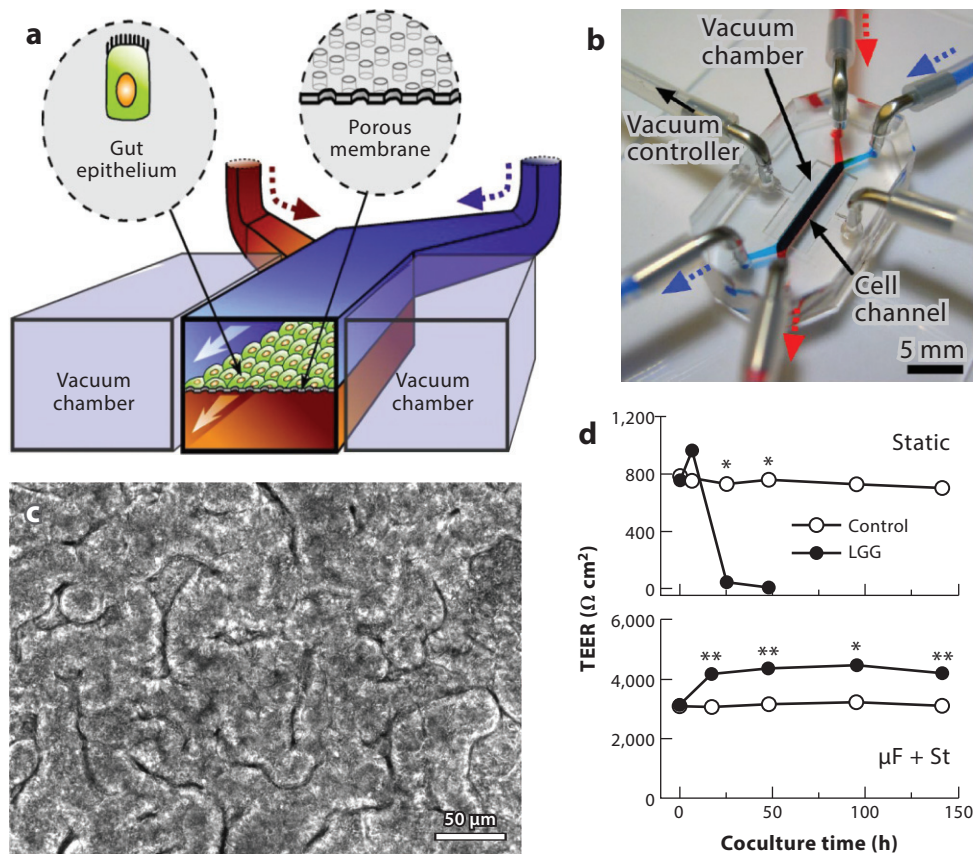
Figure 3

Human gut-on-a-chip. (*a*) A schematic of the gut-on-a-chip device, which is similar in design to the lung-on-a-chip. In this case, the flexible porous extracellular matrix–coated membrane in the central microfluidic channel is lined by human intestinal epithelial cells, which are exposed to trickling flow and peristalsis-like cyclic mechanical deformation by using a controlled vacuum in the side channels. (*b*) A photograph of the gut-on-a-chip microdevice, made of optically clear silicone polymer (polydimethylsiloxane). Blue and red dyes indicate the upper and lower microchannels, respectively, to allow visualization of the flow of culture medium. (*c*) A phase contrast image of human Caco-2 intestinal cells that undergo spontaneous villus morphogenesis after 100 h (shear stress of 0.02 dyn/cm^2; 10% cyclic strain at 0.15 Hz). (*d*) Graphs of transepithelial electrical resistance (TEER) measurements in a Caco-2 monolayer in a static Transwell culture (*top*) compared with those in the microfluidic gut-on-a-chip with cyclic mechanical strain (μF + St) measured over time in the absence (control) or presence (LGG) of the probiotic bacterium *Lactobacillus rhamnosus* GG (LGG). In the static culture, intestinal barrier function was rapidly compromised, whereas the presence of this naturally occurring microbe increased epithelial barrier integrity on-chip. A single asterisk denotes $p < 0.01$; a double asterisk denotes $p < 0.05$. Figure modified with permission from References 152 and 157.

Contributions of the Microbiome

The human body harbors a stunningly diverse array of microbial species (500–1,000 species) and a tremendous number of microbial cells (10 times more than the number of human cells in the body) and genes (100 times more than the number of genes in the human genome) (158, 159). In the intestine, these microbes play essential roles in metabolizing nutrients and xenobiotics (i.e., drugs,

chemical compounds), regulating immune responses, and maintaining gut homeostasis (160), and not surprisingly given these diverse functions, intestinal microbes contribute significantly to human health and disease. Thus, controlling host-microbe interactions in engineered disease models is extremely important.

Investigators have used Transwell systems (142–148, 161, 162), 3D culture models with cell-coated microbeads (163–171), hydrogel-based organoids (150, 151, 172–176), and the microfluidic gut-on-a-chip device (14, 152, 157, 177) to recreate the host-microbe ecosystem in vitro. Static Transwell cultures commonly utilize established intestinal cell lines, such as Caco-2 or HT-29 cells (161), in short-term (<24 h) cultures with live probiotic gut microbes or pathogenic bacteria. For example, some of the pathological features of celiac disease were recapitulated in a Transwell culture by exposing the Caco-2 cell monolayer to known triggers of this disease (e.g., gluten-derived gliadin peptides and gram-positive or -negative bacteria on the apical side; blood mononuclear cells on the basolateral side) (162). In this study, inflammatory responses (e.g., production of the proinflammatory cytokines IL-12 and IFN-γ) induced by gliadin were suppressed by the addition of probiotic strains of bacteria (e.g., *Bifidobacterium* spp.), whereas they were increased by the addition of opportunistic or pathogenic gram-negative bacteria (e.g., *Bacteroides fragilis*, *Escherichia coli*, and *Shigella* spp.). These findings suggest that interactions between gut bacteria, epithelial cells, and immune cells play a key role in celiac disease progression.

Transwell intestinal cell cultures also have been used to model infectious pathogenesis by enterovirulent bacteria (145) and chronic inflammation (142–144), as well as immunomodulatory (146, 148) and anti-inflammatory effects (147) of host-probiotic interactions. However, because Transwell cultures are static, these studies are commonly limited to less than 1 day in duration due to bacterial overgrowth, and the absence of peristalsis-like motions and fluid flow brings the physiological relevance into question given that these mechanical motions are known to contribute to control of microbial overgrowth in the living intestine (e.g., cessation of peristalsis leads to ileus) (178–180).

To conserve the histological architecture of human tissues during host-microbe interactions, ex vivo models have been developed in which human tissue sections from clinical biopsies are maintained in culture. For example, to model an intestinal infection, a human intestinal tissue biopsy specimen was mounted on a modified Transwell-like porous insert, and a circular disk was glued on its apical surface to provide a leakage-free space for the introduction of enteropathogenic *E. coli*. Colonization of the tissue section by these bacteria resulted in an increased innate immune response, including rises in the levels of IL-8 and induction of Toll-like receptor 5 (181). The protective effects of probiotic *Lactobacillus* strains also were demonstrated against invasion by a pathogenic *Salmonella* strain using intestinal tissue biopsy samples from healthy or IBD patient donors (182). In addition, the mechanism of enterohemorrhagic *E. coli* invasion under anaerobic or oxygenated conditions was studied by embedding a polarized intestinal epithelium in a modified Ussing chamber (183). Although these ex vivo intestinal tissue models provide a more in vivo–like microenvironment than conventional Transwell cultures, they require high levels of oxygenation due to the lack of vasculature, they are limited by the availability and variability of clinical biopsy specimens, and they permit analysis only of short-term interactions between intestinal epithelium and pathogenic bacteria in the absence of any peristalsis-associated mechanical cues.

Some researchers have attempted to integrate the microbiome into 3D cultures by using microbead-based rotation chambers (termed microgravity cultures) or organoids. The microgravity cultures use a rotating vessel bioreactor containing multiple ECM-coated porous microbeads lined by human epithelial cells cultured in medium with a central gas-exchange port. In contrast to other in vitro models, cells on the surface of individual 3D microbeads experience low levels of shear stress, because this bioreactor is continuously rotating at a defined speed, and this property

apparently results in increased cell differentiation (163). This approach has been used in a model of norovirus infection, which causes diarrheal diseases in humans. 3D cultures of human embryonic intestinal epithelial INT-407 cells (169) or Caco-2 human intestinal cells (171) have demonstrated cytopathic effects (e.g., loss of apical microvilli, vacuolization) as well as evidence of virus replication; however, there were concerns regarding the reproducibility of viral infection and replication (170). In other studies, 3D microbead cultures of human HT-29 colon cells (164) or embryonic intestinal epithelial INT-407 cells (166) were used to study *Salmonella enterica* serovar Typhimurium pathogenesis. The *Salmonella* cells exhibited decreased pathogenicity and lower levels of basal and infection-induced cytokine secretion when cultured with intestinal cells on the 3D microbeads than when cultured with cells in the conventional monolayer cultures. Using bioreactors, it may be possible to prevent outgrowth of microbes in host-microbe cocultures by maintaining continuous flow in the system, although this has not yet been demonstrated experimentally. However, despite the flexibility of growing host cells and applying various microbial species in rotation cultures, microbead cultures do not permit analysis of other key contributing factors, such as immune cells recruited from lamina propria or cytokine release from the basolateral surface of the epithelium.

Whereas the rotation cultures use microbeads as culture substrates, 3D organoid cultures leverage ECM or synthetic polymer hydrogels as scaffolds to support the growth and differentiation of human intestinal tissues derived from iPSCs (149–151) or disease-specific tissue biopsies (176). Rotavirus infection (172) and host-parasite interactions (174) have been reported using organoids, but the difficulty in introducing pathogens into the lumen of these closed structures and in preventing rapid microbial overgrowth severely limits the utility of this model system. It is also difficult to introduce immune cells into these models, and again, they lack the normal mechanical cues that play a key role in the regulation of intestinal development and physiology.

Microfluidic culture devices provide a way to circumvent these limitations. For example, because human intestinal cells produce mucus and experience continuous fluid flow in the human gut-on-a-chip microdevice (152, 157), it is possible to coculture them with a living microbiome. Specifically, when probiotic normal gut flora (e.g., *Lactobacillus rhamnosus* GG) was introduced in the upper channel (intestinal lumen) of the human gut-on-a-chip, they successfully colonized the villus microenvironment and showed health-promoting activities, such as increased barrier function (**Figure 3d**) (152). Because the continuous fluid flow of fresh culture medium constantly supplies nutrients and removes unbound residual bacterial cells as well as metabolic wastes in these microfluidic devices, this steady-state chemical microenvironment helps to establish a stable coculture condition in vitro (184). Thus, the gut-on-a-chip could be used to study how the microbiome contributes to intestinal diseases, such as IBD or infection with pathogenic microbes. However, challenges remain, including the need to establish robust control over aerobic and anaerobic conditions, which perhaps can be met by engineering devices that create a defined oxygen gradient (185).

LIVER

Although in vitro models of liver function have a long history in <u>a</u>dsorption, <u>d</u>istribution, <u>m</u>etabolism, <u>e</u>limination, and <u>t</u>oxicity (ADMET) and pharmacokinetics studies of drugs, there are fewer models of liver disease. To model disease in a meaningful way, it is necessary to achieve high in vivo–like functionality. Thus, it is important to consider that many liver metabolic disorders, as well as hepatotoxicity, are dependent on interactions between hepatocytes and other nonparenchymal cells of the liver or ECM. It is also important to recapitulate vascular perfusion as in vitro studies with hepatocytes cultured in bioreactors and miniaturized microfluidic systems have been shown to increase cell viability and to upregulate the expression of liver-specific differentiated cell functions (186). Here, we summarize in vitro models that have been developed to

study infectious liver diseases and inherited metabolic liver disorders; a discussion of liver cancer models can be found in the Cancer section.

Infectious Liver Diseases

Infectious hepatitis C virus (HCV) virions have been generated in a radial flow bioreactor lined by hepatoma-derived FLC4 cells, whereas this could not be accomplished in monolayer cultures (187). Human hepatoma Huh7 cells were permissive for HCV infection and acquired a more differentiated hepatocyte-like phenotype when cultured in a 3D rotation wall vessel bioreactor compared with a monolayer culture (168). A PDMS-based microfluidic system also supported viral transduction of rat hepatocytes and human HepG2 hepatoblastoma cells in vitro (188). However, it is necessary to maintain long-term stability of differentiated liver functions at physiologically relevant levels to support a persistent HCV infection, which has not yet been possible with bioreactor models. In the future, it also might be possible to study patient-specific aspects of HCV infection, as iPSC-derived hepatocyte-like cells can support the entire viral life cycle (189).

To meet this challenge, a multiwell system was fabricated in which microislands of hepatocytes are surrounded by supportive stromal cells (3T3 rat fibroblasts) (190). The micropatterning method is performed by applying a PDMS stencil in conventional 24- or 96-well plates to deposit microdomains of collagen. Hepatocytes selectively adhere to the collagen, and in a second step, fibroblasts are seeded to surround these domains. The micropatterns maintain essential hepatocytic functions, such as high albumin expression and cytochrome P-450 activities, for several weeks. This coculture microsystem also supported persistent HCV replication for more than 12 days and led to the generation of infectious virions, which cannot be achieved with conventional hepatocyte cultures (191). More recently, this micropatterned hepatocyte coculture system was shown to support the stages of liver infection by the malaria parasites *Plasmodium falciparum* and *Plasmodium vivax* (192). As this model of liver infection appears to be robust, it should aid in the development of therapeutics and vaccines against *Plasmodium* infections, because reproduction within hepatocytes is an indispensable stage in the pathogen life cycle and occurs at the very beginning of infection, making it an especially attractive target. Microengineered in vitro liver systems such as these that support long-term differentiated function could potentially be used to model other types of liver diseases, such as hepatic steatosis (fatty liver disease) induced by alcohol or metabolic disease. More refined models with increasing levels of complexity could be developed to mimic the inflammatory responses, oxidative stress, apoptosis, and fibrosis that often accompany these diseases.

Inherited Metabolic Liver Disorders

It may be possible to model inheritable metabolic disorders affecting the liver, as well as to evaluate patient-specific disease mechanisms, by incorporating primary patient-derived cells or iPSCs into these engineered liver models. Differentiation protocols have been developed that specify iPSCs along the endoderm lineage to become cells displaying bona fide hepatocyte features, including apolipoprotein B, albumin, and urea secretion as well as low-density lipoprotein uptake, glycogen storage, and functional bile transport (193). There are very few reports of iPSC-derived nonparenchymal liver cells, but protocols have been developed that generate bipotential progenitors that differentiate into cholangiocytes and hepatocytes (194, 195).

Models of liver disease that incorporate iPSC-derived cells have primarily focused on monogenetic metabolic disorders, which, although rare individually, account for 15% to 20% of liver

transplantation indications in children (196). Phenotypes of liver diseases that have been modeled with iPSC technology include progressive familial hereditary cholestasis, α_1-antitrypsin deficiency, glycogen storage disease type 1α, familial hypercholesterolemia, hereditary tyrosinemia, and Crigler–Najjar syndrome (197–199). These reports evaluated effects on relevant functions in differentiated hepatocyte-like cells in static monolayer cultures, and they could recapitulate characteristic molecular alterations of these major disease phenotypes. However, to perform deeper studies of disease mechanisms and evaluate treatment strategies, hepatocyte differentiation must be maintained at in vivo–like levels in long-term cultures, which cannot be achieved in these monolayer cultures. Hence, this is an area where engineered models could have a major impact in the future.

KIDNEY

Drug-Induced Nephrotoxicity

Although the kidney is a major site of organ damage caused by drug toxicity, few engineered human kidney models have been developed that recapitulate responses to toxic drugs in vitro. Recently, a microfluidic kidney-on-a-chip device was developed that is lined by living primary human kidney proximal tubule epithelial cells and exposed to fluid flow with a low level of shear stress (0.2 dyn/cm^2) that mimics the conditions observed in the living kidney proximal tubule (**Figure 4***a*) (200). This microfluidic device contains a "luminal" flow channel separated from an "interstitial" compartment by an ECM-coated porous membrane upon which the kidney cells are cultured. By effectively recapitulating the tubulointerstitial interface of the kidney proximal tubule, the device permits real-time analysis of transepithelial transport. Studies with this microfluidic device revealed that exposure of the human kidney proximal tubular cells to physiological fluid flow resulted in enhanced differentiation, as evidenced by increased primary cilium formation, alkaline phosphatase activity, albumin transport, glucose reabsorption, and Pgp transport function compared with cells in static Transwell culture. Importantly, under these conditions, the human kidney cells exhibited toxicity responses to the anticancer drug cisplatin that could be completely prevented by inhibiting human organic cation transporter 2 (OCT-2), a major contributor to cisplatin toxicity in humans (201). In contrast, although cisplatin induced injury in cells in Transwell culture, these responses were nonspecific and could not be suppressed by inhibiting OCT-2. Moreover, the proximal tubular cells recovered more effectively after the removal of cisplatin when exposed to continuous fluid flow compared with cells under static conditions, which also mimics the effects of clinical interventions that involve excessive hydration in humans (202–204).

Polycystic Kidney Disease

Human polycystic kidney disease (PKD) has been modeled using 3D cultures in which primary kidney epithelial cells isolated from cysts of autosomal dominant PKD (ADPKD) patients are cultured in type I collagen gels (205–208). This facilitates the formation of cysts and induces kidney-specific gene expression and cell functions in vitro. In one recent study, the cellular responses to the Na^+/K^+-ATPase inhibitor ouabain were compared in epithelial cells isolated from normal human kidney and from cysts from ADPKD patients, cultured in a 3D collagen matrix (**Figure 4***b*) (208). Ouabain is a steroid hormone synthesized by the adrenal glands that stimulates fluid secretion and induces cystic cell proliferation, two fundamental features of cyst development. These studies revealed that, when added at a physiological level, ouabain has synergetic effects on cAMP-mediated fluid secretion and cyst growth via activation of the EGFR-Src-MEK pathway in ADPKD cells and that this contributes to the overall expansion of renal cysts.
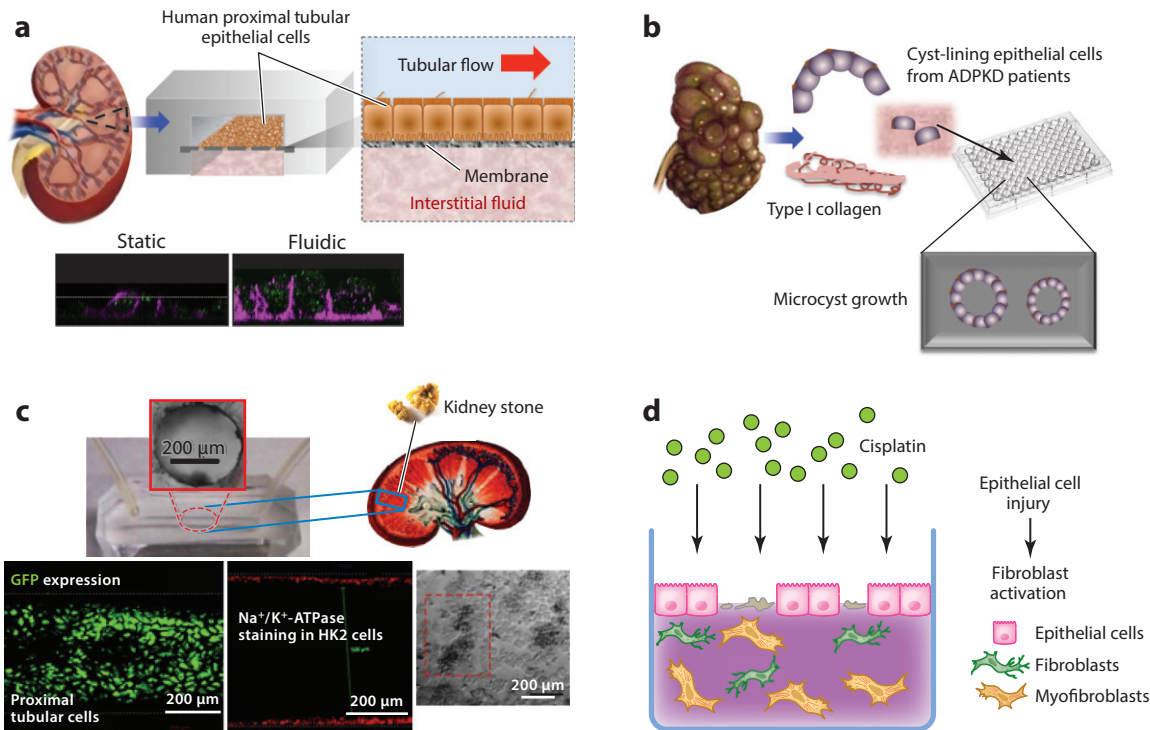
Figure 4

Engineered kidney disease models. (*a*) Drug-induced nephrotoxicity demonstrated in a human kidney-on-a-chip consisting of a microfluidic device with an upper channel (tubular lumen) separated from a bottom reservoir (interstitial space) by an extracellular matrix–coated porous membrane upon which primary human proximal tubule epithelial cells were cultured in the presence of a physiological fluid shear stress. In this device, proximal tubular epithelial cells exhibited a polarized morphology that more closely mimicked that seen in vivo, as shown in the cross-sectional fluorescent views, which demonstrate basolateral distribution of Na^+/K^+-ATPase (*magenta*) and apical distribution of aquaporin 1 (*green*), as well as a more columnar cell–like shape in cells under flow (*right*) compared with cells in static culture (*left*). The more differentiated cells in the chip also exhibited a specific toxicity response to the cancer drug cisplatin, whereas the static cells did not (200). (*b*) A 3D culture model of human polycystic kidney disease (PKD). When cyst-lining renal epithelial cells from kidneys of patients with autosomal dominant PKD (ADPKD) were cultured in type I collagen gels, ouabain was shown to stimulate fluid secretion and induce cystic cell proliferation, the two fundamental mechanisms for ADPKD cyst development (208). (*c*) Kidney stone formation on-chip. A photograph shows a polydimethylsiloxane microdevice and a cross section of a microfluidic channel (*top*) in which HK-2 proximal tubular cells were cultured and then stained for Na^+/K^+-ATPase (*bottom left* and *middle*). An optical microscopic image (*bottom right*) shows calcium phosphate crystals (*black clusters*) deposited in the lumen of the microfluidic channel side of the cells in the microfluidic device. Panel modified with permission from Reference 210. (*d*) Schematic of a 3D coculture model of renal fibrosis in which human HKC-8 proximal renal tubular epithelial cells and human WS-1 dermal fibroblasts were combined in an extracellular matrix gel and challenged with toxic doses of cisplatin. Injured epithelial cells induced the fibroblasts to differentiate into activated myofibroblasts. Panel modified with permission from Reference 211.

Kidney Stones

Kidney stones are irregular solid concretions that form inside the kidney, can obstruct urinary outflow, and cause great pain and inflammation (209). To model this condition in vitro, a cylindrical microfluidic device was created with an inner diameter of ∼400 μm, and the microchannel was coated with a layer of glass using a sol-gel method and then coated with fibronectin and plated with human proximal tubular (HK-2) cells (**Figure 4c**) (210). A solution containing $CaCl_2$ and Na_3PO_4 was injected into the microchannel lined with HK-2 cells, and in situ formation of calcium

phosphate stone deposits was detected in real time using confocal Raman spectroscopy. This in vitro model may prove useful for studying the mechanism and kinetics of kidney stone formation, which are virtually impossible to study in vivo.

Renal Fibrosis

Renal fibrosis results from the excessive accumulation of ECM that occurs in many types of chronic kidney diseases. The role of kidney epithelial cells in renal fibrosis was studied in vitro using a simple 3D coculture system that mimics the tubulointerstitial renal microenvironment and the acute tubular injury produced by cisplatin (211). Human dermal fibroblasts were cultured within a type I collagen gel, then human proximal tubular epithelial cells were plated on top of the gel to investigate how interactions between the two cell types contribute to cisplatin-induced kidney injury (**Figure 4d**). These studies showed that the epithelial cells can affect fibroblast gene expression, as measured by RT-qPCR analysis of key regulatory pathways involved in tissue fibrosis.

BONE MARROW AND HEMATOPOIESIS

Engineering artificial bone marrow capable of reproducing the complicated bone marrow microenvironment that enables pathophysiological hematopoietic responses would provide a powerful platform to study hematologic diseases. Porous ceramic scaffolds have been used to develop a 3D perfusion culture system (212, 213) that enables efficient expansion of bone marrow stromal cells and better maintenance of hematopoietic progenitors compared with 2D cultures. A biomimetic scaffold was developed using inverted colloidal crystal to mimic the structural topology of bone marrow (214), which was then seeded with stromal cells that support expansion of CD34$^+$ human hematopoietic stem cells and differentiation of B lymphocytes in vitro. Another 3D bioreactor was developed to sustain long-term erythropoiesis (215). In this device, human bone marrow mononuclear cells that were cultured in a packed bed of microcarrier beads generated reticulocytes and red blood cells continuously for up to 4 weeks, and exposure of the bioreactor to γ-radiation resulted in time- and dose-dependent induction of reticulocyte micronucleation. A membrane-based 3D bioreactor also has been developed that mimics the architecture of the lymph node (216, 217). Dendritic cells were captured within macroporous matrix sheets inside the bioreactor and cocultured with lymphocytes while being perfused with culture medium. This system recapitulated adaptive immune responses in vitro.

Although various culture systems and bioreactors have been developed to maintain hematopoietic cells in vitro, they do not recreate the entire bone marrow microenvironment or enable analysis of the response of its resident hematopoietic cells when present in their normal positions and proportions. Very recently, a bone marrow–on–a–chip device was developed by combining tissue engineering approaches with microfluidics techniques that enable investigators to culture intact living bone marrow with a functional hematopoietic niche in vitro (218). In this technique, artificial bone is first generated in mice using tissue engineering strategies, and then the engineered bone with functional marrow is explanted whole and maintained in vitro within a microfluidic device (**Figure 5**). Fluorescence-activated cell sorting analysis revealed that the engineered marrow contains a hematopoietic niche that is virtually identical to natural marrow. The bone marrow cultured on-chip also retained hematopoietic cells in normal proportions for at least 1 week in vitro. This system faithfully mimicked complex organ-level responses to radiation toxicity normally observed only in vivo as well as the myeloproliferative response to a therapeutic countermeasure agent (G-CSF) known to accelerate recovery from radiation-induced toxicity in patients. In contrast, conventional 2D stroma-supported (Dexter) cultures did not mimic these responses and were significantly more resistant to the effects of radiation toxicity. Thus, this bone marrow–on–a–chip
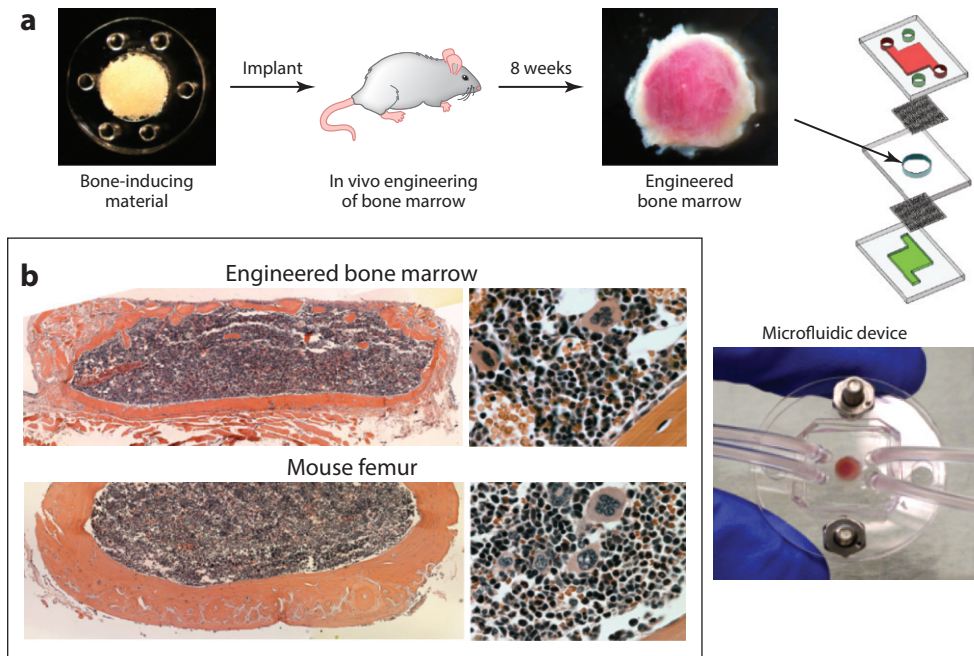
Figure 5

Bone marrow–on–a–chip system. (*a*) To engineer living marrow, polydimethylsiloxane (PDMS) devices containing a cylindrical chamber filled with bone-inducing materials were implanted subcutaneously on the back of a mouse for up to 8 weeks and then surgically removed. The cylindrically shaped engineered bone marrow that formed within the PDMS device was placed into a similarly shaped central chamber in a microfluidic system, punctured with a needle, and then maintained in culture in vitro. (*b*) Low-magnification (*left*) and high-magnification (*right*) views of histological hematoxylin and eosin (H&E)-stained sections of the engineered bone marrow formed in the PDMS device at 8 weeks following implantation (*top*) compared with a cross section of bone marrow within the normal adult mouse femur (*bottom*). Figure modified with permission from Reference 218.

offers a new in vitro strategy for studying hematologic diseases, as well as for analyzing drug responses and toxicities in living marrow.

Interestingly, this tissue engineering approach also produced living bones with predefined size and shape that contained an internal trabecular bone network and had architectural and compositional properties virtually identical to those of natural bone. Thus, this bone marrow–on–a–chip might also provide a tool to study bone matrix remodeling and bone pathophysiology in vitro. For example, it might be used to study osteoporosis by altering bone mineral density using decalcification agents (219).

VASCULAR SYSTEM

Atherosclerosis

Atherosclerosis is a chronic inflammation of the vessel wall; its initiation involves endothelial dysfunction in response to disturbed blood flow patterns. Subsequent influx of inflammatory cells and local smooth muscle cell hyperproliferation result in the formation of an atherosclerotic plaque that penetrates the vessel lumen. Rupture of the plaque often leads to thromboembolism, which is

a major cause of heart attacks and strokes. Basic human in vitro models of atherosclerosis mainly consist of endothelial cultures that are treated with presumed risk factors, such as inflammatory factors, oxidized low-density lipoprotein, or high levels of glucose, followed by characterization of their dysfunction. Sometimes, the models involve cocultures with human smooth muscle cells or human leukocytes, so the roles of these cell types in an atherogenic environment can also be studied.

Advanced in vitro models of atherosclerosis mostly rely on the use of flow culture chambers in which medium or human blood is pumped over a surface with defined geometry containing cultured endothelium under realistic arterial flow conditions. Flow chamber setups are versatile and allow for controlled variation of surface composition and geometry, cell types, and fluid dynamical conditions. As a result, flow chamber–based models have been used to study both early- and late-stage pathogenic processes in atherosclerosis.

Early onset of atherosclerosis results from disturbed blood flow and endothelial dysfunction, so many in vitro models of the disease feature cultures of endothelial cells under disturbed flow. Disturbed flow can be generated in a flow chamber by changing the pump mode from continuous to oscillatory, or by adding a lowered geometrical step in the flow chamber, which generates recirculation and reattachment zones in the flow over the cell layer (220). These studies have revealed that disturbed flow directly leads to endothelial dysfunction, including increased apoptosis and upregulation of inflammatory markers (221).

Because of the lack of plaque rupture and thrombosis in animal models, a unique opportunity for in vitro models of atherosclerosis lies in mimicking events that are hallmarks of late stages of the disease. The formation of thrombi in flow chambers can be induced by coating the flow chamber surface with collagen, plaque material, and thrombus material (such as von Willebrand factor and fibrinogen) and then plating human vascular endothelium in the chamber (222, 223). For example, in one study, the flow chambers were coated with the contents of human atherosclerotic plaques, and anticoagulated human blood was flowed over this surface under arterial conditions (224). By using this approach, investigators identified a clear role for platelet activation and aggregation in the formation of an atherosclerotic thrombus. Platelets responded specifically to collagens I and III in the plaque material, and blocking of platelet receptors for these collagens abolished their activation. Thus, this model led to identification of a new potential target for therapy in late-stage atherosclerosis.

Recently, microfluidic versions of flow chambers have been developed using microengineering techniques, such as soft lithography, in which a mold with microstructures is used to create channels in a silicone rubber (PDMS) slab. After the micromolded PDMS is bonded to a flat surface, the channels can be perfused with medium or blood. In addition, cells can be cultured in the microfluidic channels prior to flow experiments. The main advantages of using microfluidic channels instead of conventional flow chambers are that they require far lower volumetric flow rates and offer increased flexibility in terms of creating precise channel geometries (225) and, hence, mimicking more pathophysiological flow distributions. For example, the geometry and the fluid dynamical environment of an atherosclerotic plaque were mimicked in a microfluidic channel that contained a localized plaque-like narrowing (226, 227). When anticoagulated blood was flowed through this channel, it formed large platelet aggregates specifically in the outlet zone of the constriction site (**Figure 6**). In a follow-up study in which the microfluidic channels were coated with human endothelium before blood was flowed, this localized platelet aggregation response synergized with endothelial cell–mediated deposition of proaggregatory von Willebrand factor in the same region (227). Together, these studies highlight the importance of comprehensive modeling of the atherosclerotic plaque in terms of fluid dynamics, mural cells, and hematologic components when trying to understand thrombosis in atherosclerosis.
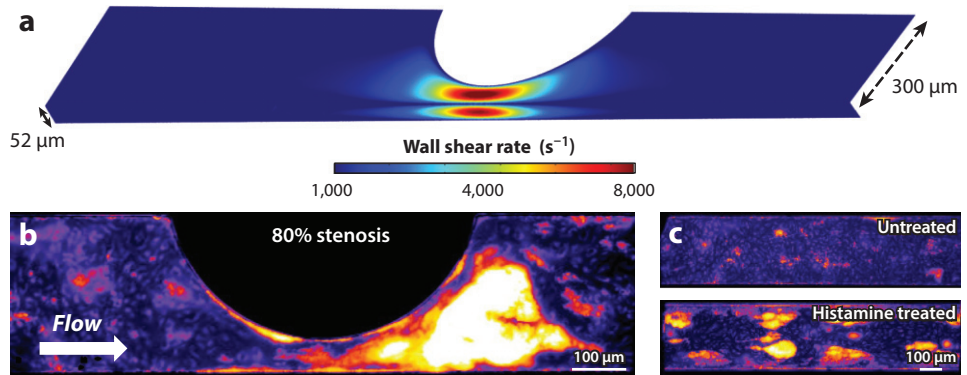
Figure 6

Induction of pathological thrombus formation in a microfluidic channel with an atherosclerotic geometry. (*a*) Schematic view of a microfluidic channel engineered with a geometric (concave semicircular) constriction to mimic a stenotic atherosclerotic vessel. The shear rates around the engineered stenosis are color coded as indicated on the scale. (*b*) Human endothelial cells lining the microfluidic channel with the engineered stenosis were subjected to blood containing platelets flowing from left to right in this view (*white arrow*) at a shear rate of $1,000 \text{ s}^{-1}$. The increased fluorescence signal in the region immediately downstream of the constriction indicates greatly enhanced platelet adhesion and preferential clot formation at this site. (*c*) Results obtained with endothelium-lined channels without a constriction that were either untreated (*top*) or treated with histamine (*bottom*) to induce endothelial activation; these were used as negative and positive controls, respectively. Figure modified with permission from Reference 227.

Deep Vein Thrombosis

Deep vein thrombosis occurs when a blood clot forms in a vein deep in the body, then releases and leads to pulmonary embolism. As described by Virchow's triad, thrombosis and venous thromboembolism occur as a result of vessel wall injury combined with abnormal flow conditions and the procoagulant state of blood components. An ideal model of thrombosis should therefore satisfy Virchow's triad, in addition to being able to mimic clinically relevant conditions and generate reliable quantitative data. Due to the inherent complexity of the disease, there are few in vitro models of deep vein thrombosis that focus on the fluid mechanical aspects near biomimetic venous valves. In one study, which used a section of vein isolated from a dog postmortem, microscopic imaging of particles in a red blood cell suspension revealed that valve pockets act as low-shear vortex traps that accelerate thrombus formation at these sites (228). In another study, human blood plasma was flowed through a microfluidic device with surface-bound clot inhibitors and variable volume-to-surface ratios, while clot formation was monitored using fluorescence microscopy. Analysis of the results accompanied by numerical simulations led to the prediction that clot propagation from superficial veins to deep veins is regulated by fluid shear rate, which might explain the correlation between superficial thrombosis and the development of deep vein thrombosis observed in patients (229).

ENDOCRINE SYSTEM

Thyroid

Changes in thyroid function, and thus in the circulating levels of thyroid hormones, are key features of a number of diseases resulting either from dysfunction of the thyroid gland or indirectly

from systemic diseases. The complex architecture of the thyroid gland requires the development of model systems that recreate the topological organization of the gland and facilitate interactions among the stromal, vascular, and follicular cells that are required for normal thyroid function. Thyrocytes show basal-apical-basal polarity in vivo, whereas in monolayer cultures, usually only apical-apical polarization is obtained, which is a major handicap given that apical-basal polarization is critical for iodine uptake (230). 3D type I collagen gel cultures have been used to induce the formation of structures containing polarized thyroid follicle cells that are responsive to thyroid-stimulating hormone (231). During the regenerative phase of subacute thyroiditis, active folliculogenesis, which is regulated by factors such as TGF-β, is observed; this response also can be mimicked by culturing thyrocytes in 3D (232). A biocompatible scaffold that replicates the geometry of both the vascular and stromal elements of the thyroid gland has been developed and seeded with rat thyrocytes (233), which may be used to support the growth of iPSCs and their differentiation into thyrocytes (234).

Ovary

Much effort has gone into developing in vitro systems for maintenance of ovarian follicles and development of meiotically active and functional oocytes, known as in vitro maturation. Current in vitro fertilization protocols are based on drug-induced oocyte maturation, followed by harvest and culture of the oocytes before fertilization (235). Although 2D culture systems are commonly used for these studies, they lack the ECM environment critical for oocyte development (236). To overcome this limitation, low-concentration alginate-based hydrogels were employed as culture systems that better maintain normal follicular architecture (237–239). 3D culture systems have been developed that contain stromal cells, clusters of multiple follicles (240), and specific hormones such as activin A (241) or other factors such as ascorbic acid (242), which greatly improve the survival of primary follicles (242–243). Recently, hydrogels containing cross-linked peptides have been developed that degrade as the follicles grow, secrete proteases, and shape their own local environment; these 3D gels allow for greater volumetric expansion of the follicles and increased development of competent oocytes (244).

A 3D artificial human ovary was recently developed that supports maturation of human oocytes (245). In this model, ovarian theca and granulosa cells are seeded into microfabricated PDMS molds designed to support the formation of relevant honeycomb and spheroid structures, respectively. Coculture of the thecal honeycomb structures with either granulosa spheroids or cumulus-oocyte complexes led to polar body exclusion from one out of the three oocytes analyzed. Although these findings suggest that this engineered microenvironment may faithfully simulate human ovarian physiology (245), the efficiency of oocyte maturation is not yet optimal, which currently precludes the use of these systems to model diseases such as infertility (244). Nonetheless, this is an interesting direction for future research.

Pancreas

Engineering of pancreas, and specifically the islets of Langerhans, has been a major focus in the tissue engineering field since its inception because of the challenge of diabetes. Current 2D culture systems fail to recapitulate the dynamics of insulin secretion in response to glucose or to maintain β cell viability for extended times. Several groups encapsulate rat, mouse, or human islet-derived cells in 3D ECM (e.g., type IV collagen) scaffolds (246) or in hydrogel scaffolds together with mesenchymal stem cells and ECM (247). Better output is obtained when the scaffolds are copopulated by islets with these stromal cells. For example, when islets from cadaveric human

donors were cultured in collagen gels with or without fibroblasts for 7 days and compared with 2D cultured cells, use of the 3D ECM scaffold alone increased cell viability and multiple functions including amyloid formation; expression of caspase 3, inflammatory markers (e.g., IL-1β), Fas, and insulin; the ratio of β to α cells; and production of functional markers such as basal and stimulated insulin secretion. However, addition of fibroblasts resulted in additional improvement of all of these parameters (248). These results are reminiscent of normal islet development, for which stromal cell–endocrine cell interactions are critical (248).

Emerging evidence suggests that vascular endothelial cells also play a critical role in supporting pancreatic islet development and function. Studies in which human endothelial cells, foreskin fibroblasts, and mouse islets were seeded on biodegradable poly(L-lactic acid)/poly(lactic-co-glycolic acid) (PLLA/PLGA) scaffolds demonstrated that islet survival and insulin secretion were improved relative to culture without the endothelial cells. Gene expression of growth factors and differentiation markers was significantly improved compared with the 2D cultures, and in vivo survival following transplantation was enhanced (249).

Nesidioblastosis refers to a process in which nonendocrine cells (i.e., ductal epithelium) differentiate into new islets; this process is observed when natural islets are lost due to toxicity or surgical removal. Nesidioblastosis was modeled by resuspending human islets obtained from young-adult brain-dead donors in gels composed of either rat tail or purified bovine type I collagen, Matrigel, or agarose and then culturing them in the presence of serum. Cell proliferation and development of islets and nonendocrine cysts were assessed over a period of 10 days. Time-dependent development of islet, ductal, and epithelial structures was evident as early as after 1 week in culture. Agarose and purified collagen gels were not effective; rat tail collagen gels supported growth of single islets, whereas in Matrigel cultures, both cell growth and formation of tubular networks were observed (250).

Better engineered cell-based models are needed to better recapitulate critical aspects of diabetes development and progression, and this might be enabled by rapid developments in the stem cell field. For example, hESCs (251, 252) and iPSCs (253) have been successfully differentiated into endoderm and pancreatic progenitors, as well as glucose-responsive, monohormonal β cells (254). Cord blood–derived mesenchymal stem cells were similarly differentiated to insulin-producing, glucose-responsive cells (255). Monohormonal, glucose-responsive cells derived from human iPSCs driven to endoderm progenitors and differentiated in the presence of growth factors and ECM-provided cues may provide the best model available for potential therapies (254).

But despite considerable progress in producing cells that make insulin, engineered systems that mimic the pancreas environment (endocrine, exocrine, and ductal compartments) and respond fully to physiological cues are still needed (256). In one recent study, microengineered concave wells were used to coculture adipose-derived stem cells with mouse pancreatic islets, and the presence of the adipose-derived stem cells increased cell viability and enabled regulated insulin secretion. Furthermore, when these encapsulated spheroids were placed within collagen-alginate microfibers using a microfluidic chip and then implanted in diabetic mice, they exerted therapeutic effects (257). This is another promising approach that could be used to analyze functional changes in human diabetic islets in the future.

Adipose Tissue

The identification of leptin as a hormone that is secreted by adipocytes and regulates energy homeostasis systemically changed our concept of adipose tissue from a nutrient-storing tissue to primary endocrine organ (258). The cardinal sign of obesity is the expansion of white adipose tissue and its acquisition of an inflammatory phenotype, driving the development of systemic

insulin resistance (259). Insulin resistance is the primary underlying cause of obesity comorbidities, including cardiovascular disease, type 2 diabetes, and cancer (260, 261). Thus, models to elucidate the molecular and cellular interactions driving adipocyte differentiation and metabolism are in great need.

Unfortunately, preadipocyte 2D cultures, which are the most widely used model today, do not capture the dynamics of adipose tissue regulation, which involves cell differentiation and proliferation occurring at the same time in the same tissue. To meet this challenge, adipose cells were cultured in 3D scaffolds composed of polyglycolic acid fiber meshes (262), electrospun polymer nanofibers (263), or collagen scaffolds (264) to differentiate preadipocytes or stem cells into mature adipocytes. Vascular endothelial cells, which are intimately linked to the expansion of adipose tissue in vivo, have been integrated into these cultures as well (265–266). Iron oxide and gold nanoparticles cross-linked to polylysine also have been used to promote the development of adipospheres via magnetic levitation of preadipocytes cocultured with stromal vascular cells derived from adipose tissue (267). The engineered 3D tissue structures show active lipogenesis, as determined by lipid droplet accumulation, but no further functional studies have been reported. Preadipocytes have been cocultured with endothelial cells on engineered silk scaffolds (266, 268), which resulted in the development of a vascular network that increases the functionality of the adipocytes, as measured by increases in both lipid storage and lipolysis. Importantly, insulin-mediated changes in lipolysis were demonstrated in this model system (266). Finally, a multicompartmental microfluidic chip has been used to culture an adipocyte cell line; the cells were shown to accumulate lipid, but no other functions were characterized (269).

Thus, although it is currently possible to maintain and differentiate adipocytes in 2D and 3D culture systems, there is still no model that effectively recapitulates the complex adipose tissue environment that is required to study obesity in vitro. This will require engineering of systems that incorporate immune, endothelial, and stromal cells as well as adipocytes under conditions in which the dynamics of nutrient and hormone delivery can be controlled in a finely tuned manner to faithfully simulate human adipose tissue in basal and hypercaloric states. Microfluidic systems are well suited for this challenge, but their use remains to be explored in the future.

SKELETAL MUSCLE

Muscular dystrophies, among the most common human genetic disorders, quickly worsen and weaken the muscles. For example, the most prevalent and most severe form of this disease—Duchenne muscular dystrophy—is caused by the absence of dystrophin protein, which results in progressive degeneration of cardiac and skeletal muscle. Functionally mature skeletal muscle has been grown on 2D or 3D flexible substrates and as freestanding self-assembled constructs (270–283). 3D skeletal muscle constructs (termed myooids) were formed by growing between two anchors a monolayer of myotubes, which detached from the substrate upon becoming contractile and rolled into cylinders while remaining attached to the anchors as if they were tendons (270). Primary rat myotubes cultured on silicon cantilevers were interrogated in real time by measuring their deflection using a detection system similar to an atomic force microscope, and stresses were calculated using a modified Stoney equation (279). When the sodium channel agonist veratridine was injected during electrical stimulation, it caused asynchronous tetanic contractions followed by inability of the muscle to further contract, as occurs in vivo. Long-term culture of these muscle cells in a combination of growth factors (e.g., creatine, cholesterol, estrogen) that are important for the development of the contractile apparatus in skeletal muscle resulted in decreased contraction time and increased contractile strength, which are characteristic of more mature phenotypes.

As impairments in glucose uptake by skeletal muscle contribute to insulin resistance in type 2 diabetes (284), this process has been studied using engineered muscle constructs. A positive correlation between contractility and glucose uptake was demonstrated by electrically stimulating C2C12 myotubes that were cultured on a microporous alumina substrate coated with an atelocollagen membrane, allowing tissue-like stiffness and contractility, and placed between two platinum ring electrodes (280, 285). Micropatterned cultures of C2C12 myotubes were also created on a fibrin gel sheet combined with a microelectrode array chip (286). Through localized electrical stimulation via microelectrode array, the contractility of each line of cells could be individually controlled. This system was used to demonstrate contraction-induced translocation of the glucose transporter GLUT4 from intracellular vesicles to the plasma membrane. GLUT4 is an important mediator of insulin- and contraction-induced glucose uptake in skeletal muscle, defects in which are closely associated with type 2 diabetes. The developed system is applicable for assaying such metabolic alterations in skeletal muscle and screening drug candidates against type 2 diabetes.

An in vitro model of aging or atrophied muscle was created using 3D bioengineered skeletal muscle constructs (287). Multiple-population-doubled C2C12 myoblasts that were previously shown to have an aged phenotype based on reduced differentiation potential (288) and zero-passage control cells were added to a collagen I/media solution and set between two mesh floatation bars attached to the containing chamber via stainless steel grips. After cell attachment, constructs were attached to a culture force monitor for measuring force and rate of force development for 24 h after seeding. The aged cells exhibited lower force generation, reduced matrix remodeling [i.e., reduced expression of matrix metalloproteinase MMP2 and MMP9 mRNAs], and smaller myotube size and diameter. They also displayed a lower potential for differentiation and hypertrophy, as shown by decreased mRNA levels of myogenin and the insulin-like growth factor family members IGF-I, IGF-IR, IGF-IEa, and MGF, as well as increased expression of catabolic transcripts (myostatin and TNF-α) in expanded myoblast populations compared with controls. Importantly, similar alterations have been observed in tissue biopsies during degeneration of whole muscle with age (289, 290) as well as in cells isolated from elderly human muscle (291–293). This engineered model could potentially be extended to incorporate diseased cells and to study muscle-wasting disorders in vitro.

The only reported in vitro disease model of skeletal muscle was engineered from myoblasts isolated from *mdx* mice with Duchenne muscular dystrophy (294). Miniature bioartificial muscles (mBAMs) were created by forming ECM gels containing muscle cells around two freestanding PDMS microposts in each well of a 96-well plate. Each hydrophobic micropost had a hydrophilic cap on its top to provide an anchoring point for the engineered tissues, and a robotic liquid-handling system was employed to mix cell suspensions with ECM solutions and to cast the tissues around the posts. A customized myoforce analysis device automatically moved electrodes into place in each well and electrically stimulated the mBAMs, which resulted in tetanic force generation. Contractions of the mBAMs were acquired using a motion tracking system, and forces were calculated from maximum bending deflection of microposts based on their dimensions and the elastic modulus of PDMS. This system was utilized to screen various doses of 31 muscle weakness–and/or muscle loss–attenuating compounds as potential treatments for Duchenne muscular dystrophy patients, and 11 compounds were identified that significantly increased tetanic force. The assay also identified beneficial and disadvantageous interactions of combinatorial therapies prescribed to some Duchenne muscular dystrophy patients.

Although this system is semiautomated and potentially high throughput, one caveat is that myosin heavy chain profiling revealed that the engineered tissues appear to have a neonatal (i.e., rather than adult) phenotype (278), and hence, they might be more appropriate for testing drugs for younger patients. Another potential limitation is that loss of dystrophin also affects muscle's

surrounding connective tissue, innervation, and vasculature (295), whereas this system permits analysis only of muscle. Consequently, the system would be unable to detect the beneficial effects of drugs acting as antifibrotic agents, through the vasculature and on the inflammatory response, as well as compounds designed to minimize contraction-induced membrane damage. Finally, as disease phenotypes in animals and humans are different, it will be necessary to incorporate human cells into this disease model in the future.

Promoting Tissue Maturation

A major challenge in skeletal muscle tissue engineering is myogenicity and the induction of adult phenotypes, as myotubes are generally arrested in an early developmental stage in vitro. Several forms of stimulation can be utilized chronically for tissue maturation, including electrical stimulation to mimic neuronal activity (296) and magnetic (297) and mechanical (298–300) means. Different outcomes in response to stimulation are to be expected from different cell sources—for example, between primary cells and cell lines (296) and between different fiber types even of the same origin (301). Use of the variety of transcription factors involved in myogenesis, the growth factors that negatively or positively affect them, and other biochemical cues also can be pursued as a means to modulate myogenesis. Optical stimulation offers a few advantages over electrical stimulation, including high spatiotemporal resolution for actuation, better flexibility for excitation under physiological conditions, and lack of toxic byproducts. In addition, because it is minimally invasive, the stimulus pulses do not damage the tissue, whereas this can be a problem with other methods that require prolonged-duration and high-magnitude electrical stimulation (275). Although optogenetics was recently shown to be applicable for controlling skeletal muscle (275, 302), the use of chronic optical stimulation for maturation of skeletal muscle has not yet been reported and may offer a suitable substitute for in-culture electrical stimulation. Contactless electrodes have also been developed to eliminate issues involved with direct electrical stimulation, including contamination, electrode corrosion, and hydrolysis and heating of the culture medium (303).

The choice of cell source is of high importance for promoting muscle differentiation. The most common skeletal muscle cell sources so far have been the mouse C2C12 and rat L6 cell lines; however, these have the drawbacks of any immortalized cell line (e.g., genetic abnormalities). Primary murine cells also have been used, but ultimately, primary human muscle cells should be more predictive for studies of disease mechanisms and screening of drugs. For example, whereas in most rodent skeletal muscles the myosin heavy chain IIb is the predominant motor protein, it is expressed in only a small number of muscles in adult large mammals (304). Importantly, primary human myoblasts recently have become available from a few commercial vendors, but they are not well characterized (305, 306). Because the differentiation potential of primary skeletal myoblasts drops rapidly after a few population doublings in culture (291), low passage numbers must be used to achieve optimal tissue maturation, which can result in higher costs. There are other cell types with myogenic potential (307) that also can be considered; however, advancement of this field will require accessible diseased human cell sources and the ability to derive mutation-specific myoblasts from humans (308) or to generate them from human iPSCs.

Incorporating Neuromuscular Interactions

Part of the challenge in inducing maturation in vitro might be due to lack of innervation, as neuronal activity is known to influence muscle maturation (309–312), expression of myosin isoforms, and phenotypic transition into different fiber types (313–315). Toward that end, functional neuron-muscle constructs have been formed in vitro on a silicon-based cantilever system (281) and

in freestanding muscle constructs (282). Using this model, successful transmission and induction of muscle contraction through the neuromuscular junction were demonstrated, as well as their blockade. These systems also were used to elicit and measure changes in contractile response as a function of the alteration of various exogenous factors (glutamic acid and tubocurarine), and hence, they provide a functional readout of muscle contractility when stimulated via the neuromuscular junction. These models could be used in the future to study the effects of muscle denervation, innervation, and reinnervation as linked with mechanical functionality. They also could be extended to utilize diseased cells to produce skeletal muscle–motoneuron–neuromuscular junction disease models, such as of amyotrophic lateral sclerosis and spinal muscular atrophy, and to serve as functional assays for drug screening.

NERVOUS SYSTEM

General Challenges

Neurological disorders, including epilepsy, Alzheimer's disease (AD), schizophrenia, Parkinson's disease (PD), amyotrophic lateral sclerosis (ALS), autism, stroke, and brain injuries, affect up to one billion people worldwide (316), yet there are a limited number of successful therapeutics. The complexity of the human brain makes it difficult to study brain disorders, as it contains 86 billion neurons and 85 billion nonneuronal cells unevenly distributed throughout various brain regions (317). The variability of cell morphology, size, functions, connections, and gene expression is also greater than that seen in any other organ (e.g., there might be ∼700 types of neurons in the hippocampus alone) (318, 319). Given the complexity of this organ, the challenge of designing an effective in vitro model is huge.

One of the major challenges in developing effective in vitro models of neurological disease is quality control: Which cell-based measurements are most relevant to define a clinically relevant diagnosis? How can those be implemented into an in vitro model? How do we analyze a psychiatric disease mechanism in vitro? However, there are some places to start. For example, schizophrenia patients show a disturbance in the synchrony of gamma oscillations (320), which possibly could be observed using MEAs in vitro. A decrease of glutamic acid decarboxylase 67 (GAD67) mRNA, γ-aminobutyric acid (GABA) receptor α subunits, and μ opioid receptors has been observed in schizophrenic patients in the dorsolateral prefrontal cortex, in layer 3 in a specific subset of neurons (321). The measurement of these molecular players could be used to qualitatively analyze and validate in vitro schizophrenia models. PD is diagnosed postmortem by the presence of Lewy bodies, which are composed of α-synuclein, and the loss of dopaminergic neurons (322). Detection and quantification of α-synuclein and neuronal loss could therefore be used as qualitative measurements for an in vitro model of PD.

The biggest challenge, however, will be developing ways to provide readouts of "cognition" in an in vitro system. The major function of the brain is to process and interpret information, and an accurate in vitro model needs to replicate this capability in some way. Interestingly, 2D rat neuronal cultures on MEAs have been used to control the behavior of a computer-generated animal (animat) using distributed patterns of neural activity. Electrical feedback to the neuronal network is provided by a computer, acting as the animat's sensory system (323). The neuronal networks also were used to control the flight of a simulated aircraft; in this case they were stimulated with high-frequency inputs to produce a system in which the living neuronal network would "learn" to control an aircraft for straight and level flight (324). Another group established bidirectional communication between a neuronal network and a mobile robot. The neural activity was decoded into motor commands for the robot, and the sensory signal from the robot was translated into

a pattern of electrical stimulation (325). By developing in vitro standards of healthy cognitive output, such as these, it may become possible to create and analyze models of neurological disease in vitro.

The ability to study diseases of the brain in vitro and observe disease-relevant phenotypes also depends on the ability to produce neuronal cultures of defined cellular composition. Recently, protocols have been developed that induce rapid and virtually complete neural conversion of human iPSCs. When combined with engineered in vitro systems, this ability is beginning to have a great impact on disease models, as described below.

Microcephaly

Microcephaly is a neurodevelopmental disorder that is usually defined as a reduction in brain size. To date, the understanding of cause and mechanisms is very limited (326), and no treatment is available yet. Human pluripotent stem cell–derived cerebral organoids have been used to study human brain development and developmental brain diseases, including microcephaly (327, 328). For example, when neuroectodermal tissues that self-organized from embryoid bodies were cultured within 3D Matrigel droplets and maintained in a spinning bioreactor to enhance nutrient absorption, rapid development of cerebral organoids resulted (**Figure 7**) (328). Neural identity was detected after only 8–10 days and defined brain regions formed after 20–30 days in culture. During intervening stages (15–20 days), the cerebral organoids contained a large continuous neuroepithelium surrounding a fluid-filled cavity reminiscent of a ventricle, with characteristic apical localization of neural-specific N-cadherin. The brain tissue reached its maximal size (∼4 mm in diameter) by 2 months, and this tissue survived for at least 10 months when maintained in the spinning bioreactor (328). The limit on organoid size was likely due to the lack of a circulatory system and limitations in oxygen and nutrient exchange. As a result, extensive cell death was observed in the core of these tissues; however, various brain regions reminiscent of the cerebral cortex, choroid plexus, retina, and meninges formed along the exterior.

Interestingly, although small embryoid bodies were obtained when similar experiments were carried out with iPSCs derived from skin fibroblasts of a patient with microcephaly, they failed to develop under the same neural induction conditions unless an increased number of initial iPSCs were utilized (328). This modification allowed the formation of neuroectoderm and subsequently of neural tissue; however, the neuroepithelial tissues that formed were smaller and had only very few progenitors, and they exhibited a larger degree of neuronal outgrowth when compared with control tissues. These overall smaller neural tissues mimicked the reduced brain size seen in microcephalic patients.

Use of this cerebral organoid model revealed that the loss of a protein implicated in microcephaly pathogenesis, called CDK5RAP2, leads to premature neural differentiation at the expense of progenitors (328). Thus, this technique, which combines the powerful self-organizing abilities of human iPSC-derived neuroprogenitor cells with 3D culture, offers a new way to investigate human neurodevelopmental processes in vitro. To be most useful, this approach will need to be modified to overcome the lack of a circulatory system and the oxygen and nutrient exchange limitations that appear to restrict 3D tissue growth and survival. Nonetheless, it is a powerful new approach to investigate human neurodevelopmental disorders, especially when using iPSCs isolated from patients with differing and well-defined genetic backgrounds.

Parkinson's Disease

PD is an incurable neurodegenerative disease that causes movement-related symptoms such as shaking, rigidity, slowness of movement, and difficulty with walking as well as cognitive and
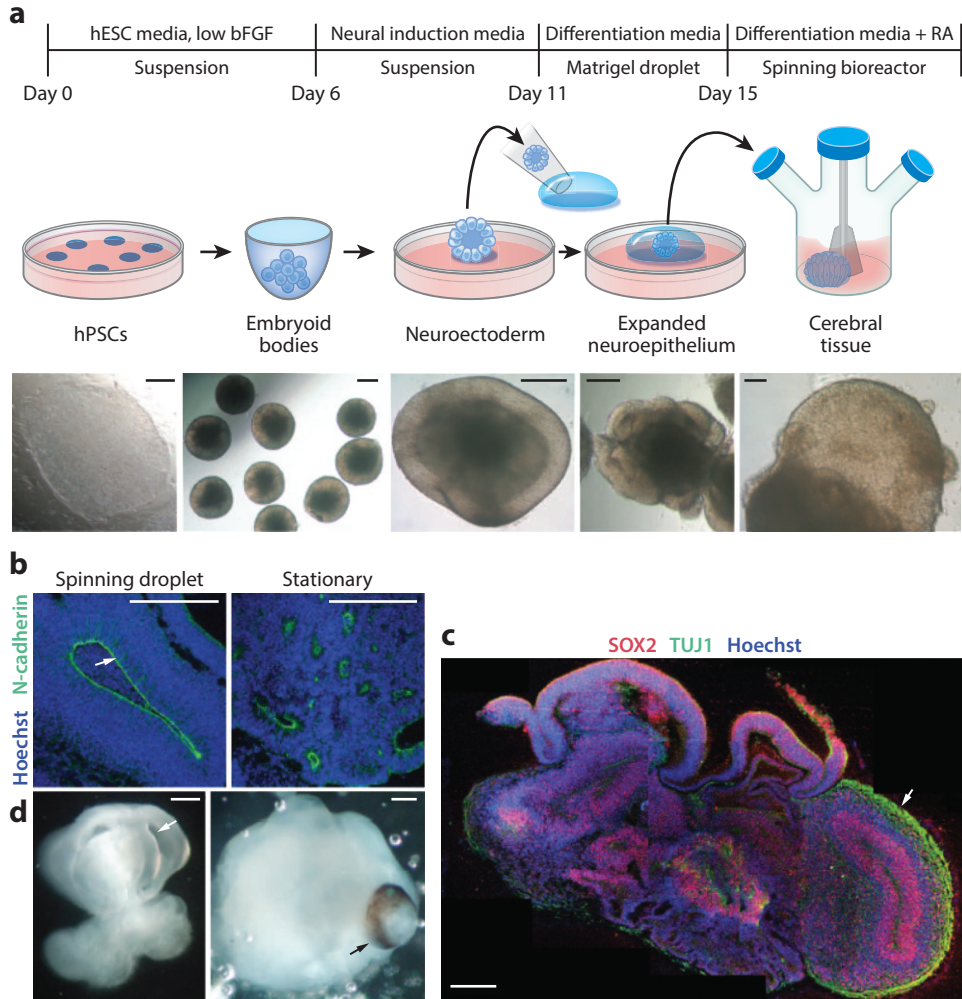
a

| hESC media, low bFGF | | Neural induction media | Differentiation media | Differentiation media + RA |
| Suspension | | Suspension | Matrigel droplet | Spinning bioreactor |

Day 0 — Day 6 — Day 11 — Day 15

hPSCs → Embryoid bodies → Neuroectoderm → Expanded neuroepithelium → Cerebral tissue

b

Spinning droplet | Stationary

Hoechst N-cadherin

c

SOX2 TUJ1 Hoechst

d

Figure 7

Cerebral organoid culture system. (*a*) Schematic of the culture system and in vitro manipulations used to induce hPSCs to form cerebral organoids. Abbreviations: bFGF, basic fibroblast growth factor; hESC, human embryonic stem cell; hPSC, human pluripotent stem cell; RA, retinoic acid. (*b*) Neuroepithelial tissues generated using this approach (*left*) were larger and more continuous and exhibited large fluid-filled cavities and typical apical localization of N-cadherin (*arrow*) compared with tissues grown in stationary suspension without Matrigel (*right*). (*c*) Immunohistocytochemical analysis revealed that the organoids exhibited complex tissue morphology with heterogeneous regions (*arrow*) containing neural progenitors (SOX2, *red*) and neurons (TUJ1, *green*). (*d*) Low-magnification bright-field images reveal fluid-filled cavities reminiscent of ventricles (*white arrow*) and retina tissue, as indicated by retinal pigmented epithelium (*black arrow*). All scale bars are 200 μm. Figure modified with permission from Reference 328.

behavioral limitations ultimately resulting in dementia. The symptoms result from the death of dopamine-generating cells in a brain region called the substantia nigra, possibly initiated by the abnormal accumulation of α-synuclein protein in the form of Lewy bodies (322, 329). The human neuroblastoma SH-SY5Y cell line has been widely used as an in vitro model for PD, because these cells possess many characteristics of dopaminergic neurons, including the ability to synthesize dopamine and noradrenaline, as determined by the expression of tyrosine hydroxylase and dopamine β-hydroxylase. They also express the dopamine transporter that regulates dopamine homeostasis, which is expressed only in dopaminergic neurons in the central nervous system (CNS) (330–332). Furthermore, dopaminergic phenotypes can be induced in these cells using retinoic acid, brain-derived neurotrophic factor (BDNF), or staurosporine. These cells also can be driven toward a PD-like state by coadministering neurotoxins, such as MPP+, 6-OHDA, or rotenone (330). The disadvantages of these conventional 2D culture models is that only neuronal cell behavior can be investigated, and the complexity of cell-cell interactions and higher-order brain architecture are neglected; as a result, these cell lines do not reliably mimic cell phenotypes observed in vivo. In the future, this approach might be advanced by including astrocytes in coculture with neuronal cells (potentially using patient-derived cell types) and by live cell imaging techniques and metabolic readouts to identify the mechanisms of dopamine-generating cell death; it also might be combined with engineered microsystems that enable analysis of cell-cell interactions and creation of electrically connected neuronal networks (333–335).

Alzheimer's Disease

AD is an incurable neurodegenerative disease accompanied by neurofibrillary tangles and β-amyloid plaques, ultimately leading to neuronal loss (336, 337). Symptoms include decreased memory abilities (eventually resulting in dementia), confusion, irritability, aggression, and mood swings. Diagnosis of AD is usually confirmed with tests that evaluate behavior and thinking abilities, followed by a brain scan (computed tomography, magnetic resonance imaging, or positron emission tomography), but a definite diagnosis is only possible postmortem (337). Research on AD is hampered by a lack of suitable in vitro models. Commonly used cell models do not include axons, synapses, or human proteins (e.g., tau), which are all implicated in the pathology of AD (338).

In an effort to develop an improved in vitro model for AD, human neuroblastoma SH-SY5Y cells were pretreated with retinoic acid for 1 week in conventional culture before being transferred into 3D culture in an ECM gel composed of laminin, type IV collagen, heparan sulfate proteoglycan, and entactin and supplemented with BDNF, neuregulin, nerve growth factor, and vitamin D_3 (338). This resulted in development of cells with neuronal morphology, expression of several neurospecific markers, formation of synapses, and axonal transport. It also induced axonal expression of mature tau protein isoforms, which reached levels found in adult human brain, making this a valuable and improved in vitro model for AD. In a separate study, cells from a neuroepithelial stem cell line derived from human iPSCs were cultured within a commercially available soft hydrogel (BD Biosciences/Corning Inc.) composed of laminin and a peptide that self-assembles into nanoscale fibers to mimic the 3D neuronal environment. These 3D culture conditions resulted in induction of in vivo–like responses related to AD, such as increased levels of p21-activated kinase activity and a higher degree of colocalization of F-actin and drebrin, which cannot be recapitulated with conventional 2D cultures (339). Thus, these studies suggest that the presence of a 3D physical microenvironment and selective biochemical initiators may provide a better platform to recapitulate in vivo aspects of tissue organization and thereby promote physiological neuronal properties reminiscent of AD (340). The problem, however, is that it is much more difficult to analyze functional responses in 3D cultures than in 2D systems (e.g., both of

these studies were solely evaluated by fluorescence imaging and Western blot analysis), and thus, the full value of these models will require development of new types of functional readouts.

Amyotrophic Lateral Sclerosis

Motor neuron loss in the spinal cord and motor cortex is the key feature of the incurable neurodegenerative disorder ALS, which is characterized by progressive weakness, muscle atrophy, paralysis, and death (341). No test can provide a definite diagnosis of ALS; instead, diagnosis is primarily based on the symptoms and signs observed in the patient and a series of tests to rule out other diseases (342). One of the main challenges in the ALS research field has been the lack of a robust supply of human motor neurons carrying the genes responsible for this condition. But in 2008, iPSCs were generated from skin fibroblasts of an 82-year-old woman suffering from a familial form of ALS. These iPSCs were successfully directed to differentiate into motor neurons and glial cells, the cell types implicated in ALS pathology, opening up a new experimental path to carry out mechanistic studies and explore cell replacement therapies (343). Another challenge that this approach might help overcome is that whereas most past work on ALS pathophysiology has involved studies of the familial form of ALS, more than 90% of ALS patients are afflicted by a sporadic form of the disease, arising from interactions between genetic and environmental factors (344). So far it has been impossible to investigate this type of disease with an in vitro model; now, with the availability of patient-derived iPSCs, it may be achievable. The iPSCs generated from patients with sporadic ALS would carry the precise constellation of genetic information associated with the pathology of the disease in that patient (343).

Autism

Autism spectrum disorder (ASD) is a neurodevelopmental disorder characterized by social deficits and communication difficulties as well as repetitive behaviors and cognitive delays. Little is known about the pathophysiological mechanisms leading to ASD (345), and specific diagnosis is challenging. This disorder cannot be fully recapitulated in animal models, and relevant models need to focus on early development, when genetic and environmental insults are thought to be causative in this disease (346). A human neural progenitor system developed from human fetal brain tissue was analyzed by whole-genome profiling to assess the functional genomics of both normal human neuronal development and autism (347). This study showed that during differentiation of normal human neural progenitors derived from early human embryos (8–19 gestational weeks), many genes and signaling pathways linked to ASD are highly coexpressed, including *CBS*, *DLX2*, *RIMS3*, and *PRKCB1*. Furthermore the expression of some of these genes is modulated during neuronal differentiation, implying that ASD has a neurodevelopmental origin. It is also possible to study ASD in a dish using patient-derived iPSCs, which enable analysis of various syndromic forms of ASD and their individual pathophysiology. The identification of phenotypes in human iPSC-based models of ASD has been achieved in four forms of ASD with known single-gene defects: Rett syndrome (*MECP2*), Phelan–McDermid syndrome (*SHANK3*), Timothy syndrome (*CACNA1C*), and fragile X syndrome (*FMR1*).

In the case of human iPSCs from Rett syndrome patients, significantly reduced cell soma and dendritic branching was demonstrated, as well as reduced frequency and amplitude of miniature excitatory and inhibitory postsynaptic currents (348). Human iPSCs from Rett syndrome patients also displayed fewer puncta (a presynaptic marker of excitatory synapses), which suggests that there might be an overall reduction in synapses in these patients (345). Human iPSCs from patients with Phelan–McDermid syndrome show significant deficits in excitatory synaptic transmission (349).

Cortical-enriched neuronal populations differentiated from human iPSCs from patients with Timothy syndrome exhibit action potentials wider than those of control cells, in addition to a loss of $Ca_V1.2$ channel inactivation. An increase in sustained intracellular calcium rise following membrane depolarization further suggested a deficiency in calcium signaling in these neurons (345, 350). Both neurite number and length were reduced in neurons derived from human iPSCs from patients with fragile X syndrome, a phenotype that resembles that seen in human fragile X syndrome postmortem tissue (345, 351, 352). However, a major challenge to modeling ASD is that it has not yet been possible to use human iPSC differentiation strategies to generate the neurons of the middle to upper cortical layers that form the intracortical circuitry that is often perturbed in ASD. More recent differentiation protocols have begun to address neuronal region specificity (353, 354), so it might be possible to overcome this limitation in the future. For example, there are modified neural differentiation protocols that enable the derivation of specialized neuronal precursor and mature neuron populations, including floor plate precursors, midbrain dopaminergic neurons, and cortical neurons (355–357).

Another challenge is that it currently takes a long time (2–4 months) to differentiate iPSC-derived neurons to the point where they exhibit a level of neuronal connectivity that allows study of synaptic physiology. In particular, given that defects in neural synchrony of oscillatory activity are associated with neuropsychiatric disorders including ASD (358), there is significant interest in establishing in vitro neuronal cultures capable of supporting synchronous neuronal activity. Culturing cells on MEAs allows repeated measurements of differentiated cells in culture over time and could be used by investigators to study and optimize cell maturation kinetics. But the key to understanding the pathophysiology of ASD is the creation of robust disease-relevant cellular models. This will require multiple efforts, including establishment of human iPSCs from biopsy material from ASD patients with different genetic backgrounds and from control individuals; genetic engineering of normal human iPSCs to generate sets of lines with targeted ASD-relevant genetic defects; development of robust, standardized, efficient, and relevant neuronal differentiation protocols; and development of better definitions of ASD-related cellular phenotypes upon which corresponding cellular assays can be built (345).

Central Nervous System and Spinal Cord Injury

Worldwide, 130,000 survivors of spinal cord injury are reported each year (359), but the majority of those survivors are left paralyzed, with no restorative treatment available as yet (360). Neurons fail to regenerate after injury, because of several inhibitory processes that become activated following injury (360). Researchers are trying to unravel these processes with the aim of enhancing regenerative capacity and functional regrowth.

Components of the brain ECM, such as hyaluronan, chondroitin sulfate proteoglycans (e.g., aggrecan, versican, brevican, and phosphacan), tenascins, and link proteins (361), are altered after CNS injury and are believed to contribute significantly to inhibition of axonal regrowth and myelin repair (362). Because proteoglycans that contain chondroitin sulfate glycosaminoglycan (CS-GAG) side chains are upregulated in the CNS after injury (363), chicken dorsal root ganglion cells were seeded into agarose gels containing differently sulfated GAGs (aggrecan, hyaluronan, or chondroitin) (363). CS-4,6 GAG, which is upregulated in astroglial scar in vivo, inhibited neurite outgrowth similarly to aggrecan, which is a known inhibitor of nerve process extension (363). This 3D in vitro model revealed that specific forms of CS-GAG have different functions in the CNS after injury, and that their sulfation state is critically related to their ability to inhibit axonal regeneration.

In another study, Cullen et al. (364) developed a 3D tissue engineered system to improve stem cell transplantation for CNS injury. Rat neurons were cocultured with rat astrocytes in Matrigel

and subjected to mechanical loading or to treatment with TGF-β1 to induce astrogliosis, a process associated with CNS injury in vivo. Mouse neural stem cells, which were delivered to the injured coculture, exhibited the highest survival rates when implanted in a methylcellulose-laminin scaffold (364). These findings suggest that it might be beneficial to use a tissue engineering approach to target neural stem cell delivery, as this can improve donor cell survival (364).

It has been difficult to study glial scar formation, which also inhibits axonal regeneration after injury in vivo, using 2D cultures because astrocytes in a monolayer are constitutively activated. A 3D type I collagen gel system was developed that maintains rat astrocytes in a more quiescent state than in monolayer cultures, thus mimicking their behavior in the undamaged CNS (365). Addition of TGF-β1 to the astrocytes cultured in these 3D gels resulted in their activation in vitro (365), mimicking the reactive astrogliosis seen in vivo after injury. This 3D culture system therefore provides a potentially powerful new tool for the investigation of CNS damage and repair.

Schizophrenia

Schizophrenia is a mental disorder characterized by delusions, paranoia, hallucinations, disorganized thinking, lack of emotion, and lack of motivation (366). Genetics, early environment, neurobiology, and psychological and social processes appear to be important factors contributing to disease onset and progression, but the mechanisms underlying the disease remain poorly understood (366, 367). Multiple studies have generated iPSC-derived neurons from fibroblasts isolated from patients diagnosed with schizophrenia by using conventional induction protocols (368, 369). It is also possible to directly convert human fibroblasts into mature induced neurons without passage through an intervening pluripotent state by overexpressing BRN2 and MYTL1 and adding microRNA-124 or NEUROD2, and similar results have been obtained by expressing ASCL1 and MYTL1 and adding microRNA-124 and microRNA-9/9 (368–370).

Importantly, researchers observed reduced activity and altered gene expression profiles in human iPSC-derived neurons from schizophrenic patients (369) and identified a number of new pathways that may contribute to schizophrenia (369). However, because this method bypasses neuronal development, it is not possible to use these cells to analyze neural cell migration, specification, or maturation, which may be critical to the progression of this disease. Furthermore, because this method results in terminally differentiated neurons that do not proliferate, the total amount of cellular material available for analysis is limited.

Another method, which results in formation of induced neural progenitor cells (iNPCs) from fibroblasts, better recapitulates neural development and offers a virtually limitless supply of neurons for models of psychiatric disorders. iNPC technology provides a fast and robust protocol to obtain proliferative neural precursors and generate more homogeneous populations than are possible with current induced neuronal differentiation methods; however, development of new strategies that permit patterning of specific regional identities also will be critical (371). Analysis of iNPCs derived from human iPSCs taken from one schizophrenic patient revealed a 2-fold increase in extramitochondrial oxygen consumption as well as elevated levels of reactive oxygen species (372). Together, these studies offer an excellent proof of concept that reprogramming-based in vitro disease models can be used to study cellular alterations in schizophrenia; however, the relevance of these alterations to disease phenotype remains unclear.

Adding 3D Complexity

Although great effort has been put into developing in vitro human brain models using iPSCs as well as 2D and 3D gel culture systems to model psychiatric and neurodegenerative disorders,

significant hurdles remain. Examples of challenges include coupling the brain to the vasculature; increasing the complexity in terms of cell type variety, axonal directionality, and structure-function relationships; and developing quantitative readouts that scale with in vivo brain functions and are relevant to the modeled disease. Whereas existing in vitro 2D neuronal cell culture models are accessible to analysis using microscopy and MEA analysis, 3D models are not yet amenable to these techniques. Methods have been developed to make large (1 × 1 mm) pieces of transparent brain tissue (the CLARITY project) (373), which could be integrated into 3D cultures; however, microscopes and objectives must be modified to fluorescently visualize cells and molecules within these tissues. The controllability and reproducibility of 3D models and cerebral organoids also need to be improved.

One major limitation of most of the current models is that they fail to combine different types of neurons, incorporate myelinated nerves (374), or establish cocultures of neurons with astrocytes in vitro. Control of axonal growth should be improved and directed to create defined neuronal network structures, for example, using axonal diodes or engineered channels that guide axons controllably in a specific direction (334). More appropriate brain ECM substrates should be incorporated in 2D and 3D in vitro models as well, because the brain ECM is unique and its importance for injury responses is well recognized. For example, in one recent study, a more complex 3D gel composed of type I collagen and hyaluronan produced a 70% increase in the number of neurons generated from embryonic mouse brain progenitor cells, compared with a 14% increase when the same cells were placed in 2D culture (375). In another study, a 3D millimeter-sized neural network was developed and then assembled with other, similar structures to create a complex 3D architecture containing broad neural networks that connected different brain regions (376). This was achieved not with a scaffold or hydrogel, but by culturing a massive amount of neurospheroids that were formed by cells from specific rat brain regions. This system promoted the formation of complex millimeter-scale axonal extensions through the 3D cellular construct that have not been observed in 2D cultures (376). It will be interesting to integrate normal and diseased human neuronal cells into such complex 3D systems.

CARTILAGE

Osteoarthritis

One of the most devastating diseases of cartilage is osteoarthritis (OA), which is the most common type of arthritis. It is a complex chronic inflammatory and metabolic disorder that results in breakdown of cartilage matrix, and it often involves adjacent synovium, underlying bone, and surrounding connective tissues. The complex nature of the disease has hindered the development of accurate disease models. Current in vitro OA models range from simple 2D monolayer cell culture models in which chondrocytes are stimulated with proinflammatory cytokines (377) to Transwell insert-based cocultures of chondrocytes and immune cells (378) to more elaborate 3D animal or human engineered cartilage inflammatory disease models (379, 380). For example, to generate an in vitro cartilage model, bovine articular chondrocytes were grown in a collagen sponge with or without IL-1β, an inflammatory cytokine reported to mediate cartilage degradation in OA in vivo (380, 381). In this model, IL-1β upregulated the degradative enzymes MMP1 and MMP3 and downregulated the ECM proteins COL2A1 and aggrecan (380). This 3D system enabled the investigators to study the responses of chondrocytes to inflammatory cytokines; however, they neither tested the ability of the platform to evaluate the efficacy of anti-inflammatory effects of drugs in vitro nor addressed the integration of inflammatory immune cells such as macrophages in the system.

In a separate study, human cartilage exhibiting normal function—evident from expression of the key matrix proteins aggrecan and type II collagen—was engineered in vitro by culturing adult human knee chondrocytes for 4 weeks within a 3D scaffold fabricated from purified silk fibroin in a differentiation medium containing TGF-β1, insulin, transferrin, fetal bovine serum, and R3-IGF-1 (379). Addition of the proinflammatory cytokines TNF-α and IL-1β or of macrophage-conditioned medium increased expression of MMP1 and MMP3, consistent with observations of inflamed cartilage in vivo. One limitation of this study is that supraphysiologic levels of cytokines were used and the chondrocytes were not cocultured in direct contact with macrophages. Moreover, the macrophages were generated by stimulation of an acute monocytic leukemia cell line (THP-1) with lectin phytohemagglutinin, a nonspecific mitosis and activation inducer, rather than derivation from freshly isolated human primary monocytes. However, chondrocyte hypertrophy and loss of the sulfated glycosaminoglycans that are hallmarks of OA could be demonstrated in this model, whereas they are not observed in conventional 2D cultures (379).

SKIN

Psoriasis

Psoriasis is a highly prevalent inflammatory skin disease that is clinically characterized by erythrosquamous plaques, and it presents with inflammation, disturbed epidermal differentiation, and expression of SKALP/elafin, hBD2, and cytokeratin 6 (382). Traditionally, keratinocytes submerged under basal medium supplemented with growth factors such as ethanolamine, phospho-ethanolamine, bovine pituitary extract, insulin, hydrocortisone, and recombinant mouse epidermal growth factor (rEGF) in 2D culture have been widely used to study psoriasis in vitro (382–384); however, these systems lack the 3D microenvironment that is found in skin. More recently, significant progress has been made towards generating 3D engineered human skin tissue equivalents. For example, in one human skin model, de-epidermized dermis and primary adult human keratinocytes were submerged under medium for 4 days, and then the medium was removed and the cells were cultured at an air-liquid interface for an additional 10 days (382). These skin constructs exhibited normal, fully stratified epidermal tissue morphology and protein expression (e.g., high levels of cytokeratin 10), as seen in normal human skin in vivo. Importantly, when this engineered tissue was stimulated with inflammatory cytokines (IL-1α, TNF-α, and IL-6), a psoriasis-like phenotype was induced, as evidenced by elevated SKALP/elafin and hBD2 mRNA and protein levels. Immune cells also were introduced into this in vitro disease model by placing activated human CD4+ human T lymphocytes underneath the skin equivalent and allowing the cells to migrate toward the epidermis for 4 days (385). The T cells produced IFN-γ, TNF-α, and IL-17 and induced an activated inflammatory phenotype in keratinocytes, with elevated expression of proteins (e.g., cytokeratin 16, hBD2, elafin) that are upregulated in psoriatic tissues. Importantly, when the anti-inflammatory drugs all-*trans*-retinoic acid and cyclosporin A were added to the model, they reduced expression of psoriasis- and inflammation-associated markers in the keratinocytes (385).

INFECTIOUS DISEASES

According to the World Health Organization, infectious diseases are the leading cause of death worldwide. Some examples of in vitro infectious disease models have been described above in the context of specific organ systems, and Transwell inserts linked by differentiated tissue-specific cell monolayers are often used for this purpose (386–394). The 3D organoids that were used to study intestinal infection by *Salmonella* Typhimurium and norovirus, formed from human A549

lung epithelial cells that were cultured in ECM gels, also have been used to study *Pseudomonas aeruginosa* pathogenesis (395). These 3D cultures displayed more relevant differentiation markers than monolayer cultures, and interestingly, pathogenesis was less severe in the organoids, although they secreted more cytokines. When human 5637 uroepithelial cells maintained in 2D and 3D cultures were infected with the uropathogenic CP9 strain of *E. coli*, the infected cells grown in monolayer were quickly obliterated, whereas the organoids were much more resistant to infectious injury (396). Taken together, these studies suggest that various types of epithelial cells are much more sensitive to infection by pathogens when they are maintained in 2D cultures than when they are grown in 3D cultures that more closely mimic tissue differentiation and morphology observed in vivo. However, all of these studies used established cell lines, and thus, it will be important to determine whether similar results are obtained with human primary cells or iPSC-derived cells.

Microfluidic culture devices also have been used to model infections in vitro. Dynamic fluid flow was shown to enhance adenovirus infection of human fibroblasts when compared with static conditions (397). This flow-enhanced infectivity was leveraged to develop a higher-sensitivity assay for vesicular stomatitis virus infection (398). Other microfluidic systems have been used to study virus infection (188, 399); however, they have not yet been used to gain new mechanistic insight into viral pathogenesis or host-pathogen interactions. Enterohemorrhagic *E. coli* has been grown with a commensal *E. coli* biofilm that formed on HeLa cells cultured in a microfluidic device (177). This study revealed that the commensal biofilm microenvironment is a key determinant of enterohemorrhagic *E. coli* virulence.

Microfluidic devices containing very narrow microchannels have been used to investigate the rigidity of *Plasmodium falciparum*–infected red blood cells and the role of this parasite in capillary blockage (400). By varying the width of microchannels from 2 to 8 μm, the investigators showed that flowing uninfected or early ring infected red blood cells (8 μm in diameter) were highly elastic and could squeeze through the 2-μm channels. Trophozoite stages failed to freely traverse the 2- to 4-μm channels, and schizont forms blocked even the 6-μm channels. Interestingly, opposite results were found in *Plasmodium vivax*–infected red blood cells using a similar setup (401). A similar microfluidic model was used to reproduce the interaction between malaria-infected red blood cells and mammalian cells expressing ICAM-1 (402). These authors also modeled the phagocytosis of infected erythrocytes by macrophages and found evidence of phagocytosis of uninfected cells, consistent with human autopsy data.

CANCER

The lack of progress in finding effective treatments for cancer may be due, in part, to the lack of accurate models that mimic the biological processes that occur in patients with this disease. Conventional 2D cell cultures have provided great insight into the ability of tumor cells to grow, but they do not provide information about the complex interactions between the cancer cells and the physicochemical environment that exists within living tumors. For this reason, many groups have explored the use of 3D in vitro models, and more recently, microfluidic devices have been applied for this purpose as well. However, there are virtually as many different types of cancers as there are organs, and each of them displays distinct behaviors. Thus, below we provide a few pertinent examples of organ-specific in vitro models of cancer, as well as models of key processes, such as angiogenesis and metastasis, that are shared by all.

Lung

When human A549 lung tumor cells were grown in 3D decellularized lung matrix, they formed nodules that grew over time, and they produced MMPs similar to those seen in human lung cancer

patients; these responses were not observed in 2D culture (403). A microfluidic chip equipped with pneumatic microvalves was used to analyze the paracrine loop between human CL1-0 lung adenocarcinoma cells and human fibroblasts. Cytokines from the cancer cells stimulated the fibroblasts to transform into myofibroblasts, which specifically produced cytokines that increased the migration speed of the cancer cells (404). A549 lung alveolar epithelial cells originally isolated from a human lung tumor were cultured in a microfluidic device with growth medium and the anticancer drug tirapazamine under various oxygen gradients. These studies demonstrated enhancement of drug-induced cancer cell killing by hypoxia in vitro (405).

Breast

Breast cancer is often modeled in vitro using multicellular tumor spheroids, which are derived from a collection of cells that aggregate under nonadherent culture conditions, or when placed in ECM gels, to form 3D cellular masses in vitro. For example, normal breast epithelial cells form hollow spheroids lined by polarized epithelium and surrounded by a basement membrane when cultured in 3D ECM gels, whereas breast cancer cells form spheroids composed of solid masses of disorganized cells that lack polarity or a continuous basement membrane. Thus, the morphology and growth kinetics, as well as cell-cell and cell-ECM interactions, within these spheroids resemble those of tumor nodules, making them potentially valuable models of tumor initiation and growth (406). This system has been leveraged, for example, to manipulate expression of potentially cancer-relevant genes and then to determine whether those genes alter the ability of malignant MDA-MB-468 breast cancer cells or nonmalignant MCF-10A cells to undergo acinar morphogenesis (407, 408). In another recent study, gene network reverse engineering approaches were used to identify genes that had a high likelihood of being causally involved in cancer progression in a mouse transgenic breast cancer model, and then these genes were silenced using siRNA in mouse breast tumor cells grown as spheroids in 3D ECM gels. This study led to the discovery that the *HoxA1* gene can induce breast cancer cells to reduce their growth, restore normal epithelial polarization, induce accumulation of basement membrane, and undergo acinar differentiation in vitro (409). Importantly, when this same siRNA bound to nanoparticles was delivered through the nipple into the breast ducts in the young transgenic mice, suppression of this gene was sufficient to prevent breast cancer development even though cancer formation was still driven by an active oncogene encoding SV40 T antigen in this model (409).

Phenotypes representative of malignant and benign breast tumors can be recapitulated in vitro by controlling cell-microenvironment interactions through modulation of β_1 integrin signaling, which is aberrantly expressed in human breast carcinomas and is thought to play a central role in cancer cell growth, apoptosis, invasion, and metastasis (410). Using a laminin-rich gel, investigators found that inhibition β_1 integrin in malignant human MDA-MB-231 breast cancer cells resulted in cell death and phenotypic reversion of malignancy. In contrast, nonmalignant HMT-3522-S-1 cells that formed tissue-like structures remained unaffected by β_1 integrin inhibition, and similar results were observed in in vivo mouse models (411–413). The reversibility of the breast cancer phenotype was also demonstrated in 3D ECM gels by combining mouse breast cancer cells with embryonic mesenchyme or ECM components, such as biglycan, that are deposited by these cells, which retain the ability to induce partial breast cancer reversion in vitro and in vivo (414).

Microfluidic devices have been used to investigate breast epithelial tumor cell–stroma interactions. For example, the laminar flow properties of microfluidic devices (which prevent mixing of neighboring flow streams) have been leveraged to compartmentalize human mammary fibroblasts in an ECM gel side-by-side with another ECM gel containing breast ductal carcinoma in situ cells; this setup enabled an investigation of the role of stromal interactions in the transition to

invasive ductal carcinoma (415). This study revealed that the fibroblasts had to be in direct contact with the tumor cells to induce the transition to the invasive phenotype. In another study using the same method, metastatic MDA-MB-231 breast cancer cells and RAW 264.1 macrophage cells were placed within neighboring ECM gels composed of type I collagen and Matrigel, respectively. In this system, the RAW 264.1 cells invaded the gels when the breast cancer cells were cultured within them, but not when the cells were absent (416).

Brain

A key aspect of this aggressive and persistent form of cancer is the high degree of vascularization of the tumor, and for this reason, many in vitro brain cancer studies focus on interactions between cancer cells and endothelial cells. To study these interactions, a microfluidic device was created with multiple parallel channels: a central channel filled with fibrin matrix, surrounded by two fluidic channels, which were in turn adjacent to stromal cell culture channels. Human umbilical vascular endothelial cells that were seeded through one fluidic channel adhered to the exposed surface of the central fibrin gel. When highly malignant human U87MG glioblastoma multiforme cells were cultured in the stromal cell culture channel on the opposite side of the fibrin gel, the endothelial cells invaded the fibrin matrix within 24 h, apparently in response to the U87MG-derived factors. Interestingly, the vascular sprouts did not grow in a direct path toward U87MG cells, and instead, some sprouts appeared convoluted and aberrantly fused with adjacent vessels, resulting in the formation of vascular patterns resembling those observed in certain brain tumors in vivo (417).

Colon

Human LS174T colon carcinoma cells that were first cultured as spheroids have been cultured in microfluidic devices and exposed continuously to flowing medium to mimic chemical gradients surrounding blood vessels in the tumor microenvironment. This device was used to characterize the transport differences between a passively diffusing therapeutic (doxorubicin) and actively penetrating vectors (*Salmonella* bacteria). The ability to quantify diffusion resistance will be essential for developing and tuning new tumor-penetrating therapeutics (nanoparticles, nanotherapeutics) (418).

Liver

A chitosan-alginate scaffold has been used to show accelerated growth of hepatocellular carcinoma–derived cell lines in mouse models, as well as increased chemotherapy resistance in vitro compared with conventional cultures (419). Comparison of hepatocellular carcinoma–derived cell lines in static cultures versus dynamic microfluidic cultures has revealed that flow conditions support gene and protein expression patterns more reminiscent of cells in the periportal zone of the liver, whereas the cells in static culture display a perivenous-like phenotype (420). Distant metastases are the major cause of cancer mortality, and the liver is a highly metastasis-permissive organ. Microreactors combining human hepatocytes and nonparenchymal liver cells were used to support the growth of prostate and breast cancer cell lines as well as primary breast cancer explants, which in some cases were not supported by static cultures (421, 422).

Hematologic Cancers

Primary multiple myeloma (MM) has been difficult to propagate ex vivo because these cells require the bone marrow microenvironment to grow (423). To sustain MM cell growth in vitro, a 3D culture model was developed that reconstituted the composition of the in vivo bone

marrow microenvironment (424). To mimic the bone marrow matrix, an endosteal niche was reconstructed by surface coating with a mixture of type I collagen and fibronectin and then overlaying bone marrow cells suspended in a mixture of fibronectin and Matrigel; this system supported proliferation of MM cells in vitro. To recapitulate interactions between MM cells and the osteoblast niche, a microfluidic 3D culture system was developed that uses 3D ossified tissue constructed from osteoblast cells cultured within a perfused microfluidic device to recreate the endosteal surface (425). Importantly, primary MM cells could be propagated in vitro by directly culturing bone marrow mononuclear cells from MM patient biopsies in this device, which confirms that the endosteal layer is critical for MM cell proliferation.

Biomimetic scaffolds have been developed to maintain leukemia cell growth in vitro; for example, an osteoblast niche was engineered to maintain chronic myelogenous leukemia (CML) cells in vitro (426). In this system, marrow mesenchymal stem cells from CML patients were cultured on decellularized human bone and induced to undergo osteoblast differentiation to recreate the osteoblastic niche where leukemic stem cells normally reside. This biomimetic culture system was able to maintain primitive CML stem and progenitor cells and to retain their proliferating potential in vitro for a longer period of time (more than 5 weeks) than is possible in 2D stroma-supported cultures. Polymeric scaffolds with a high porosity that were fabricated and coated with type I collagen and fibronectin to mimic the bone marrow (427) can maintain acute myeloid leukemia cells in vitro for over 6 weeks in the absence of exogenous growth factors. When bone marrow stromal cells and leukemic cells were cultured in these 3D scaffolds, the tumor cells were more resistant to drug-induced apoptosis compared with cells in 2D cultures (428).

Angiogenesis

Tumor angiogenesis is the growth of new capillaries that are required for supplying nutrients and oxygen and removing waste products and hence are necessary for the growth and expansion of solid tumors. Due to its inherent complexity and the involvement of flow, many microfluidic models have been developed to study angiogenesis in vitro. Biodegradable microfluidic devices composed entirely of ECM have been developed by using photolithographic and replica molding methods to fabricate internal networks of microchannels filled with sacrificial material (sugar crystals) that are dissolved prior to seeding cells in the device. This model is interesting because endothelial cells may be plated inside the channels while tumor cells are grown within the surrounding 3D ECM (429, 430), and all the structures within the system have well-defined and controllable geometries. This property is significant because, for the first time, the relationship between the geometry of the initial (unsprouted) vessel and the location of the source of vessel growth factor signals could be controlled and explored. It was found that vessel geometries and the location of the source of growth factors (and, thus, the resulting diffusion patterns) dictate the location and morphology of 3D, sprouting endothelial cells, and that these parameters also influence the ability of angiogenic inhibitors to antagonize the formation of filopodia.

Other on-chip angiogenesis models generate functional capillary networks that sprout freely within a 3D matrix of stroma and ECM (431–433). Importantly, these in vitro angiogenesis models enable high-resolution analysis and have provided new insights into the molecular mechanisms of angiogenesis inhibitors, including how spatial patterns of diffusive gradients influence the position of angiogenic sprouting (429–433).

The power of microfluidic systems—namely, the ability to multiplex—has been employed to develop nearly identical human microtissues containing vascularized networks in a parallelized PDMS platform. The fluidic layout, which connects the microtissue chambers, was designed using a circuit analog such that each chamber may be observed in series or in parallel with respect

to other chambers. This capability provides precise control of the chemical (e.g., growth factors) and mechanical (pressure) microenvironment. Modulating the interstitial pressure greatly affects the growth characteristics of sprouting vessels, a phenomenon that has been observed during tumor angiogenesis in vivo but had not previously been recapitulated in vitro. Thus, the effects of multiple microenvironmental variations on angiogenic responses can now be multiplexed and studied on a single chip, providing a large amount of insight into the process of microenvironmental perturbation to pathology in a short amount of time (434).

Metastasis

Cancer metastasis involves physical invasion of cancer cells through their natural tissue boundary (e.g., basement membrane), translocation through the interstitium, intravasation into the bloodstream or lymphatics, circulation through the body, adhesion and extravasation out of a distant blood vessel or lymphatic, and implantation into the interstitium of a distant site, where new growth of the cells leads to a secondary, metastatic lesion. Recently, there has been a transition from using static transmigration chambers to analyze tumor cell migration in vitro to using more sophisticated microfluidic devices, which permit analysis of more complex interactions between tumor cells and other cells, as well as ECM, under physiological flow conditions. For example, a microfluidics-based in vitro assay was developed that enables real-time visualization and quantification of interactions between tumor cells and endothelial cells to mimic physiological processes involved in tumor cell intravasation. Studies with highly invasive fibrosarcoma cells revealed that treatment of the endothelium with TNF-α results in a higher number of tumor–endothelial cell binding interactions with faster dynamics, providing evidence that the endothelium poses a barrier to tumor cell intravasation that can be regulated by factors present in the tumor microenvironment (435).

Prior to extravasation, tumor cells are believed to undergo mechanical deformation as they squeeze through small capillaries before adhering to the endothelium and transmigrating through the underlying basement membrane. This process was modeled in a microfluidic device by flowing tumor cells through small (10 μm in diameter) channels of variable length; the more mechanical strain a tumor cell experienced, the greater was its ability to adhere to the endothelium and the higher its migration rate (436). Moreover, similar results were obtained with three different types of cancer cell lines (HepG2 liver, HeLa cervical, and MDA-MB-435S breast), suggesting that this may a fundamental response involved in tumor cell extravasation. In a separate study, MDA-MB-231 breast cancer cells were flowed through the top channel of a two-layered microfluidic device in which a 0.4-μm polyester membrane separated the channels and the top of the membrane was lined with endothelium; cytokines also were flowed through the lower channel to simulate the presence or absence of stimulants. This study reproduced the preferential adhesion of circulating cancer cells to endothelium in organs and tissues that express high levels of CXCL12, as has been observed in vivo (437).

Bone is the most common site for metastasis, and advanced breast and prostate cancer patients almost always develop bone metastases. A microfluidic 3D culture model has been developed to analyze the specificity of human breast cancer metastases to bone by recreating a vascularized bone-like microenvironment (**Figure 8**) (438). Osteodifferentiated human bone marrow–derived mesenchymal stem cells were mixed with collagen solution, introduced into a microfluidic channel, and gelled; 3 days later, endothelial cells were seeded in the adjacent channel, separated by posts, to create a monolayer covering the adjacent channel walls and the gel-channel interfaces. When human breast cancer cells were injected into the channel, it was possible to quantitate tumor cell extravasation and micrometastasis generation within a bone-like microenvironment in vitro. These
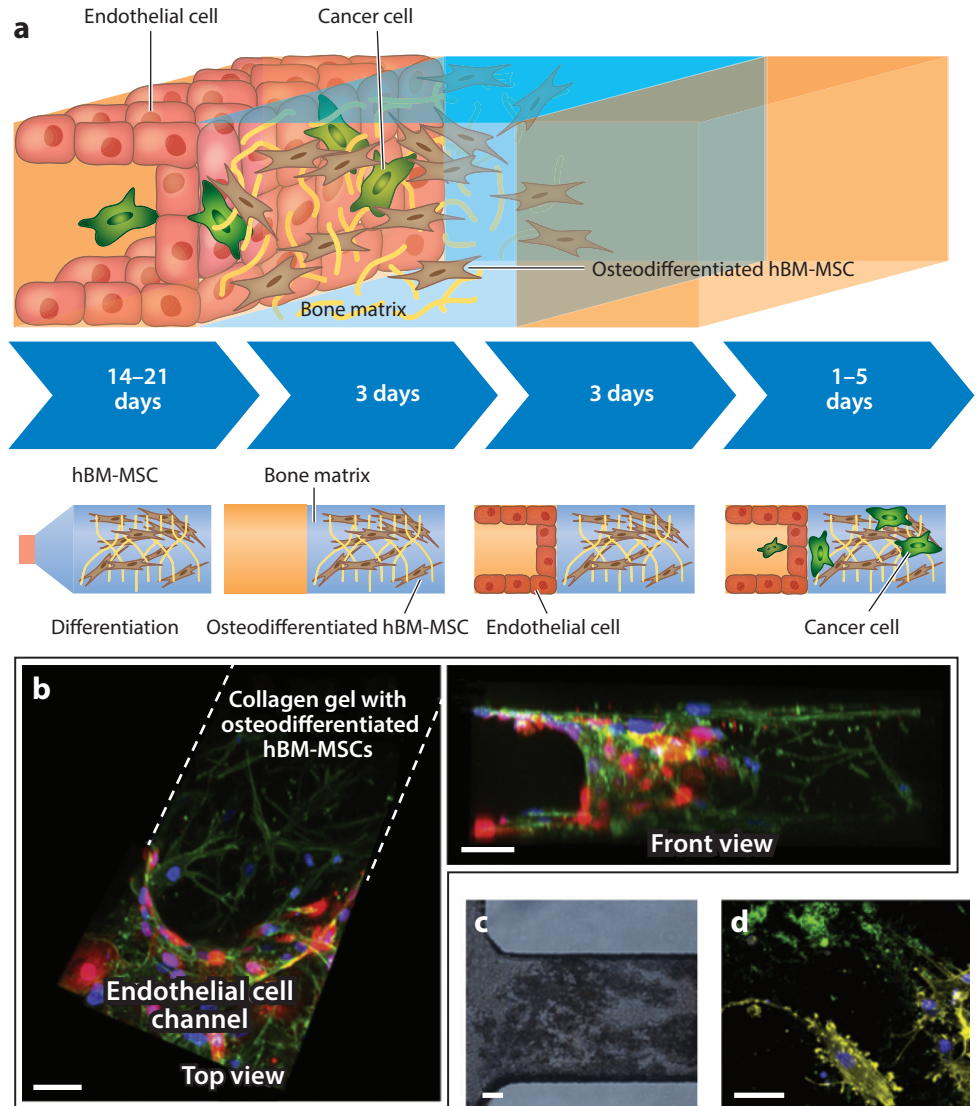
Figure 8

Microengineered cancer metastasis model. (*a*) Osteodifferentiated human bone marrow–derived mesenchymal stem cells (hBM-MSCs) (*brown*) were mixed with a collagen solution and gelled within a microfluidic device. Endothelial cells (*red*) were seeded 3 days later to generate a monolayer covering the channel walls and the gel-channel interfaces. Cancer cells (*green*) were introduced into the channel after 3 additional days of culture, and their extravasation ability and metastasis capacity were monitored for up to 5 days. (*b*) Top and front fluorescent microscopic views of the microfluidic device, showing that endothelial cells (transfected with red fluorescent protein) completely covered the channel walls while the osteodifferentiated hBM-MSCs were homogeneously distributed within the collagen gel; cells were stained with DAPI (*blue*) and phalloidin (*green*). (*c*) Alizarin red staining of calcium deposits (*dark regions*) within a collagen gel in which the osteodifferentiated hBM-MSCs were cultured. (*d*) Fluorescent microscopic views showing that the osteodifferentiated hBM-MSCs secreted osteocalcin (*yellow*) in the 3D microenvironment (DAPI, *blue*; phalloidin, *green*). All scale bars are 50 μm. Figure modified with permission from Reference 438.

studies demonstrated that coculture of cancer cells with osteoblast-like cells significantly increases drug resistance, invasiveness, and angiogenic potential (439–441). Furthermore, the cancer cells were observed to self-organize into microcolonies in these cultures, and this process was associated with a reduction in osteoblastic tissue thickness as well as an increase in osteoclastogenesis, reminiscent of the vicious cycle of bone metastasis observed in vivo (441).

CONCLUSION

The inability of animal models to faithfully mimic many human diseases, combined with the desire to be able to study disease under controlled conditions, has led to the emergence of a new field at the intersection between pathology and tissue engineering that is focused on creation of in vitro disease models. Models have been created that can be used to study facets of a large range of different diseases that occur in virtually every organ system of the body. Many of these models are still relatively simple; for example, Transwell inserts that merely permit culture of cells at an air-liquid interface or culture of two different cell types separated by a porous membrane probably remain the most commonly used experimental system. However, increasingly complex and sophisticated models of human tissues and organs are being engineered and modified to create unique disease models. A simple example is the way in which advances in our ability to engineer heart tissues, and to measure electrical conduction as well as quantitate contractile stresses in real time while carrying out high-resolution imaging in vitro, have opened up entirely new ways to study how disease processes influence these structures and functions.

The application of microfabrication techniques has permitted construction of microfluidic systems with complex functionalities such that it is now possible to recapitulate organ-level structures and to study, for example, how the alveolar-capillary interface of the lung responds to infectious microbes or toxic particulates in vitro while immune cells are flowed simultaneously through a capillary endothelium-lined vascular channel. Although these systems are still simplified, they have led to new insights into the contribution of the mechanical microenvironment to disease (e.g., pulmonary edema). Given that mechanical, chemical, and cellular components can be manipulated individually in these engineered systems, greater insights are likely to come as more researchers embrace these technologies. Although most of the current in vitro disease models utilize nonhuman cells or established human cell lines, primary cells and iPSC-derived cells isolated from diseased patients and healthy cohorts are starting to be integrated into these systems. This combination of tissue engineering with stem cell engineering has led to the development of new models of neurological and heart disorders, for example, that recapitulate some of the hallmarks of human disease. It also could be used in the future for personalized medicine and to enable personalized pathological investigations using living organ mimics rather than histological samples of fixed organs.

Numerous challenges remain, however, because many diseases are chronic in nature, involve complex interactions between different organs, and manifest at the whole-organism level. It will be difficult to model all of these factors, but it might be possible to establish long-term cultures (e.g., using controlled microperfusion devices in bioreactors or microfluidic devices) that could recapitulate central features of particular chronic diseases. Given the key role of recruitment of circulating immune cell and inflammatory responses in disease etiology, it is critical that these components be integrated into engineered in vitro disease models, an achievement that is now possible using microfluidic organ-on-a-chip devices. The function of all organs is also regulated by humoral, neurogenic, and metabolic factors that can be accounted for only in whole-animal models. That said, there are ongoing efforts in the organs-on-chips field focused on linking multiple different engineered organs via fluidic coupling of their vascular channels to create a "human

body–on–a–chip," which could potentially be used to mimic some key features of system-level disease states.

Because of their potential to faithfully mimic the functions of normal human tissues and organs and to enable a new form of personalized medicine, engineered tissues and organs-on-chips have captured the attention of the medical, pharmaceutical, chemical, and cosmetics industries as well as government regulatory agencies (e.g., the US Food and Drug Administration and the US Environmental Protection Agency). On the basis of the accomplishments we have reviewed here, we believe that there is great potential to advance fundamental research into disease mechanisms and to revolutionize clinical pathology as well.

DISCLOSURE STATEMENT

LITERATURE CITED

1. Seok J, Warren HS, Cuenca AG, Mindrinos MN, Baker HV, et al. 2013. Genomic responses in mouse models poorly mimic human inflammatory diseases. *PNAS* 110:3507–12
2. Takahashi K, Yamanaka S. 2006. Induction of pluripotent stem cells from mouse embryonic and adult fibroblast cultures by defined factors. *Cell* 126:663–76
3. Takahashi K, Tanabe K, Ohnuki M, Narita M, Ichisaka T, et al. 2007. Induction of pluripotent stem cells from adult human fibroblasts by defined factors. *Cell* 131:861–72
4. Yu JY, Vodyanik MA, Smuga-Otto K, Antosiewicz-Bourget J, Frane JL, et al. 2007. Induced pluripotent stem cell lines derived from human somatic cells. *Science* 318:1917–20
5. Ieda M, Fu JD, Delgado-Olguin P, Vedantham V, Hayashi Y, et al. 2010. Direct reprogramming of fibroblasts into functional cardiomyocytes by defined factors. *Cell* 142:375–86
6. Pang ZP, Yang N, Vierbuchen T, Ostermeier A, Fuentes DR, et al. 2011. Induction of human neuronal cells by defined transcription factors. *Nature* 476:220–23
7. Son EY, Ichida JK, Wainger BJ, Toma JS, Rafuse VF, et al. 2011. Conversion of mouse and human fibroblasts into functional spinal motor neurons. *Cell Stem Cell* 9:205–18
8. Singhvi R, Kumar A, Lopez G, Stephanopoulos GN, Wang DIC, et al. 1994. Engineering cell shape and function. *Science* 264:696–98
9. Chen CS, Mrksich M, Huang S, Whitesides G, Ingber DE. 1997. Geometric control of cell life and death. *Science* 276:1425–28
10. Derda R, Musah S, Orner BP, Klim JR, Li L, Kiessling LL. 2010. High-throughput discovery of synthetic surfaces that support proliferation of pluripotent cells. *J. Am. Chem. Soc.* 132:1289–95
11. Musah S, Morin SA, Wrighton PJ, Zwick DB, Jin S, Kiessling LL. 2012. Glycosaminoglycan-binding hydrogels enable mechanical control of human pluripotent stem cell self-renewal. *ACS Nano* 6:10168–77
12. Shin SR, Jung SM, Zalabany M, Kim K, Zorlutuna P, et al. 2013. Carbon-nanotube-embedded hydrogel sheets for engineering cardiac constructs and bioactuators. *ACS Nano* 7:2369–80
13. Martin I, Wendt D, Heberer M. 2004. The role of bioreactors in tissue engineering. *Trends Biotechnol.* 22:80–86
14. Huh D, Kim HJ, Fraser JP, Shea DE, Khan M, et al. 2013. Microfabrication of human organs-on-chips. *Nat. Protoc.* 8:2135–57
15. Kolesky DB, Truby RL, Gladman AS, Busbee TA, Homan KA, Lewis JA. 2014. 3D bioprinting of vascularized, heterogeneous cell-laden tissue constructs. *Adv. Mater.* 26:3124–30
16. Yadid M, Sela G, Amiad Pavlov D, Landesberg A. 2011. Adaptive control of cardiac contraction to changes in loading: from theory of sarcomere dynamics to whole-heart function. *Pflügers Arch.* 462:49–60

17. Itzhaki I, Maizels L, Huber I, Zwi-Dantsis L, Caspi O, et al. 2011. Modelling the long QT syndrome with induced pluripotent stem cells. *Nature* 471:225–29

18. Moretti A, Bellin M, Welling A, Jung CB, Lam JT, et al. 2010. Patient-specific induced pluripotent stem-cell models for long-QT syndrome. *N. Engl. J. Med.* 363:1397–409

19. Davis RP, Casini S, van den Berg CW, Hoekstra M, Remme CA, et al. 2012. Cardiomyocytes derived from pluripotent stem cells recapitulate electrophysiological characteristics of an overlap syndrome of cardiac sodium channel disease. *Circulation* 125:3079–91

20. Jung CB, Moretti A, Mederos y Schnitzler M, Iop L, Storch U, et al. 2012. Dantrolene rescues arrhythmogenic RYR2 defect in a patient-specific stem cell model of catecholaminergic polymorphic ventricular tachycardia. *EMBO Mol. Med.* 4:180–91

21. Sun N, Yazawa M, Liu J, Han L, Sanchez-Freire V, et al. 2012. Patient-specific induced pluripotent stem cells as a model for familial dilated cardiomyopathy. *Sci. Transl. Med.* 4:130ra47

22. Morita H, Seidman J, Seidman CE. 2005. Genetic causes of human heart failure. *J. Clin. Investig.* 115:518–26

23. Hajjar RJ, Zsebo K, Deckelbaum L, Thompson C, Rudy J, et al. 2008. Design of a phase 1/2 trial of intracoronary administration of AAV1/SERCA2a in patients with heart failure. *J. Card. Fail.* 14:355–67

24. Seidman JG, Seidman C. 2001. The genetic basis for cardiomyopathy: from mutation identification to mechanistic paradigms. *Cell* 104:557–67

25. Maron BJ. 2002. Hypertrophic cardiomyopathy: a systematic review. *JAMA* 287:1308–20

26. Lan F, Lee AS, Liang P, Sanchez-Freire V, Nguyen PK, et al. 2013. Abnormal calcium handling properties underlie familial hypertrophic cardiomyopathy pathology in patient-specific induced pluripotent stem cells. *Cell Stem Cell* 12:101–13

27. Burridge PW, Keller G, Gold JD, Wu JC. 2012. Production of de novo cardiomyocytes: human pluripotent stem cell differentiation and direct reprogramming. *Cell Stem Cell* 10:16–28

28. Thomas SP, Kucera JP, Bircher-Lehmann L, Rudy Y, Saffitz JE, Kleber AG. 2003. Impulse propagation in synthetic strands of neonatal cardiac myocytes with genetically reduced levels of connexin43. *Circ. Res.* 92:1209–16

29. Beauchamp P, Choby C, Desplantez T, de Peyer K, Green K, et al. 2004. Electrical propagation in synthetic ventricular myocyte strands from germline connexin43 knockout mice. *Circ. Res.* 95:170–78

30. Beauchamp P, Desplantez T, McCain ML, Li W, Asimaki A, et al. 2012. Electrical coupling and propagation in engineered ventricular myocardium with heterogeneous expression of connexin43. *Circ. Res.* 110:1445–53

31. Alford PW, Feinberg AW, Sheehy SP, Parker KK. 2010. Biohybrid thin films for measuring contractility in engineered cardiovascular muscle. *Biomaterials* 31:3613–21

32. Bursac N, Parker KK, Iravanian S, Tung L. 2002. Cardiomyocyte cultures with controlled macroscopic anisotropy: a model for functional electrophysiological studies of cardiac muscle. *Circ. Res.* 91:E45–54

33. Grosberg A, Alford PW, McCain ML, Parker KK. 2011. Ensembles of engineered cardiac tissues for physiological and pharmacological study: heart on a chip. *Lab Chip* 11:4165–73

34. McCain ML, Parker KK. 2011. Mechanotransduction: the role of mechanical stress, myocyte shape, and cytoskeletal architecture on cardiac function. *Pflügers Arch.* 462:89–104

35. Pong T, Adams WJ, Bray MA, Feinberg AW, Sheehy SP, et al. 2011. Hierarchical architecture influences calcium dynamics in engineered cardiac muscle. *Exp. Biol. Med.* 236:366–73

36. Kim DH, Lipke EA, Kim P, Cheong R, Thompson S, et al. 2010. Nanoscale cues regulate the structure and function of macroscopic cardiac tissue constructs. *PNAS* 107:565–70

37. Chung CY, Bien H, Sobie EA, Dasari V, McKinnon D, et al. 2011. Hypertrophic phenotype in cardiac cell assemblies solely by structural cues and ensuing self-organization. *FASEB J.* 25:851–62

38. Desplantez T, McCain ML, Beauchamp P, Rigoli G, Rothen-Rutishauser B, et al. 2012. Connexin43 ablation in foetal atrial myocytes decreases electrical coupling, partner connexins, and sodium current. *Cardiovasc. Res.* 94:58–65

39. Chang MG, Zhang YB, Chang CY, Xu LM, Emokpae R, et al. 2009. Spiral waves and reentry dynamics in an in vitro model of the healed infarct border zone. *Circ. Res.* 105:1062–71

40. Ursell PC, Gardner PI, Albala A, Fenoglio JJ, Wit AL. 1985. Structural and electrophysiological changes in the epicardial border zone of canine myocardial infarcts during infarct healing. *Circ. Res.* 56:436–51

41. Saffitz JE. 2000. Regulation of intercellular coupling in acute and chronic heart disease. *Braz. J. Med. Biol. Res.* 33:407–13

42. Brown RD, Ambler SK, Mitchell MD, Long CS. 2005. The cardiac fibroblast: therapeutic target in myocardial remodeling and failure. *Annu. Rev. Pharmacol. Toxicol.* 45:657–87

43. Thompson SA, Copeland CR, Reich DH, Tung L. 2011. Mechanical coupling between myofibroblasts and cardiomyocytes slows electric conduction in fibrotic cell monolayers. *Circulation* 123:2083–93

44. Dobaczewski M, Bujak M, Zymek P, Ren G, Entman ML, Frangogiannis NG. 2006. Extracellular matrix remodeling in canine and mouse myocardial infarcts. *Cell Tissue Res.* 324:475–88

45. Souders CA, Bowers SL, Baudino TA. 2009. Cardiac fibroblast: the renaissance cell. *Circ. Res.* 105:1164–76

46. Rohr S. 2012. Arrhythmogenic implications of fibroblast-myocyte interactions. *Circ. Arrhythm. Electrophysiol.* 5:442–52

47. Thompson SA, Blazeski A, Copeland CR, Cohen DM, Chen CS, et al. 2014. Acute slowing of cardiac conduction in response to myofibroblast coupling to cardiomyocytes through N-cadherin. *J. Mol. Cell. Cardiol.* 68:29–37

48. Boulaksil M, Winckel SK, Engelen MA, Stein M, van Veen TA, et al. 2010. Heterogeneous Connexin43 distribution in heart failure is associated with dispersed conduction and enhanced susceptibility to ventricular arrhythmias. *Eur. J. Heart Fail.* 12:913–21

49. Kitamura H, Ohnishi Y, Yoshida A, Okajima K, Azumi H, et al. 2002. Heterogeneous loss of connexin43 protein in nonischemic dilated cardiomyopathy with ventricular tachycardia. *J. Cardiovasc. Electrophysiol.* 13:865–70

50. Gutstein DE, Morley GE, Vaidya D, Liu F, Chen FL, et al. 2001. Heterogeneous expression of gap junction channels in the heart leads to conduction defects and ventricular dysfunction. *Circulation* 104:1194–99

51. Feinberg AW, Feigel A, Shevkoplyas SS, Sheehy S, Whitesides GM, Parker KK. 2007. Muscular thin films for building actuators and powering devices. *Science* 317:1366–70

52. McCain ML, Sheehy SP, Grosberg A, Goss JA, Parker KK. 2013. Recapitulating maladaptive, multiscale remodeling of failing myocardium on a chip. *PNAS* 110:9770–75

53. Gomez AM, Valdivia HH, Cheng H, Lederer MR, Santana LF, et al. 1997. Defective excitation-contraction coupling in experimental cardiac hypertrophy and heart failure. *Science* 276:800–6

54. Piacentino V III, Weber CR, Chen X, Weisser-Thomas J, Margulies KB, et al. 2003. Cellular basis of abnormal calcium transients of failing human ventricular myocytes. *Circ. Res.* 92:651–58

55. Eschenhagen T, Fink C, Remmers U, Scholz H, Wattchow J, et al. 1997. Three-dimensional reconstitution of embryonic cardiomyocytes in a collagen matrix: a new heart muscle model system. *FASEB J.* 11:683–94

56. Zimmermann WH, Fink C, Kralisch D, Remmers U, Weil J, Eschenhagen T. 2000. Three-dimensional engineered heart tissue from neonatal rat cardiac myocytes. *Biotechnol. Bioeng.* 68:106–14

57. Tobita K, Liu LJ, Janczewski AM, Tinney JP, Nonemaker JM, et al. 2006. Engineered early embryonic cardiac tissue retains proliferative and contractile properties of developing embryonic myocardium. *Am. J. Physiol. Heart Circ. Physiol.* 291:H1829–37

58. Ralphe JC, de Lange WJ. 2013. 3D engineered cardiac tissue models of human heart disease: learning more from our mice. *Trends Cardiovasc. Med.* 23:27–32

59. Hansen A, Eder A, Bonstrup M, Flato M, Mewe M, et al. 2010. Development of a drug screening platform based on engineered heart tissue. *Circ. Res.* 107:35–44

60. Stohr A, Friedrich FW, Flenner F, Geertz B, Eder A, et al. 2013. Contractile abnormalities and altered drug response in engineered heart tissue from Mybpc3-targeted knock-in mice. *J. Mol. Cell. Cardiol.* 63:189–98

61. Vignier N, Schlossarek S, Fraysse B, Mearini G, Kramer E, et al. 2009. Nonsense-mediated mRNA decay and ubiquitin-proteasome system regulate cardiac myosin-binding protein C mutant levels in cardiomyopathic mice. *Circ. Res.* 105:239–48

62. Fraysse B, Weinberger F, Bardswell SC, Cuello F, Vignier N, et al. 2012. Increased myofilament Ca^{2+} sensitivity and diastolic dysfunction as early consequences of Mybpc3 mutation in heterozygous knock-in mice. *J. Mol. Cell. Cardiol.* 52:1299–307

63. Pohlmann L, Kroger I, Vignier N, Schlossarek S, Kramer E, et al. 2007. Cardiac myosin-binding protein C is required for complete relaxation in intact myocytes. *Circ. Res.* 101:928–38

64. de Lange WJ, Hegge LF, Grimes AC, Tong CW, Brost TM, et al. 2011. Neonatal mouse-derived engineered cardiac tissue: a novel model system for studying genetic heart disease. *Circ. Res.* 109:8–19

65. Radisic M, Park H, Gerecht S, Cannizzaro C, Langer R, Vunjak-Novakovic G. 2007. Biomimetic approach to cardiac tissue engineering. *Philos. Trans. R. Soc. B* 362:1357–68

66. Song H, Zandstra PW, Radisic M. 2011. Engineered heart tissue model of diabetic myocardium. *Tissue Eng. A* 17:1869–78

67. Katare RG, Ando M, Kakinuma Y, Sato T. 2010. Engineered heart tissue: a novel tool to study the ischemic changes of the heart in vitro. *PLOS ONE* 5:e9275

68. Ando M, Katare RG, Kakinuma Y, Zhang D, Yamasaki F, et al. 2005. Efferent vagal nerve stimulation protects heart against ischemia-induced arrhythmias by preserving connexin43 protein. *Circulation* 112:164–70

69. Katare RG, Ando M, Kakinuma Y, Arikawa M, Handa T, et al. 2009. Vagal nerve stimulation prevents reperfusion injury through inhibition of opening of mitochondrial permeability transition pore independent of the bradycardiac effect. *J. Thorac. Cardiovasc. Surg.* 137:223–31

70. Kakinuma Y, Ando M, Kuwabara M, Katare RG, Okudela K, et al. 2005. Acetylcholine from vagal stimulation protects cardiomyocytes against ischemia and hypoxia involving additive non-hypoxic induction of HIF-1α. *FEBS Lett.* 579:2111–18

71. Mosadegh B, Dabiri BE, Lockett MR, Derda R, Campbell P, et al. 2014. Three-dimensional paper-based model for cardiac ischemia. *Adv. Healthc. Mater.* 3:1036–43

72. Deiss F, Mazzeo A, Hong E, Ingber DE, Derda R, Whitesides GM. 2013. Platform for high-throughput testing of the effect of soluble compounds on 3D cell cultures. *Anal. Chem.* 85:8085–94

73. Derda R, Laromaine A, Mammoto A, Tang SK, Mammoto T, et al. 2009. Paper-supported 3D cell culture for tissue-based bioassays. *PNAS* 106:18457–62

74. Derda R, Tang SK, Laromaine A, Mosadegh B, Hong E, et al. 2011. Multizone paper platform for 3D cell cultures. *PLOS ONE* 6:e18940

75. Ma Z, Koo S, Finnegan MA, Loskill P, Huebsch N, et al. 2014. Three-dimensional filamentous human diseased cardiac tissue model. *Biomaterials* 35:1367–77

76. Koroleva A, Gill AA, Ortega I, Haycock JW, Schlie S, et al. 2012. Two-photon polymerization-generated and micromolding-replicated 3D scaffolds for peripheral neural tissue engineering applications. *Biofabrication* 4:025005

77. Hinton RB Jr, Lincoln J, Deutsch GH, Osinska H, Manning PB, et al. 2006. Extracellular matrix remodeling and organization in developing and diseased aortic valves. *Circ. Res.* 98:1431–38

78. Butcher JT, Mahler GJ, Hockaday LA. 2011. Aortic valve disease and treatment: the need for naturally engineered solutions. *Adv. Drug Deliv. Rev.* 63:242–68

79. Brinkley DM, Gelfand EV. 2013. Valvular heart disease: classic teaching and emerging paradigms. *Am. J. Med.* 126:1035–42

80. Liu AC, Joag VR, Gotlieb AI. 2007. The emerging role of valve interstitial cell phenotypes in regulating heart valve pathobiology. *Am. J. Pathol.* 171:1407–18

81. Rajamannan NM, Evans FJ, Aikawa E, Grande-Allen KJ, Demer LL, et al. 2011. Calcific aortic valve disease: not simply a degenerative process. A review and agenda for research from the National Heart and Lung and Blood Institute Aortic Stenosis Working Group. Executive summary: calcific aortic valve disease—2011 update. *Circulation* 124:1783–91

82. Yip CY, Simmons CA. 2011. The aortic valve microenvironment and its role in calcific aortic valve disease. *Cardiovasc. Pathol.* 20:177–82

83. Wylie-Sears J, Aikawa E, Levine RA, Yang JH, Bischoff J. 2011. Mitral valve endothelial cells with osteogenic differentiation potential. *Arterioscler. Thromb. Vasc. Biol.* 31:598–607

84. Gould ST, Srigunapalan S, Simmons CA, Anseth KS. 2013. Hemodynamic and cellular response feedback in calcific aortic valve disease. *Circ. Res.* 113:186–97

85. van der Linde D, Konings EEM, Slager MA, Witsenburg M, Helbing WA, et al. 2011. Birth prevalence of congenital heart disease worldwide: a systematic review and meta-analysis. *J. Am. Coll. Cardiol.* 58:2241–47

86. Sider KL, Blaser MC, Simmons CA. 2011. Animal models of calcific aortic valve disease. *Int. J. Inflamm.* 2011:364310

87. Arden C, Chambers JB, Sandoe J, Ray S, Prendergast B, et al. 2014. Can we improve the detection of heart valve disease? *Heart* 100:271–73

88. Yip CY, Chen JH, Zhao R, Simmons CA. 2009. Calcification by valve interstitial cells is regulated by the stiffness of the extracellular matrix. *Arterioscler. Thromb. Vasc. Biol.* 29:936–42

89. Chen JH, Chen WL, Sider KL, Yip CY, Simmons CA. 2011. β-Catenin mediates mechanically regulated, transforming growth factor-β1–induced myofibroblast differentiation of aortic valve interstitial cells. *Arterioscler. Thromb Vasc. Biol.* 31:590–97

90. Wang H, Haeger SM, Kloxin AM, Leinwand LA, Anseth KS. 2012. Redirecting valvular myofibroblasts into dormant fibroblasts through light-mediated reduction in substrate modulus. *PLOS ONE* 7:e39969

91. Richards J, El-Hamamsy I, Chen S, Sarang Z, Sarathchandra P, et al. 2013. Side-specific endothelial-dependent regulation of aortic valve calcification: interplay of hemodynamics and nitric oxide signaling. *Am. J. Pathol.* 182:1922–31

92. Tseng H, Cuchiara ML, Durst CA, Cuchiara MP, Lin CJ, et al. 2013. Fabrication and mechanical evaluation of anatomically-inspired quasilaminate hydrogel structures with layer-specific formulations. *Ann. Biomed. Eng.* 41:398–407

93. Hockaday LA, Kang KH, Colangelo NW, Cheung PY, Duan B, et al. 2012. Rapid 3D printing of anatomically accurate and mechanically heterogeneous aortic valve hydrogel scaffolds. *Biofabrication* 4:035005

94. Duan B, Kapetanovic E, Hockaday LA, Butcher JT. 2013. Three-dimensional printed trileaflet valve conduits using biological hydrogels and human valve interstitial cells. *Acta Biomater.* 10:1836–46

95. Young EW, Wheeler AR, Simmons CA. 2007. Matrix-dependent adhesion of vascular and valvular endothelial cells in microfluidic channels. *Lab Chip* 7:1759–66

96. Chen MB, Srigunapalan S, Wheeler AR, Simmons CA. 2013. A 3D microfluidic platform incorporating methacrylated gelatin hydrogels to study physiological cardiovascular cell-cell interactions. *Lab Chip* 13:2591–98

97. Thayer P, Balachandran K, Rathan S, Yap CH, Arjunon S, et al. 2011. The effects of combined cyclic stretch and pressure on the aortic valve interstitial cell phenotype. *Ann. Biomed. Eng.* 39:1654–67

98. Balachandran K, Alford PW, Wylie-Sears J, Goss JA, Grosberg A, et al. 2011. Cyclic strain induces dual-mode endothelial-mesenchymal transformation of the cardiac valve. *PNAS* 108:19943–48

99. Moraes C, Likhitpanichkul M, Lam CJ, Beca BM, Sun Y, Simmons CA. 2013. Microdevice array-based identification of distinct mechanobiological response profiles in layer-specific valve interstitial cells. *Integr. Biol.* 5:673–80

100. Wikswo JP, Curtis EL, Eagleton ZE, Evans BC, Kole A, et al. 2013. Scaling and systems biology for integrating multiple organs-on-a-chip. *Lab Chip* 13:3496–511

101. Moraes C, Labuz JM, Leung BM, Inoue M, Chun TH, Takayama S. 2013. On being the right size: scaling effects in designing a human-on-a-chip. *Integr. Biol.* 5:1149–61

102. Holgate ST. 2008. Pathogenesis of asthma. *Clin. Exp. Allergy* 38:872–97

103. Szelenyi I. 2000. Animal models of bronchial asthma. *Inflamm. Res.* 49:639–54

104. Borish LC, Nelson HS, Lanz MJ, Claussen L, Whitmore JB, et al. 1999. Interleukin-4 receptor in moderate atopic asthma: a phase I/II randomized, placebo-controlled trial. *Am. J. Respir. Crit. Care Med.* 160:1816–23

105. Cho JY, Miller M, Baek KJ, Han JW, Nayar J, et al. 2004. Inhibition of airway remodeling in IL-5-deficient mice. *J. Clin. Investig.* 113:551–60

106. Foster PS, Hogan SP, Ramsay AJ, Matthaei KI, Young IG. 1996. Interleukin 5 deficiency abolishes eosinophilia, airways hyperreactivity, and lung damage in a mouse asthma model. *J. Exp. Med.* 183:195–201

107. Hozawa S, Haruta Y, Ishioka S, Yamakido M. 1995. Effects of a PAF antagonist, Y-24180, on bronchial hyperresponsiveness in patients with asthma. *Am. J. Respir. Crit. Care Med.* 152:1198–202

108. Leckie MJ, ten Brinke A, Khan J, Diamant Z, O'Connor BJ, et al. 2000. Effects of an interleukin-5 blocking monoclonal antibody on eosinophils, airway hyper-responsiveness, and the late asthmatic response. *Lancet* 356:2144–48

109. Norris V, Choong L, Tran D, Corden Z, Boyce M, et al. 2005. Effect of IVL745, a VLA-4 antagonist, on allergen-induced bronchoconstriction in patients with asthma. *J. Allergy Clin. Immunol.* 116:761–67

110. Hirst SJ. 1996. Airway smooth muscle cell culture: application to studies of airway wall remodelling and phenotype plasticity in asthma. *Eur. Respir. J.* 9:808–20

111. Royce SG, Tan L, Koek AA, Tang ML. 2009. Effect of extracellular matrix composition on airway epithelial cell and fibroblast structure: implications for airway remodeling in asthma. *Ann. Allergy Asthma Immunol.* 102:238–46

112. Ingram JL, Huggins MJ, Church TD, Li Y, Francisco DC, et al. 2011. Airway fibroblasts in asthma manifest an invasive phenotype. *Am. J. Respir. Crit. Care Med.* 183:1625–32

113. Barbato A, Turato G, Baraldo S, Bazzan E, Calabrese F, et al. 2006. Epithelial damage and angiogenesis in the airways of children with asthma. *Am. J. Respir. Crit. Care Med.* 174:975–81

114. Yick CY, Ferreira DS, Annoni R, von der Thusen JH, Kunst PW, et al. 2012. Extracellular matrix in airway smooth muscle is associated with dynamics of airway function in asthma. *Allergy* 67:552–59

115. Parker J, Sarlang S, Thavagnanam S, Williamson G, O'Donoghue D, et al. 2010. A 3-D well-differentiated model of pediatric bronchial epithelium demonstrates unstimulated morphological differences between asthmatic and nonasthmatic cells. *Pediatr. Res.* 67:17–22

116. Blume C, Davies DE. 2013. In vitro and ex vivo models of human asthma. *Eur. J. Pharm. Biopharm.* 84:394–400

117. Whitcutt MJ, Adler KB, Wu R. 1988. A biphasic chamber system for maintaining polarity of differentiation of cultured respiratory tract epithelial cells. *In Vitro Cell. Dev. Biol.* 24:420–28

118. Gray TE, Guzman K, Davis CW, Abdullah LH, Nettesheim P. 1996. Mucociliary differentiation of serially passaged normal human tracheobronchial epithelial cells. *Am. J. Respir. Cell Mol. Biol.* 14:104–12

119. Thavagnanam S, Parker JC, McBrien ME, Skibinski G, Heaney LG, et al. 2011. Effects of IL-13 on mucociliary differentiation of pediatric asthmatic bronchial epithelial cells. *Pediatr. Res.* 69:95–100

120. Choe MM, Tomei AA, Swartz MA. 2006. Physiological 3D tissue model of the airway wall and mucosa. *Nat. Protoc.* 1:357–62

121. Elias JA. 2000. Airway remodeling in asthma: unanswered questions. *Am. J. Respir. Crit. Care Med.* 161:S168–71

122. Huang X, Yang N, Fiore VF, Barker TH, Sun Y, et al. 2012. Matrix stiffness–induced myofibroblast differentiation is mediated by intrinsic mechanotransduction. *Am. J. Respir Cell Mol. Biol.* 47:340–48

123. Miller C, George S, Niklason L. 2010. Developing a tissue-engineered model of the human bronchiole. *J. Tissue Eng. Regen. Med.* 4:619–27

124. Krimmer DI, Oliver BG. 2011. What can in vitro models of COPD tell us? *Pulm. Pharmacol. Ther.* 24:471–77

125. Adamson J, Haswell LE, Phillips G, Gaça MD. 2011. In vitro models of chronic obstructive pulmonary disease (COPD). In *Bronchitis*, ed. I Martin-Loeches, pp. 41–66. Rijeka, Croat.: InTech

126. Rogers DF. 2007. Physiology of airway mucus secretion and pathophysiology of hypersecretion. *Respir. Care* 52:1134–46; discussion 1146–49

127. Haswell LE, Hewitt K, Thorne D, Richter A, Gaça MD. 2010. Cigarette smoke total particulate matter increases mucous secreting cell numbers in vitro: a potential model of goblet cell hyperplasia. *Toxicol. In Vitro* 24:981–87

128. Kreindler JL, Jackson AD, Kemp PA, Bridges RJ, Danahay H. 2005. Inhibition of chloride secretion in human bronchial epithelial cells by cigarette smoke extract. *Am. J. Physiol. Lung Cell. Mol. Physiol.* 288:L894–902

129. Comer DM, Kidney JC, Ennis M, Elborn JS. 2013. Airway epithelial cell apoptosis and inflammation in COPD, smokers and nonsmokers. *Eur. Respir. J.* 41:1058–67

130. Gray AC, McLeod JD, Clothier RH. 2007. A review of in vitro modelling approaches to the identification and modulation of squamous metaplasia in the human tracheobronchial epithelium. *Altern. Lab. Anim.* 35:493–504

131. Korpi-Steiner NL, Valkenaar SM, Bates ME, Evans MD, Gern JE, et al. 2010. Human monocytic cells direct the robust release of CXCL10 by bronchial epithelial cells during rhinovirus infection. *Clin. Exp. Allergy* 40:1203–13

132. Araya J, Cambier S, Markovics JA, Wolters P, Jablons D, et al. 2007. Squamous metaplasia amplifies pathologic epithelial-mesenchymal interactions in COPD patients. *J. Clin. Investig.* 117:3551–62

133. Mukhopadhyay S, Gal AA. 2010. Granulomatous lung disease: an approach to the differential diagnosis. *Arch. Pathol. Lab. Med.* 134:667–90

134. Heinemann DE, Peters JH, Gahr M. 1997. A human in vitro granuloma model using heat killed *Candida albicans* cells immobilized on plastic culture wells. *Scand. J. Immunol.* 45:596–604

135. Puissegur MP, Botanch C, Duteyrat JL, Delsol G, Caratero C, et al. 2004. An in vitro dual model of mycobacterial granulomas to investigate the molecular interactions between mycobacteria and human host cells. *Cell. Microbiol.* 6:423–33

136. Shikama Y, Kobayashi K, Kasahara K, Kaga S, Hashimoto M, et al. 1989. Granuloma formation by artificial microparticles in vitro: Macrophages and monokines play a critical role in granuloma formation. *Am. J. Pathol.* 134:1189–99

137. Sanchez VC, Weston P, Yan A, Hurt RH, Kane AB. 2011. A 3-dimensional in vitro model of epithelioid granulomas induced by high aspect ratio nanomaterials. *Part. Fibre Toxicol.* 8:17

138. Huh D, Matthews BD, Mammoto A, Montoya-Zavala M, Hsin HY, et al. 2010. Reconstituting organ-level lung functions on a chip. *Science* 328:1662–68

139. Huh D, Leslie DC, Matthews BD, Fraser JP, Jurek S, et al. 2012. A human disease model of drug toxicity–induced pulmonary edema in a lung-on-a-chip microdevice. *Sci. Transl. Med.* 4:159ra47

140. Rutgeerts P, Geboes K, Vantrappen G, Kerremans R, Coenegrachts JL, et al. 1984. Natural history of recurrent Crohn's disease at the ileocolonic anastomosis after curative surgery. *Gut* 25:665–72

141. Kaser A, Zeissig S, Blumberg RS. 2010. Inflammatory bowel disease. *Annu. Rev. Immunol.* 28:573–621

142. Fang HW, Fang SB, Chiang Chiau JS, Yeung CY, Chan WT, et al. 2010. Inhibitory effects of *Lactobacillus casei* subsp. *rhamnosus* on *Salmonella* lipopolysaccharide-induced inflammation and epithelial barrier dysfunction in a co-culture model using Caco-2/peripheral blood mononuclear cells. *J. Med. Microbiol.* 59:573–79

143. Haller D, Bode C, Hammes WP, Pfeifer AM, Schiffrin EJ, et al. 2000. Non-pathogenic bacteria elicit a differential cytokine response by intestinal epithelial cell/leucocyte co-cultures. *Gut* 47:79–87

144. Parlesak A, Haller D, Brinz S, Baeuerlein A, Bode C. 2004. Modulation of cytokine release by differentiated CACO-2 cells in a compartmentalized co-culture model with mononuclear leucocytes and nonpathogenic bacteria. *Scand. J. Immunol.* 60:477–85

145. Lievin-Le Moal V, Servin AL. 2013. Pathogenesis of human enterovirulent bacteria: lessons from cultured, fully differentiated human colon cancer cell lines. *Microbiol. Mol. Biol. Rev.* 77:380–439

146. Mileti E, Matteoli G, Iliev ID, Rescigno M. 2009. Comparison of the immunomodulatory properties of three probiotic strains of *Lactobacilli* using complex culture systems: prediction for in vivo efficacy. *PLOS ONE* 4:e7056

147. Nurmi JT, Puolakkainen PA, Rautonen NE. 2005. *Bifidobacterium lactis* sp. 420 up-regulates cyclooxygenase (Cox)-1 and down-regulates Cox-2 gene expression in a Caco-2 cell culture model. *Nutr. Cancer* 51:83–92

148. Pozo-Rubio T, Mujico JR, Marcos A, Puertollano E, Nadal I, et al. 2011. Immunostimulatory effect of faecal *Bifidobacterium* species of breast-fed and formula-fed infants in a peripheral blood mononuclear cell/Caco-2 co-culture system. *Br. J. Nutr.* 106:1216–23

149. Sato T, Clevers H. 2013. Growing self-organizing mini-guts from a single intestinal stem cell: mechanism and applications. *Science* 340:1190–94

150. Spence JR, Mayhew CN, Rankin SA, Kuhar MF, Vallance JE, et al. 2011. Directed differentiation of human pluripotent stem cells into intestinal tissue in vitro. *Nature* 470:105–9

151. McCracken KW, Howell JC, Wells JM, Spence JR. 2011. Generating human intestinal tissue from pluripotent stem cells in vitro. *Nat. Protoc.* 6:1920–28

152. Kim HJ, Huh D, Hamilton G, Ingber DE. 2012. Human gut-on-a-chip inhabited by microbial flora that experiences intestinal peristalsis–like motions and flow. *Lab Chip* 12:2165–74

153. Fiocchi C. 1998. Inflammatory bowel disease: etiology and pathogenesis. *Gastroenterology* 115:182–205

154. Basson MD. 2003. Paradigms for mechanical signal transduction in the intestinal epithelium. *Digestion* 68:217–25

155. Vantrappen G, Janssens J, Hellemans J, Ghoos Y. 1977. The interdigestive motor complex of normal subjects and patients with bacterial overgrowth of the small intestine. *J. Clin. Investig.* 59:1158–66

156. Quigley EM. 2011. Microflora modulation of motility. *J. Neurogastroenterol. Motil.* 17:140–47

157. Kim HJ, Ingber DE. 2013. Gut-on-a-chip microenvironment induces human intestinal cells to undergo villus differentiation. *Integr. Biol.* 5:1130–40

158. Gill SR, Pop M, Deboy RT, Eckburg PB, Turnbaugh PJ, et al. 2006. Metagenomic analysis of the human distal gut microbiome. *Science* 312:1355–59

159. Ley RE, Peterson DA, Gordon JI. 2006. Ecological and evolutionary forces shaping microbial diversity in the human intestine. *Cell* 124:837–48

160. Tremaroli V, Backhed F. 2012. Functional interactions between the gut microbiota and host metabolism. *Nature* 489:242–49

161. Chantret I, Barbat A, Dussaulx E, Brattain MG, Zweibaum A. 1988. Epithelial polarity, villin expression, and enterocytic differentiation of cultured human colon carcinoma cells: a survey of twenty cell lines. *Cancer Res.* 48:1936–42

162. De Palma G, Cinova J, Stepankova R, Tuckova L, Sanz Y. 2010. Pivotal advance: Bifidobacteria and gram-negative bacteria differentially influence immune responses in the proinflammatory milieu of celiac disease. *J. Leukoc. Biol.* 87:765–78

163. Barrila J, Radtke AL, Crabbe A, Sarker SF, Herbst-Kralovetz MM, et al. 2010. Organotypic 3D cell culture models: using the rotating wall vessel to study host-pathogen interactions. *Nat. Rev. Microbiol.* 8:791–801

164. Höner zu Bentrup K, Ramamurthy R, Ott CM, Emami K, Nelman-Gonzalez M, et al. 2006. Three-dimensional organotypic models of human colonic epithelium to study the early stages of enteric salmonellosis. *Microbes Infect.* 8:1813–25

165. Margolis LB, Fitzgerald W, Glushakova S, Hatfill S, Amichay N, et al. 1997. Lymphocyte trafficking and HIV infection of human lymphoid tissue in a rotating wall vessel bioreactor. *AIDS Res. Hum. Retrovir.* 13:1411–20

166. Nickerson CA, Goodwin TJ, Terlonge J, Ott CM, Buchanan KL, et al. 2001. Three-dimensional tissue assemblies: novel models for the study of *Salmonella enterica* serovar Typhimurium pathogenesis. *Infect. Immun.* 69:7106–20

167. Nickerson CA, Richter EG, Ott CM. 2007. Studying host-pathogen interactions in 3-D: organotypic models for infectious disease and drug development. *J. Neuroimmune Pharmacol.* 2:26–31

168. Sainz B Jr, TenCate V, Uprichard SL. 2009. Three-dimensional Huh7 cell culture system for the study of hepatitis C virus infection. *Virol. J.* 6:103

169. Straub TM, Höner zu Bentrup K, Orosz-Coghlan P, Dohnalkova A, Mayer BK, et al. 2007. In vitro cell culture infectivity assay for human noroviruses. *Emerg. Infect. Dis.* 13:396–403

170. Papafragkou E, Hewitt J, Park GW, Greening G, Vinje J. 2013. Challenges of culturing human norovirus in three-dimensional organoid intestinal cell culture models. *PLOS ONE* 8:e63485

171. Straub TM, Bartholomew RA, Valdez CO, Valentine NB, Dohnalkova A, et al. 2011. Human norovirus infection of Caco-2 cells grown as a three-dimensional tissue structure. *J. Water Health* 9:225–40

172. Finkbeiner SR, Zeng XL, Utama B, Atmar RL, Shroyer NF, et al. 2012. Stem cell–derived human intestinal organoids as an infection model for rotaviruses. *mBio* 3:e00159-12

173. Kalabis J, Wong GS, Vega ME, Natsuizaka M, Robertson ES, et al. 2012. Isolation and characterization of mouse and human esophageal epithelial cells in 3D organotypic culture. *Nat. Protoc.* 7:235–46

174. Klotz C, Aebischer T, Seeber F. 2012. Stem cell–derived cell cultures and organoids for protozoan parasite propagation and studying host-parasite interaction. *Int. J. Med. Microbiol.* 302:203–9

175. Kuratnik A, Giardina C. 2013. Intestinal organoids as tissue surrogates for toxicological and pharmacological studies. *Biochem. Pharmacol.* 85:1721–26

176. Sato T, Stange DE, Ferrante M, Vries RG, Van Es JH, et al. 2011. Long-term expansion of epithelial organoids from human colon, adenoma, adenocarcinoma, and Barrett's epithelium. *Gastroenterology* 141:1762–72

177. Kim J, Hegde M, Jayaraman A. 2010. Co-culture of epithelial cells and bacteria for investigating host-pathogen interactions. *Lab Chip* 10:43–50

178. Madl C, Druml W. 2003. Systemic consequences of ileus. *Best Pract. Res. Clin. Gastroenterol.* 17:445–56

179. Lin HC. 2004. Small intestinal bacterial overgrowth: a framework for understanding irritable bowel syndrome. *JAMA* 292:852–58

180. Bures J, Cyrany J, Kohoutova D, Forstl M, Rejchrt S, et al. 2010. Small intestinal bacterial overgrowth syndrome. *World J. Gastroenterol.* 16:2978–90

181. Schuller S, Lucas M, Kaper JB, Giron JA, Phillips AD. 2009. The ex vivo response of human intestinal mucosa to enteropathogenic *Escherichia coli* infection. *Cell. Microbiol.* 11:521–30

182. Tsilingiri K, Barbosa T, Penna G, Caprioli F, Sonzogni A, et al. 2012. Probiotic and postbiotic activity in health and disease: comparison on a novel polarised ex-vivo organ culture model. *Gut* 61:1007–15

183. Schuller S, Phillips AD. 2010. Microaerobic conditions enhance type III secretion and adherence of enterohaemorrhagic *Escherichia coli* to polarized human intestinal epithelial cells. *Environ. Microbiol.* 12:2426–35

184. Duell BL, Cripps AW, Schembri MA, Ulett GC. 2011. Epithelial cell co-culture models for studying infectious diseases: benefits and limitations. *J. Biomed. Biotechnol.* 2011:852419

185. Fritz JV, Desai MS, Shah P, Schneider JG, Wilmes P. 2013. From meta-omics to causality: experimental models for human microbiome research. *Microbiome* 1:14

186. Soldatow VY, Lecluyse EL, Griffith LG, Rusyn I. 2013. In vitro models for liver toxicity testing. *Toxicol. Res.* 2:23–39

187. Aizaki H, Nagamori S, Matsuda M, Kawakami H, Hashimoto O, et al. 2003. Production and release of infectious hepatitis C virus from human liver cell cultures in the three-dimensional radial-flow bioreactor. *Virology* 314:16–25

188. Sodunke TR, Bouchard MJ, Noh HM. 2008. Microfluidic platform for hepatitis B viral replication study. *Biomed. Microdevices* 10:393–402

189. Schwartz RE, Trehan K, Andrus L, Sheahan TP, Ploss A, et al. 2012. Modeling hepatitis C virus infection using human induced pluripotent stem cells. *PNAS* 109:2544–48

190. Khetani SR, Bhatia SN. 2008. Microscale culture of human liver cells for drug development. *Nat. Biotechnol.* 26:120–26

191. Ploss A, Khetani SR, Jones CT, Syder AJ, Trehan K, et al. 2010. Persistent hepatitis C virus infection in microscale primary human hepatocyte cultures. *PNAS* 107:3141–45

192. March S, Ng S, Velmurugan S, Galstian A, Shan J, et al. 2013. A microscale human liver platform that supports the hepatic stages of *Plasmodium falciparum* and *vivax*. *Cell Host Microbe.* 14:104–15

193. Gerbal-Chaloin S, Funakoshi N, Caillaud A, Gondeau C, Champon B, Si-Tayeb K. 2014. Human induced pluripotent stem cells in hepatology: beyond the proof of concept. *Am. J. Pathol.* 184:332–47

194. Yanagida A, Ito K, Chikada H, Nakauchi H, Kamiya A. 2013. An in vitro expansion system for generation of human IPS cell–derived hepatic progenitor–like cells exhibiting a bipotent differentiation potential. *PLOS ONE* 8:e67541

195. Nakamura N, Saeki K, Mitsumoto M, Matsuyama S, Nishio M, et al. 2012. Feeder-free and serum-free production of hepatocytes, cholangiocytes, and their proliferating progenitors from human pluripotent stem cells: application to liver-specific functional and cytotoxic assays. *Cell. Reprogram.* 14:171–85

196. Ordonez MP, Goldstein LSB. 2012. Using human-induced pluripotent stem cells to model monogenic metabolic disorders of the liver. *Semin. Liver Dis.* 32:298–306

197. Fattahi F, Asgari S, Pournasr B, Seifinejad A, Totonchi M, et al. 2013. Disease-corrected hepatocyte-like cells from familial hypercholesterolemia–induced pluripotent stem cells. *Mol. Biotechnol.* 54:863–73

198. Rashid ST, Corbineau S, Hannan N, Marciniak SJ, Miranda E, et al. 2010. Modeling inherited metabolic disorders of the liver using human induced pluripotent stem cells. *J. Clin. Investig.* 120:3127–36

199. Ghodsizadeh A, Taei A, Totonchi M, Seifinejad A, Gourabi H, et al. 2010. Generation of liver disease–specific induced pluripotent stem cells along with efficient differentiation to functional hepatocyte-like cells. *Stem Cell Rev.* 6:622–32

200. Jang KJ, Mehr AP, Hamilton GA, McPartlin LA, Chung S, et al. 2013. Human kidney proximal tubule–on–a–chip for drug transport and nephrotoxicity assessment. *Integr. Biol.* 5:119–1129

201. Ludwig T, Riethmüller C, Gekle M, Schwerdt G, Oberleithner H. 2004. Nephrotoxicity of platinum complexes is related to basolateral organic cation transport. *Kidney Int.* 66:196–202

202. Cornelison TL, Reed E. 1993. Nephrotoxicity and hydration management for cisplatin, carboplatin, and ormaplatin. *Gynecol. Oncol.* 50:147–58

203. Yamada Y, Ikuta Y, Nosaka K, Miyanari N, Hayashi N, et al. 2010. Successful treatment of cisplatin overdose with plasma exchange. *Case Rep. Med.* 2010:802312

204. Yao X, Panichpisal K, Kurtzman N, Nugent K. 2007. Cisplatin nephrotoxicity: a review. *Am. J. Med. Sci.* 334:115–24

205. Wallace DP, Grantham JJ, Sullivan LP. 1996. Chloride and fluid secretion by cultured human polycystic kidney cells. *Kidney Int.* 50:1327–36

206. Yamaguchi T, Reif GA, Calvet JP, Wallace DP. 2010. Sorafenib inhibits cAMP-dependent ERK activation, cell proliferation, and in vitro cyst growth of human ADPKD cyst epithelial cells. *Am. J. Physiol. Ren. Physiol.* 299:F944–51

207. DesRochers TM, Palma E, Kaplan DL. 2014. Tissue-engineered kidney disease models. *Adv. Drug Deliv. Rev.* 69–70:67–80

208. Jansson K, Nguyen AT, Magenheimer BS, Reif GA, Aramadhaka LR, et al. 2012. Endogenous concentrations of ouabain act as a cofactor to stimulate fluid secretion and cyst growth of in vitro ADPKD models via cAMP and EGFR-Src-MEK pathways. *Am. J. Physiol. Ren. Physiol.* 303:F982–90

209. Aggarwal KP, Narula S, Kakkar M, Tandon C. 2013. Nephrolithiasis: molecular mechanism of renal stone formation and the critical role played by modulators. *Biomed. Res. Int.* 2013:292953

210. Wei Z, Amponsah PK, Al-Shatti M, Nie Z, Bandyopadhyay BC. 2012. Engineering of polarized tubular structures in a microfluidic device to study calcium phosphate stone formation. *Lab Chip* 12:4037–40

211. Moll S, Ebeling M, Weibel F, Farina A, Araujo Del Rosario A, et al. 2013. Epithelial cells as active player in fibrosis: findings from an in vitro model. *PLOS ONE* 8:e56575

212. Braccini A, Wendt JC, Jakob M, Heberer M, Jaquiery C, et al. 2005. Three-dimensional perfusion culture of human bone marrow cells and generation of osteoinductive grafts. *Stem Cells* 23:1066–72

213. Maggio ND, Piccinini E, Jaworski M, Trumpp A, Wendt DJ, et al. 2011. Toward modeling the bone marrow niche using scaffold-based 3D culture systems. *Biomaterials* 32:321–29

214. Nichols JE, Cortiella J, Lee J, Niles JA, Cuddihy M, et al. 2009. In vitro analog of human bone marrow from 3D scaffolds with biomimetic inverted colloidal crystal geometry. *Biomaterials* 30:1071–79

215. Sun H, Tsai Y, Nowak I, Dertinger SD, Wu JHD, et al. 2011. Response kinetics of radiation-induced micronucleated reticulocytes in human bone marrow culture. *Mutat. Res.* 718:38–43

216. Giese C, Demmler CD, Ammer R, Hartmann S, Lubitz A, et al. 2006. A human lymph node in vitro—challenges and progress. *Artif. Organs* 30:803–8

217. Giese C, Lubitz A, Demmler CD, Reuschel J, Bergner K, et al. 2010. Immunological substance testing on human lymphatic micro-organoids in vitro. *J. Biotechnol.* 148:38–45

218. Torisawa Y, Spina CS, Mammoto T, Mammoto A, Weaver JC, et al. 2014. Bone marrow–on–a–chip replicates hematopoietic niche physiology in vitro. *Nat. Methods* 11:663–69

219. Lee CY, Chan SH, Lai HY, Lee ST. 2011. A method to develop an in vitro osteoporosis model of porcine vertebrae: histological and biomechanical study. *J. Neurosurg. Spine* 14:789–98

220. Chien S. 2008. Effects of disturbed flow on endothelial cells. *Ann. Biomed. Eng.* 36:554–62

221. Li YS, Haga JH, Chien S. 2005. Molecular basis of the effects of shear stress on vascular endothelial cells. *J. Biomech.* 38:1949–71

222. Sakariassen KS, Aarts PA, de Groot PG, Houdijk WP, Sixma JJ. 1983. A perfusion chamber developed to investigate platelet interaction in flowing blood with human vessel wall cells, their extracellular matrix, and purified components. *J. Lab. Clin. Med.* 102:522–35

223. Van Kruchten R, Cosemans JM, Heemskerk JW. 2012. Measurement of whole blood thrombus formation using parallel-plate flow chambers—a practical guide. *Platelets* 23:229–42

224. Penz S, Reininger AJ, Brandl R, Goyal P, Rabie T, et al. 2005. Human atheromatous plaques stimulate thrombus formation by activating platelet glycoprotein VI. *FASEB J.* 19:898–909

225. Westein E, de Witt S, Lamers M, Cosemans JM, Heemskerk JW. 2012. Monitoring in vitro thrombus formation with novel microfluidic devices. *Platelets* 23:501–9

226. Nesbitt WS, Westein E, Tovar-Lopez FJ, Tolouei E, Mitchell A, et al. 2009. A shear gradient–dependent platelet aggregation mechanism drives thrombus formation. *Nat. Med.* 15:665–73

227. Westein E, van der Meer AD, Kuijpers MJ, Frimat JP, van den Berg A, Heemskerk JW. 2013. Atherosclerotic geometries exacerbate pathological thrombus formation poststenosis in a von Willebrand factor–dependent manner. *PNAS* 110:1357–62

228. Karino T, Motomiya M. 1984. Flow through a venous valve and its implication for thrombus formation. *Thromb. Res.* 36:245–57

229. Runyon MK, Kastrup CJ, Johnson-Kerner BL, Ha TG, Ismagilov RF. 2008. Effects of shear rate on propagation of blood clotting determined using microfluidics and numerical simulations. *J. Am. Chem. Soc.* 130:3458–64

230. Takasu N, Ohno S, Komiya I, Yamada T. 1992. Requirements of follicle structure for thyroid hormone synthesis; cytoskeletons and iodine metabolism in polarized monolayer cells on collagen gel and in double layered, follicle-forming cells. *Endocrinology* 131:1143–48

231. Toda S, Koike N, Sugihara H. 2001. Cellular integration of thyrocytes and thyroid folliculogenesis: a perspective for thyroid tissue regeneration and engineering. *Endocr. J.* 48:407–25

232. Toda S, Koike N, Sugihara H. 2001. Thyrocyte integration, and thyroid folliculogenesis and tissue regeneration: perspective for thyroid tissue engineering. *Pathol. Int.* 51:403–17

233. Toni R, Casa CD, Spaletta G, Marchetti G, Mazzoni P, et al. 2007. The bioartificial thyroid: a biotechnological perspective in endocrine organ engineering for transplantation replacement. *Acta Biomed.* 78(Suppl. 1):129–55

234. Toni R, Tampieri A, Zini N, Strusi V, Sandri M, et al. 2011. Ex situ bioengineering of bioartificial endocrine glands: a new frontier in regenerative medicine of soft tissue organs. *Ann. Anat.* 193:381–94

235. Xu M, West E, Shea LD, Woodruff TK. 2006. Identification of a stage-specific permissive in vitro culture environment for follicle growth and oocyte development. *Biol. Reprod.* 75:916–23

236. Hovatta O, Silye R, Abir R, Krausz T, Winston RM. 1997. Extracellular matrix improves survival of both stored and fresh human primordial and primary ovarian follicles in long-term culture. *Hum. Reprod.* 12:1032–36

237. Augst AD, Kong HJ, Mooney DJ. 2006. Alginate hydrogels as biomaterials. *Macromol. Biosci.* 6:623–33

238. Kreeger PK, Deck JW, Woodruff TK, Shea LD. 2006. The in vitro regulation of ovarian follicle development using alginate–extracellular matrix gels. *Biomaterials* 27:714–23

239. Pangas SA, Saudye H, Shea LD, Woodruff TK. 2003. Novel approach for the three-dimensional culture of granulosa cell–oocyte complexes. *Tissue Eng.* 9:1013–21

240. Hornick JE, Duncan FE, Shea LD, Woodruff TK. 2013 Multiple follicle culture supports primary follicle growth through paracrine-acting signals. *Reproduction* 145:19–32

241. Telfer EE, McLaughlin M, Ding C, Thong KJ. 2008. A two-step serum-free culture system supports development of human oocytes from primordial follicles in the presence of activin. *Hum. Reprod.* 23:1151–58

242. Tagler D, Makanji Y, Tu T, Bernabe BP, Lee R, et al. 2013. Promoting extracellular matrix remodeling via ascorbic acid enhances the survival of primary ovarian follicles encapsulated in alginate hydrogels. *Biotechnol. Bioeng.* 111:1417–29

243. Ting AY, Yeoman RR, Lawson MS, Zelinski MB. 2012. Synthetic polymers improve vitrification outcomes of macaque ovarian tissue as assessed by histological integrity and the in vitro development of secondary follicles. *Cryobiology* 65:1–11

244. Telfer EE, Zelinski MB. 2013. Ovarian follicle culture: advances and challenges for human and nonhuman primates. *Fertil. Steril.* 99:1523–33

245. Krotz SP, Robins JC, Ferruccio TM, Moore R, Steinhoff MM, et al. 2013. In vitro maturation of oocytes via the pre-fabricated self-assembled artificial human ovary. *J. Assist. Reprod. Genet.* 27:743–50

246. Coronel MM, Stabler CL. 2013. Engineering a local microenvironment for pancreatic islet replacement. *Curr. Opin. Biotechnol.* 24:900–8

247. Phelps EA, Headen DM, Taylor WR, Thule PM, Garcia AJ. 2013. Vasculogenic bio-synthetic hydrogel for enhancement of pancreatic islet engraftment and function in type 1 diabetes. *Biomaterials* 34:4602–11

248. Zhang Y, Jalili RB, Warnock GL, Ao Z, Marzban L, Ghahary A. 2012. Three-dimensional scaffolds reduce islet amyloid formation and enhance survival and function of cultured human islets. *Am. J. Pathol.* 181:1296–305

249. Kaufman-Francis K, Koffler J, Weinberg N, Dor Y, Levenberg S. 2012. Engineered vascular beds provide key signals to pancreatic hormone–producing cells. *PLOS ONE* 7:e40741

250. Kerr-Conte J, Pattou F, Lecomte-Houcke M, Xia Y, Boilly B, et al. 1996. Ductal cyst formation in collagen-embedded adult human islet preparations: a means to the reproduction of nesidioblastosis in vitro. *Diabetes* 45:1108–14

251. Kroon E, Martinson LA, Kadoya K, Bang AG, Kelly OG, et al. 2008. Pancreatic endoderm derived from human embryonic stem cells generates glucose-responsive insulin-secreting cells in vivo. *Nat. Biotechnol.* 26:443–52

252. Jiang J, Au M, Lu K, Eshpeter A, Korbutt G, et al. 2007. Generation of insulin-producing islet-like clusters from human embryonic stem cells. *Stem Cells* 25:1940–53

253. Thatava T, Armstrong AS, De Lamo JG, Edukulla R, Khan YK, et al. 2011. Successful disease-specific induced pluripotent stem cell generation from patients with kidney transplantation. *Stem Cell Res. Ther.* 2:48

254. Cheng X, Ying L, Lu L, Galvao AM, Mills JA, et al. 2012. Self-renewing endodermal progenitor lines generated from human pluripotent stem cells. *Cell Stem Cell* 10:371–84

255. Prabakar KR, Domínguez-Bendala J, Molano RD, Pileggi A, Villate S, et al. 2012. Generation of glucose-responsive, insulin-producing cells from human umbilical cord blood–derived mesenchymal stem cells. *Cell Transplant.* 21:1321–39

256. Woodford C, Zandstra PW. 2012. Tissue engineering 2.0: guiding self-organization during pluripotent stem cell differentiation. *Curr. Opin. Biotechnol.* 23:810–19

257. Jun Y, Kang AR, Lee JS, Park SJ, Lee DY, et al. 2014. Microchip-based engineering of super-pancreatic islets supported by adipose-derived stem cells. *Biomaterials* 35:4815–26

258. Spiegelman BM. 2013. Banting Lecture 2012. Regulation of adipogenesis: toward new therapeutics for metabolic disease. *Diabetes* 62:1774–82

259. Hotamisligil GS. 2006. Inflammation and metabolic disorders. *Nature* 444:860–67

260. Gilbert CA, Slingerland JM. 2013. Cytokines, obesity, and cancer: new insights on mechanisms linking obesity to cancer risk and progression. *Annu. Rev. Med.* 64:45–57

261. Johnson AM, Olefsky JM. 2012. The origins and drivers of insulin resistance. *Cell* 152:673–84

262. Fischbach C, Seufert J, Staiger H, Hacker M, Neubauer M, et al. 2004. Three-dimensional in vitro model of adipogenesis: comparison of culture conditions. *Tissue Eng.* 10:215–29

263. Kang X, Xie Y, Powell HM, Lee LJ, Belury MA, et al. 2007. Adipogenesis of murine embryonic stem cells in a three-dimensional culture system using electrospun polymer scaffolds. *Biomaterials* 28:450–58

264. Kang X, Xie Y, Kniss DA. 2005. Adipose tissue model using three-dimensional cultivation of preadipocytes seeded onto fibrous polymer scaffolds. *Tissue Eng.* 11:458–68

265. Aoki S, Toda S, Sakemi T, Sugihara H. 2003. Co-culture of endothelial cells and mature adipocytes actively promotes immature preadipocyte development in vitro. *Cell Struct. Funct.* 28:55–60

266. Choi JH, Bellas E, Vunjak-Novakovic G, Kaplan DL. 2011. Adipogenic differentiation of human adipose-derived stem cells on 3D silk scaffolds. *Methods Mol. Biol.* 702:319–30

267. Daquinag AC, Souza GR, Kolonin MG. 2013. Adipose tissue engineering in three-dimensional levitation tissue culture system based on magnetic nanoparticles. *Tissue Eng. C* 19:336–44

268. Choi JH, Gimble JM, Lee K, Marra KG, Rubin JP, et al. 2010. Adipose tissue engineering for soft tissue regeneration. *Tissue Eng. B* 16:413–26

269. Lai N, Sims JK, Jeon NL, Lee K. 2012. Adipocyte induction of preadipocyte differentiation in a gradient chamber. *Tissue Eng. C* 18:958–67

270. Dennis RG, Kosnik PF. 2000. Excitability and isometric contractile properties of mammalian skeletal muscle constructs engineered in vitro. *In Vitro Cell. Dev. Biol. Anim.* 36:327–35

271. Hosseini V, Ahadian S, Ostrovidov S, Camci-Unal G, Chen S, et al. 2012. Engineered contractile skeletal muscle tissue on a microgrooved methacrylated gelatin substrate. *Tissue Eng. A* 18:2453–65

272. Khodabukus A, Baar K. 2012. Defined electrical stimulation emphasizing excitability for the development and testing of engineered skeletal muscle. *Tissue Eng. C* 18:349–57

273. Nagamine K, Kawashima T, Ishibashi T, Kaji H, Kanzaki M, Nishizawa M. 2010. Micropatterning contractile C_2C_{12} myotubes embedded in a fibrin gel. *Biotechnol. Bioeng.* 105:1161–67

274. Ramón-Azcón J, Ahadian S, Estili M, Liang X, Ostrovidov S, et al. 2013. Dielectrophoretically aligned carbon nanotubes to control electrical and mechanical properties of hydrogels to fabricate contractile muscle myofibers. *Adv. Mater.* 25:4028–34

275. Sakar MS, Neal D, Boudou T, Borochin MA, Li Y, et al. 2012. Formation and optogenetic control of engineered 3D skeletal muscle bioactuators. *Lab Chip* 12:4976–85

276. Shimizu FHK, Nagamori E. 2010. Novel method for measuring active tension generation by C2C12 myotube using UV-crosslinked collagen film. *Biotechnol. Bioeng.* 106:482–89

277. Shimizu FHK, Sasaki H, Hida H, Fujita H, Obinata K, et al. 2010. Assembly of skeletal muscle cells on a Si-MEMS device and their generative force measurement. *Biomed. Microdevices* 12:247–52

278. Vandenburgh H, Shansky J, Benesch-Lee F, Barbata V, Reid J, et al. 2008. A drug screening platform based on the contractility of tissue engineered muscle. *Muscle Nerve* 37:438–47

279. Wilson K, Das M, Wahl KJ, Colton RJ, Hickman JJ. 2010. Measurement of contractile stress generated by cultured rat muscle on silicon cantilevers for toxin detection and muscle performance enhancement. *PLOS ONE* 5:e11042

280. Kaji H, Ishibashi T, Nagamine K, Kanzaki M, Nishizawa M. 2010. Electrically induced contraction of C2C12 myotubes cultured on a porous membrane-based substrate with muscle tissue–like stiffness. *Biomaterials* 31:6981–86

281. Smith AST, Long CJ, Pirozzi K, Hickman JJ. 2013. A functional system for high-content screening of neuromuscular junctions in vitro. *Technology* 1:1–12

282. Morimoto Y, Kato-Negishi M, Onoe H, Takeuchi S. 2013. Three-dimensional neuron-muscle constructs with neuromuscular junctions. *Biomaterials* 34:9413–19

283. Sun Y, Duffy R, Lee A, Feinberg AW. 2013. Optimizing the structure and contractility of engineered skeletal muscle thin films. *Acta Biomater.* 9:7885–94

284. Krook A, Björnholm M, Galuska D, Jiang XJ, Fahlman R, et al. 2000. Characterization of signal transduction and glucose transport in skeletal muscle from type 2 diabetic patients. *Diabetes* 49:284–92

285. Ishibashi T, Hoshino Y, Kaji H, Kanzaki M, Sato M, Nishizawa M. 2009. Localized electrical stimulation to C2C12 myotubes cultured on a porous membrane-based substrate. *Biomed. Microdevices* 11:413–19

286. Nagamine K, Kawashima T, Sekine S, Ido Y, Kanzaki M, Nishizawa M. 2010. Spatiotemporally controlled contraction of micropatterned skeletal muscle cells on a hydrogel sheet. *Lab Chip* 11:513–17

287. Sharples AP, Player DJ, Martin NR, Mudera V, Stewart CE, Lewis MP. 2012. Modelling in vivo skeletal muscle ageing in vitro using three-dimensional bioengineered constructs. *Aging Cell* 11:986–95

288. Sharples AP, Al-Shanti N, Lewis MP, Stewart CE. 2011. Reduction of myoblast differentiation following multiple population doublings in mouse C_2C_{12} cells: a model to investigate ageing? *J. Cell. Biochem.* 112:3773–85

289. Cuthbertson D, Smith K, Babraj J, Leese G, Waddell T, et al. 2005. Anabolic signaling deficits underlie amino acid resistance of wasting, aging muscle. *FASEB J.* 19:422–24

290. Leger B, Derave W, De Bock K, Hespel P, Russell AP. 2008. Human sarcopenia reveals an increase in SOCS-3 and myostatin and a reduced efficiency of Akt phosphorylation. *Rejuvenation Res.* 11:163–75B

291. Bigot A, Jacquemin V, Debacq-Chainiaux F, Butler-Browne GS, Toussaint O, et al. 2008. Replicative aging down-regulates the myogenic regulatory factors in human myoblasts. *Biol. Cell* 100:189–99

292. Pietrangelo T, Puglielli C, Mancinelli R, Beccafico S, Fano G, Fulle S. 2009. Molecular basis of the myogenic profile of aged human skeletal muscle satellite cells during differentiation. *Exp. Gerontol.* 44:523–31

293. Beccafico S, Riuzzi F, Puglielli C, Mancinelli R, Fulle S, et al. 2011. Human muscle satellite cells show age-related differential expression of S100B protein and RAGE. *Age* 33:523–41

294. Vandenburgh H, Shansky J, Benesch-Lee F, Skelly K, Spinazzola JM, et al. 2009. Automated drug screening with contractile muscle tissue engineered from dystrophic myoblasts. *FASEB J.* 23:3325–34

295. Chamberlain JS, Rando TA, eds. 2006. *Duchenne Muscular Dystrophy: Advances in Therapeutics.* New York: Taylor & Francis

296. Langelaan ML, Boonen KJ, Rosaria-Chak KY, van der Schaft DW, Post MJ, Baaijens FP. 2011. Advanced maturation by electrical stimulation: differences in response between C2C12 and primary muscle progenitor cells. *J. Tissue Eng. Regen. Med.* 5:529–39

297. Yuge L, Kataoka K. 2000. Differentiation of myoblasts is accelerated in culture in a magnetic field. *In Vitro Cell. Dev. Biol. Anim.* 36:383–86

298. Goldspink G, Scutt A, Loughna PT, Wells DJ, Jaenicke T, Gerlach GF. 1992. Gene expression in skeletal muscle in response to stretch and force generation. *Am. J. Physiol. Regul. Integr. Comp. Physiol.* 262:R356–63

299. Powell CA, Smiley BL, Mills J, Vandenburgh HH. 2002. Mechanical stimulation improves tissue-engineered human skeletal muscle. *Am. J. Physiol. Cell Physiol.* 283:C1557–65

300. Moon DG, Christ G, Stitzel JD, Atala A, Yoo JJ. 2008. Cyclic mechanical preconditioning improves engineered muscle contraction. *Tissue Eng.* 14:848

301. Huang YC, Dennis RG, Baar K. 2006. Cultured slow versus fast skeletal muscle cells differ in physiology and responsiveness to stimulation. *Am. J. Physiol. Cell Physiol.* 291:C11–17

302. Asano T, Ishizua T, Yawo H. 2012. Optically controlled contraction of photosensitive skeletal muscle cells. *Biotechnol. Bioeng.* 109:199–204

303. Ahadian S, Ramón-Azcón J, Ostrovidov S, Camci-Unal G, Kaji H, et al. 2013. A contactless electrical stimulator: application to fabricate functional skeletal muscle tissue. *Biomed. Microdevices* 15:109–15

304. Harrison BC, Allen DL, Leinwand LA. 2011. IIb or not IIb? Regulation of myosin heavy chain gene expression in mice and men. *Skelet. Muscle* 1:1–9

305. Jankowski R. 2011. A comparison of commercially-available human skeletal muscle cells and media for research applications. *Nat. Methods Appl. Notes.* **http://www.nature.com/app_notes/nmeth/2011/111406/full/an7998.html**

306. Owens J, Moreira K, Bain G. 2013. Characterization of primary human skeletal muscle cells from multiple commercial sources. *In Vitro Cell. Dev. Biol. Anim.* 49:695–705

307. Fishman JM, Tyraskis A, Maghsoudlou P, Urbani L, Totonelli G, et al. 2013. Skeletal muscle tissue engineering: which cell to use? *Tissue Eng. B* 19:503–15

308. Zhu CH, Mouly V, Cooper RN, Mamchaoui K, Bigot A, et al. 2007. Cellular senescence in human myoblasts is overcome by human telomerase reverse transcriptase and cyclin-dependent kinase 4: consequences in aging muscle and therapeutic strategies for muscular dystrophies. *Aging Cell* 6:515–23

309. Larkin LM, van der Meulen JH, Dennis RG, Kennedy JB. 2006. Functional evaluation of nerve–skeletal muscle constructs engineered in vitro. *In Vitro Cell. Dev. Biol. Anim.* 42:75–82

310. Dhawan V, Lytle IF, Dow DE, Huang YC, Brown DL. 2007. Neurotization improves contractile forces of tissue-engineered skeletal muscle. *Tissue Eng.* 13:2813–21

311. Das M, Rumsey JW, Bhargava N, Stancescu M, Hickman JJ. 2009. Skeletal muscle tissue engineering: a maturation model promoting long-term survival of myotubes, structural development of the excitation-contraction coupling apparatus and neonatal myosin heavy chain expression. *Biomaterials* 30:5392–402

312. Das M, Rumsey JW, Bhargava N, Stancescu M, Hickman JJ. 2010. A defined long-term in vitro tissue engineered model of neuromuscular junctions. *Biomaterials* 31:4880–88

313. Buller AJ, Eccles JC, Eccles RM. 1960. Differentiation of fast and slow muscles in the cat hind limb. *J. Physiol.* 150:399–416

314. Bacou F, Rouanet P, Barjot C, Janmot C, Vigneron P, d'Albis A. 1996. Expression of myosin isoforms in denervated, cross-reinnervated, and electrically stimulated rabbit muscles. *Eur. J. Biochem.* 236:539–47

315. Salmons S, Sreter FA. 1976. Significance of impulse activity in the transformation of skeletal muscle type. *Nature* 263:30–34

316. WHO (World Health Organ.). 2006. *Neurological Disorders: Public Health Challenges.* Geneva: WHO

317. Herculano-Houzel S. 2009. The human brain in numbers: a linearly scaled-up primate brain. *Front. Hum. Neurosci.* 3:31

318. Masland RH. 2004. Neuronal cell types. *Curr. Biol.* 14:R497–500

319. Stevens CF. 1998. Neuronal diversity: too many cell types for comfort? *Curr. Biol.* 8:R708–10

320. Gonzalez-Burgos G, Lewis DA. 2012. NMDA receptor hypofunction, parvalbumin-positive neurons, and cortical gamma oscillations in schizophrenia. *Schizophr. Bull.* 38:950–57

321. Curley AA, Lewis DA. 2012. Cortical basket cell dysfunction in schizophrenia. *J. Physiol.* 590:715–24

322. Samii A, Nutt JG, Ransom BR. 2004. Parkinson's disease. *Lancet* 363:1783–93

323. DeMarse TB, Wagenaar DA, Blau AW, Potter SM. 2001. The neurally controlled animat: biological brains acting with simulated bodies. *Auton. Robots* 11:305–10

324. DeMarse TB, Dockendorf KP. 2005. Adaptive flight control with living neuronal networks on micro-electrode arrays. *Proc. Int. Joint Conf. Neural Netw. (IJCNN) 2005*, Vol. 3, pp. 1548–51. Piscataway, NJ: IEEE

325. Novellino A, D'Angelo P, Cozzi L, Chiappalone M, Sanguineti V, Martinoia S. 2007. Connecting neurons to a mobile robot: an in vitro bidirectional neural interface. *Comput. Intell. Neurosci.* 2007:12725

326. Abuelo D. 2007. Microcephaly syndromes. *Semin. Pediatr. Neurol.* 14:118–27

327. Brustle O. 2013. Developmental neuroscience: miniature human brains. *Nature* 501:319–20

328. Lancaster MA, Renner M, Martin CA, Wenzel D, Bicknell LS, et al. 2013. Cerebral organoids model human brain development and microcephaly. *Nature* 501:373–79

329. Jankovic J. 2008. Parkinson's disease: clinical features and diagnosis. *J. Neurol. Neurosurg. Psychiatry* 79:368–76

330. Xie HR, Hu LS, Li GY. 2010. SH-SY5Y human neuroblastoma cell line: in vitro cell model of dopamin-ergic neurons in Parkinson's disease. *Chin. Med. J.* 123:1086–92

331. Presgraves SP, Ahmed T, Borwege S, Joyce JN. 2004. Terminally differentiated SH-SY5Y cells provide a model system for studying neuroprotective effects of dopamine agonists. *Neurotox. Res.* 5:579–98

332. Oyarce AM, Fleming PJ. 1991. Multiple forms of human dopamine β-hydroxylase in SH-SY5Y neuro-blastoma cells. *Arch. Biochem. Biophys.* 290:503–10

333. Wilson NR, Ty MT, Ingber DE, Sur M, Liu G. 2007. Synaptic reorganization in scaled networks of controlled size. *J. Neurosci.* 27:13581–89

334. Peyrin JM, Deleglise B, Saias L, Vignes M, Gougis P, et al. 2011. Axon diodes for the reconstruction of oriented neuronal networks in microfluidic chambers. *Lab Chip* 11:3663–73

335. Suter DM. 2011. Live cell imaging of neuronal growth cone motility and guidance in vitro. *Methods Mol. Biol.* 769:65–86

336. Castellani RJ, Perry G. 2014. The complexities of the pathology-pathogenesis relationship in Alzheimer disease. *Biochem. Pharmacol.* 88:671–76

337. Reitz C, Mayeux R. 2014. Alzheimer disease: epidemiology, diagnostic criteria, risk factors and biomark-ers. *Biochem. Pharmacol.* 88:640–51

338. Agholme L, Lindstrom T, Kagedal K, Marcusson J, Hallbeck M. 2010. An in vitro model for neuro-science: differentiation of SH-SY5Y cells into cells with morphological and biochemical characteristics of mature neurons. *J. Alzheimer's Dis.* 20:1069–82

339. Zhang D, Pekkanen-Mattila M, Shahsavani M, Falk A, Teixeira AI, Herland A. 2014. A 3D Alzheimer's disease culture model and the induction of P21-activated kinase mediated sensing in iPSC derived neurons. *Biomaterials* 35:1420–28

340. Franze K, Janmey PA, Guck J. 2013. Mechanics in neuronal development and repair. *Annu. Rev. Biomed. Eng.* 15:227–51

341. Pasinelli P, Brown RH. 2006. Molecular biology of amyotrophic lateral sclerosis: insights from genetics. *Nat. Rev. Neurosci.* 7:710–23

342. Phukan J, Pender NP, Hardiman O. 2007. Cognitive impairment in amyotrophic lateral sclerosis. *Lancet Neurol.* 6:994–1003

343. Dimos JT, Rodolfa KT, Niakan KK, Weisenthal LM, Mitsumoto H, et al. 2008. Induced pluripotent stem cells generated from patients with ALS can be differentiated into motor neurons. *Science* 321:1218–21

344. Dunckley T, Huentelman MJ, Craig DW, Pearson JV, Szelinger S, et al. 2007. Whole-genome analysis of sporadic amyotrophic lateral sclerosis. *N. Engl. J. Med.* 357:775–88

345. Aigner S, Heckel T, Zhang JD, Andreae LC, Jagasia R. 2013. Human pluripotent stem cell models of autism spectrum disorder: emerging frontiers, opportunities, and challenges towards neuronal networks in a dish. *Psychopharmacology* 231:1089–104

346. Bauman ML, Kemper TL. 2005. Neuroanatomic observations of the brain in autism: a review and future directions. *Int. J. Dev. Neurosci.* 23:183–87

347. Konopka G, Wexler E, Rosen E, Mukamel Z, Osborn GE, et al. 2012. Modeling the functional genomics of autism using human neurons. *Mol. Psychiatry* 17:202–14

348. Marchetto MC, Carromeu C, Acab A, Yu D, Yeo GW, et al. 2010. A model for neural development and treatment of Rett syndrome using human induced pluripotent stem cells. *Cell* 143:527–39

349. Shcheglovitov A, Shcheglovitova O, Yazawa M, Portmann T, Shu R, et al. 2013. SHANK3 and IGF1 restore synaptic deficits in neurons from 22q13 deletion syndrome patients. *Nature* 503:267–71

350. Pasca SP, Portmann T, Voineagu I, Yazawa M, Shcheglovitov A, et al. 2011. Using iPSC-derived neurons to uncover cellular phenotypes associated with Timothy syndrome. *Nat. Med.* 17:1657–62

351. Sheridan SD, Theriault KM, Reis SA, Zhou F, Madison JM, et al. 2011. Epigenetic characterization of the *FMR1* gene and aberrant neurodevelopment in human induced pluripotent stem cell models of fragile X syndrome. *PLOS ONE* 6:e26203

352. Castren M, Tervonen T, Karkkainen V, Heinonen S, Castren E, et al. 2005. Altered differentiation of neural stem cells in fragile X syndrome. *PNAS* 102:17834–39

353. Brennand KJ, Simone A, Tran N, Gage FH. 2012. Modeling psychiatric disorders at the cellular and network levels. *Mol. Psychiatry* 17:1239–53

354. Durnaoglu S, Genc S, Genc K. 2011. Patient-specific pluripotent stem cells in neurological diseases. *Stem Cells Int.* 2011:212487

355. Fasano C, Kortleven C, Trudeau LE. 2010. Chronic activation of the D2 autoreceptor inhibits both glutamate and dopamine synapse formation and alters the intrinsic properties of mesencephalic dopamine neurons in vitro. *Eur. J. Neurosci.* 32:1433–41

356. Kriks S, Shim JW, Piao J, Ganat YM, Wakeman DR, et al. 2011. Dopamine neurons derived from human ES cells efficiently engraft in animal models of Parkinson's disease. *Nature* 480:547–51

357. Shi Y, Kirwan P, Smith J, Robinson HP, Livesey FJ. 2012. Human cerebral cortex development from pluripotent stem cells to functional excitatory synapses. *Nat. Neurosci.* 15:477–86

358. Penzes P, Buonanno A, Passafaro M, Sala C, Sweet RA. 2013. Developmental vulnerability of synapses and circuits associated with neuropsychiatric disorders. *J. Neurochem.* 126:165–82

359. Thuret S, Moon LD, Gage FH. 2006. Therapeutic interventions after spinal cord injury. *Nat. Rev. Neurosci.* 7:628–43

360. Abu-Rub M, McMahon S, Zeugolis DI, Windebank A, Pandit A. 2010. Spinal cord injury in vitro: modelling axon growth inhibition. *Drug Discov. Today* 15:436–43

361. Zimmermann DR, Dours-Zimmermann MT. 2008. Extracellular matrix of the central nervous system: from neglect to challenge. *Histochem. Cell Biol.* 130:635–53

362. Lau LW, Cua R, Keough MB, Haylock-Jacobs S, Yong VW. 2013. Pathophysiology of the brain extra-cellular matrix: a new target for remyelination. *Nat. Rev. Neurosci.* 14:722–29

363. Gilbert RJ, McKeon RJ, Darr A, Calabro A, Hascall VC, Bellamkonda RV. 2005. CS-4,6 is differentially up-regulated in glial scar and is a potent inhibitor of neurite extension. *Mol. Cell. Neurosci.* 29:545–58

364. Cullen DK, Stabenfeldt SE, Simon CM, Tate CC, LaPlaca MC. 2007. In vitro neural injury model for optimization of tissue-engineered constructs. *J. Neurosci. Res.* 85:3642–51

365. East E, Golding JP, Phillips JB. 2009. A versatile 3D culture model facilitates monitoring of astrocytes undergoing reactive gliosis. *J. Tissue Eng. Regen. Med.* 3:634–46

366. Smyth AM, Lawrie SM. 2013. The neuroimmunology of schizophrenia. *Clin. Psychopharmacol. Neurosci.* 11:107–11

367. Roussos P, Haroutunian V. 2014. Schizophrenia: susceptibility genes and oligodendroglial and myelin related abnormalities. *Front. Cell. Neurosci.* 8:5

368. Ambasudhan R, Talantova M, Coleman R, Yuan X, Zhu S, et al. 2011. Direct reprogramming of adult human fibroblasts to functional neurons under defined conditions. *Cell Stem Cell* 9:113–18

369. Brennand KJ, Gage FH. 2012. Modeling psychiatric disorders through reprogramming. *Dis. Models Mech.* 5:26–32

370. Yoo AS, Sun AX, Li L, Shcheglovitov A, Portmann T, et al. 2011. MicroRNA-mediated conversion of human fibroblasts to neurons. *Nature* 476:228–31

371. Tran NN, Ladran IG, Brennand KJ. 2013. Modeling schizophrenia using induced pluripotent stem cell–derived and fibroblast-induced neurons. *Schizophr. Bull.* 39:4–10

372. Paulsen BdS, da Silveira MS, Galina A, Rehen SK. 2013. Pluripotent stem cells as a model to study oxygen metabolism in neurogenesis and neurodevelopmental disorders. *Arch. Biochem. Biophys.* 534:3–10

373. Chung K, Wallace J, Kim SY, Kalyanasundaram S, Andalman AS, et al. 2013. Structural and molecular interrogation of intact biological systems. *Nature* 497:332–37

374. Park J, Koito H, Li J, Han A. 2009. Microfluidic compartmentalized co-culture platform for CNS axon myelination research. *Biomed. Microdevices* 11:1145–53

375. Brannvall K, Bergman K, Wallenquist U, Svahn S, Bowden T, et al. 2007. Enhanced neuronal differentiation in a three-dimensional collagen-hyaluronan matrix. *J. Neurosci. Res.* 85:2138–46

376. Kato-Negishi M, Morimoto Y, Onoe H, Takeuchi S. 2013. Millimeter-sized neural building blocks for 3D heterogeneous neural network assembly. *Adv. Healthc. Mater.* 2:1564–70

377. Akhtar N, Rasheed Z, Ramamurthy S, Anbazhagan AN, Voss FR, et al. 2010. MicroRNA-27b regulates the expression of matrix metalloproteinase 13 in human osteoarthritis chondrocytes. *Arthritis Rheum.* 62:1361–71

378. Blasioli DJ, Matthews GL, Kaplan DL. 2014. The degradation of chondrogenic pellets using co-cultures of synovial fibroblasts and U937 cells. *Biomaterials* 35:1185–91

379. Sun L, Wang X, Kaplan DL. 2011. A 3D cartilage–inflammatory cell culture system for the modeling of human osteoarthritis. *Biomaterials* 32:5581–89

380. Cortial D, Gouttenoire J, Rousseau CF, Ronziere MC, Piccardi N, et al. 2006. Activation by IL-1 of bovine articular chondrocytes in culture within a 3D collagen-based scaffold. An in vitro model to address the effect of compounds with therapeutic potential in osteoarthritis. *Osteoarthr. Cartil.* 14:631–40

381. Towle CA, Hung HH, Bonassar LJ, Treadwell BV, Mangham DC. 1997. Detection of interleukin-1 in the cartilage of patients with osteoarthritis: a possible autocrine/paracrine role in pathogenesis. *Osteoarthr. Cartil.* 5:293–300

382. Pol A, Bergers M, van Ruissen F, Pfundt R, Schalkwijk J. 2002. A simple technique for high-throughput screening of drugs that modulate normal and psoriasis-like differentiation in cultured human keratinocytes. *Skin Pharmacol. Appl. Skin Physiol.* 15:252–61

383. Pol A, Bergers M, Schalkwijk J. 2003. Comparison of antiproliferative effects of experimental and established antipsoriatic drugs on human keratinocytes, using a simple 96-well-plate assay. *In Vitro Cell. Dev. Biol. Anim.* 39:36–42

384. Amigo M, Schalkwijk J, Olthuis D, De Rosa S, Paya M, et al. 2006. Identification of avarol derivatives as potential antipsoriatic drugs using an in vitro model for keratinocyte growth and differentiation. *Life Sci.* 79:2395–404

385. van den Bogaard EH, Tjabringa GS, Joosten I, Vonk-Bergers M, van Rijssen E, et al. 2014. Crosstalk between keratinocytes and T cells in a 3D microenvironment: a model to study inflammatory skin diseases. *J. Investig. Dermatol.* 134:719–27

386. Villenave R, Thavagnanam S, Sarlang S, Parker J, Douglas I, et al. 2012. In vitro modeling of respiratory syncytial virus infection of pediatric bronchial epithelium, the primary target of infection in vivo. *PNAS* 109:5040–45

387. Matrosovich MN, Matrosovich TY, Gray T, Roberts NA, Klenk HD. 2004. Human and avian influenza viruses target different cell types in cultures of human airway epithelium. *PNAS* 101:4620–24

388. Ludlow M, Rennick LJ, Sarlang S, Skibinski G, McQuaid S, et al. 2010. Wild-type measles virus infection of primary epithelial cells occurs via the basolateral surface without syncytium formation or release of infectious virus. *J. Gen. Virol.* 91:971–79

389. Sims AC, Burkett SE, Yount B, Pickles RJ. 2008. SARS-CoV replication and pathogenesis in an in vitro model of the human conducting airway epithelium. *Virus Res.* 133:33–44

390. Zhang L, Bukreyev A, Thompson CI, Watson B, Peeples ME, et al. 2005. Infection of ciliated cells by human parainfluenza virus type 3 in an in vitro model of human airway epithelium. *J. Virol.* 79:1113–24

391. Bermudez LE. 2002. The efficiency of the translocation of *Mycobacterium tuberculosis* across a bilayer of epithelial and endothelial cells as a model of the alveolar wall is a consequence of transport within mononuclear phagocytes and invasion of alveolar epithelial cells. *Infect. Immun.* 70:140–46

392. Bhat P, Snooks MJ, Anderson DA. 2011. Hepatocytes traffic and export hepatitis B virus basolaterally by polarity-dependent mechanisms. *J. Virol.* 85:12474–81

393. Ren D, Nelson KL, Uchakin PN, Smith AL, Gu XX, et al. 2012. Characterization of extended co-culture of non-typeable *Haemophilus influenzae* with primary human respiratory tissues. *Exp. Biol. Med.* 237:540–47

394. Lamers RP, Eade CR, Waring AJ, Cole AL, Cole AM. 2011. Characterization of the retrocyclin analogue RC-101 as a preventative of *Staphylococcus aureus* nasal colonization. *Antimicrob. Agents Chemother.* 55:5338–46

395. Carterson AJ, Höner zu Bentrup K, Ott CM, Clarke MS, Pierson DL, et al. 2005. A549 lung epithelial cells grown as three-dimensional aggregates: alternative tissue culture model for *Pseudomonas aeruginosa* pathogenesis. *Infect. Immun.* 73:1129–40

396. Smith YC, Grande KK, Rasmussen SB, O'Brien AD. 2006. Novel three-dimensional organoid model for evaluation of the interaction of uropathogenic *Escherichia coli* with terminally differentiated human urothelial cells. *Infect. Immun.* 74:750–57

397. Cimetta E, Franzoso M, Trevisan M, Serena E, Zambon A, et al. 2012. Microfluidic-driven viral infection on cell cultures: theoretical and experimental study. *Biomicrofluidics* 6:24127–712

398. Zhu Y, Warrick JW, Haubert K, Beebe DJ, Yin J. 2009. Infection on a chip: a microscale platform for simple and sensitive cell-based virus assays. *Biomed. Microdevices* 11:565–70

399. Walker G. 2004. Cell infection within a microfluidic device using virus gradients. *Sens. Actuators B* 98:347–55

400. Shelby JP, White J, Ganesan K, Rathod PK, Chiu DT. 2003. A microfluidic model for single-cell capillary obstruction by *Plasmodium falciparum*–infected erythrocytes. *PNAS* 100:14618–22

401. Handayani S, Chiu DT, Tjitra E, Kuo JS, Lampah D, et al. 2009. High deformability of *Plasmodium vivax*–infected red blood cells under microfluidic conditions. *J. Infect. Dis.* 199:445–50

402. Antia M, Herricks T, Rathod PK. 2007. Microfluidic modeling of cell-cell interactions in malaria pathogenesis. *PLOS Pathog.* 3:e99

403. Mishra DK, Sakamoto JH, Thrall MJ, Baird BN, Blackmon SH, et al. 2012. Human lung cancer cells grown in an ex vivo 3D lung model produce matrix metalloproteinases not produced in 2D culture. *PLOS ONE* 7:e45308

404. Hsu TH, Xiao JL, Tsao YW, Kao YL, Huang SH, et al. 2011. Analysis of the paracrine loop between cancer cells and fibroblasts using a microfluidic chip. *Lab Chip* 11:1808–14

405. Chen YA, King AD, Shih HC, Peng CC, Wu CY, et al. 2011. Generation of oxygen gradients in microfluidic devices for cell culture using spatially confined chemical reactions. *Lab Chip* 11:3626–33

406. Mehta G, Hsiao AY, Ingram M, Luker GD, Takayama S. 2012. Opportunities and challenges for use of tumor spheroids as models to test drug delivery and efficacy. *J. Control. Release* 164:92–204

407. Debnath J, Mills KR, Collins NL, Reginato MJ, Muthuswamy SK, Brugge JS. 2002. The role of apoptosis in creating and maintaining luminal space within normal and oncogene-expressing mammary acini. *Cell* 111:29–40

408. Kenny PA, Lee GY, Myers CA, Neve RM, Semeiks JR, et al. 2007. The morphologies of breast cancer cell lines in three-dimensional assays correlate with their profiles of gene expression. *Mol. Oncol.* 1:84–96

409. Brock A, Krause S, Li H, Kowalski M, Goldberg MS, et al. 2014. Silencing *HoxA1* by intraductal injection of siRNA lipidoid nanoparticles prevents mammary tumor progression in mice. *Sci. Transl. Med.* 6:217ra2

410. White DE, Kurpios NA, Zuo D, et al. 2004. Targeted disruption of β1-integrin in a transgenic mouse model of human breast cancer reveals an essential role in mammary tumor induction. *Cancer Cell* 6:159–70

411. Bissell MJ, Weaver VM, Lelievre SA, et al. 1999. Tissue structure, nuclear organization, and gene expression in normal and malignant breast. *Cancer Res.* 59:1757s–63s; discussion 1763s–64s

412. Weaver VM, Petersen OW, Wang F, et al. 1997. Reversion of the malignant phenotype of human breast cells in three-dimensional culture and in vivo by integrin blocking antibodies. *J. Cell Biol.* 137:231–45

413. Park CC, Zhang H, Pallavicini M, Gray JW, Baehner F, et al. 2006. β1 integrin inhibitory antibody induces apoptosis of breast cancer cells, inhibits growth, and distinguishes malignant from normal phenotype in three dimensional cultures and in vivo. *Cancer Res.* 66:1526–35

414. Bischof AG, Yüksel D, Mammoto T, Mammoto A, Krause S, Ingber DE. 2013. Breast cancer normalization induced by embryonic mesenchyme is mediated by extracellular matrix biglycan. *Integr. Biol.* 5:1045–56

415. Sung KE, Yang N, Pehlke C, Keely PJ, Eliceiri KW, et al. 2011. Transition to invasion in breast cancer: a microfluidic in vitro model enables examination of spatial and temporal effects. *Integr. Biol.* 3:439–50

416. Huang CP, Lu J, Seon H, Lee AP, Flanagan L, et al. 2009. Engineering microscale cellular niches for three-dimensional multicellular co-cultures. *Lab Chip* 9:1740–48

417. Kim S, Lee H, Chung M, Jeon NL. 2013. Engineering of functional, perfusable 3D microvascular networks on a chip. *Lab Chip* 13:1489–500

418. Walsh CL, Babin BM, Kasinskas RW, Foster JA, McGarry MJ, Forbes NS. 2009. A multipurpose microfluidic device designed to mimic microenvironment gradients and develop targeted cancer therapeutics. *Lab Chip* 9:545–54

419. Leung M, Kievit FM, Florczyk SJ, Veiseh O, Wu J, et al. 2010. Chitosan-alginate scaffold culture system for hepatocellular carcinoma increases malignancy and drug resistance. *Pharm. Res.* 27:1939–48

420. Cheng S, Prot JM, Leclerc E, Bois FY. 2012. Zonation related function and ubiquitination regulation in human hepatocellular carcinoma cells in dynamic versus static culture conditions. *BMC Genomics* 13:54

421. Yates C, Shepard CR, Papworth G, Dash A, Stolz DB, et al. 2007. Novel three-dimensional organotypic liver bioreactor to directly visualize early events in metastatic progression. *Adv. Cancer Res.* 97:225–46

422. Wheeler SE, Borenstein JT, Clark AM, Ebrahimkhani MR, Fox IJ, et al. 2013. All-human microphysical model of metastasis therapy. *Stem Cell Res. Ther.* 4(Suppl. 1):S11

423. Abe M. 2011. Targeting the interplay between myeloma cells and the bone marrow microenvironment in myeloma. *Int. J. Hematol.* 94:334–43

424. Kirshner J, Thulien KJ, Martin LD, Marun CD, Reiman T, et al. 2008. A unique three-dimensional model for evaluating the impact of therapy on multiple myeloma. *Blood* 112:2935–45

425. Zhang W, Lee WY, Siegel DS, Tolias P, Zilberberg J. 2014. Patient-specific 3D microfluidic tissue model for multiple myeloma. *Tissue Eng. C* 20:663–70

426. Hou L, Liu T, Tan J, Meng W, Deng L, et al. 2009. Long-term culture of leukemic bone marrow primary cells in biomimetic osteoblast niche. *Int. J. Hematol.* 90:281–91

427. Blanco TM, Mantalaris A, Bismarck A, Panoskaltsis N. 2010. The development of a three-dimensional scaffold for ex vivo biomimicry of human acute myeloid leukemia. *Biomaterials* 31:2243–51

428. Aljitawi OS, Li D, Xiao Y, Zhang D, Ramachandran K, et al. 2014. A novel three-dimensional stromal-based model for in vitro chemotherapy sensitivity testing of leukemia cells. *Leuk. Lymphoma* 55:378–91

429. Baker BM, Trappmann B, Stapleton SC, Toro E, Chen CS. 2013. Microfluidics embedded within extracellular matrix to define vascular architectures and pattern diffusive gradients. *Lab Chip.* 13:3246–52

430. Nguyen DHT, Stapleton SC, Yang MT, Cha SS, Choi CK, et al. 2013. Biomimetic model to reconstitute angiogenic sprouting morphogenesis in vitro. *PNAS* 110:6712–17

431. Chen MB, Whisler JA, Jeon JS, Kamm RD. 2013. Mechanisms of tumor cell extravasation in an in vitro microvascular network platform. *Integr. Biol.* 5:1262–71

432. Moya ML, Hsu YH, Lee AP, Hughes CC, George SC. 2013. In vitro perfused human capillary networks. *Tissue Eng.* 19:730–37

433. Bischel LL, Young EW, Mader BR, Beebe DJ. 2013. Tubeless microfluidic angiogenesis assay with three-dimensional endothelial-lined microvessels. *Biomaterials* 34:1471–77

434. Hsu YH, Moya ML, Hughes CC, George SC, Lee AP. 2013. A microfluidic platform for generating large-scale nearly identical human microphysiological vascularized tissue arrays. *Lab Chip* 13:2990–98

435. Zervantonakis IK, Hughes-Alford SK, Charest JL, Condeelis JS, Gertler FB, Kamm RD. 2012. Three-dimensional microfluidic model for tumor cell intravasation and endothelial barrier function. *PNAS* 109:13515–20

436. Chaw KC, Manimaran M, Tay EH, Swaminathan S. 2007. Multi-step microfluidic device for studying cancer metastasis. *Lab Chip* 7:1041–47

437. Song JW, Cavnar SP, Walker AC, Luker KE, Gupta M, et al. 2009. Microfluidic endothelium for studying the intravascular adhesion of metastatic breast cancer cells. *PLOS ONE* 4:5756

438. Bersini S, Jeon JS, Dubini G, Arrigoni C, Chung S, et al. 2014. A microfluidic 3D in vitro model for specificity of breast cancer metastasis to bone. *Biomaterials* 35:2454–61

439. Mastro AM, Vogler EA. 2009. A three-dimensional osteogenic tissue model for the study of metastatic tumor cell interactions with bone. *Cancer Res.* 69:4097–100

440. Talukdar S, Kundu SC. 2013. Engineered 3D silk-based metastasis models: interactions between human breast adenocarcinoma, mesenchymal stem cells and osteoblast-like cells. *Adv. Funct. Mater.* 23:5249–60

441. Krishnan V, Vogler EA, Sosnoski DM, Mastro AM. 2014. In vitro mimics of bone remodeling and the vicious cycle of cancer in bone. *J. Cell. Physiol.* 229:453–62